



ELSEVIER

Contents lists available at ScienceDirect

Surface Science Reports

journal homepage: www.elsevier.com/locate/surfrep

Electronic, structural and chemical effects of charge-transfer at organic/inorganic interfaces



R. Otero^{b,c,*}, A.L. Vázquez de Parga^{b,c}, J.M. Gallego^{a,b}

^a Instituto de Ciencia de Materiales de Madrid-CSIC, Cantoblanco, 28049 Madrid, Spain

^b IMDEA-Nanoscience, 28049 Madrid, Spain

^c Dep. de Física de la Materia Condensada, Universidad Autónoma de Madrid, 28049 Madrid, Spain

ARTICLE INFO

Article history:

Received 30 June 2016

Received in revised form

3 March 2017

Accepted 5 March 2017

Available online 28 March 2017

Keywords:

Organic adsorbates

Self-assembly

Charge transfer

ABSTRACT

During the last decade, interest on the growth and self-assembly of organic molecular species on solid surfaces spread over the scientific community, largely motivated by the promise of cheap, flexible and tunable organic electronic and optoelectronic devices. These efforts lead to important advances in our understanding of the nature and strength of the non-bonding intermolecular interactions that control the assembly of the organic building blocks on solid surfaces, which have been recently reviewed in a number of excellent papers. To a large extent, such studies were possible because of a smart choice of model substrate-adsorbate systems where the molecule-substrate interactions were purposefully kept low, so that most of the observed supramolecular structures could be understood simply by considering intermolecular interactions, keeping the role of the surface always relatively small (although not completely negligible). On the other hand, the systems which are more relevant for the development of organic electronic devices include molecular species which are electron donors, acceptors or blends of donors and acceptors. Adsorption of such organic species on solid surfaces is bound to be accompanied by charge-transfer processes between the substrate and the adsorbates, and the physical and chemical properties of the molecules cannot be expected any longer to be the same as in solution phase. In recent years, a number of groups around the world have started tackling the problem of the adsorption, self-assembly and electronic and chemical properties of organic species which interact rather strongly with the surface, and for which charge-transfer must be considered. The picture that is emerging shows that charge transfer can lead to a plethora of new phenomena, from the development of delocalized band-like electron states at molecular overlayers, to the existence of new substrate-mediated intermolecular interactions or the strong modification of the chemical reactivity of the adsorbates. The aim of this review is to start drawing general conclusions and developing new concepts which will help the scientific community to proceed more efficiently towards the understanding of organic/inorganic interfaces in the strong interaction limit, where charge-transfer effects must be taken into consideration.

© 2017 The Authors. Published by Elsevier B.V. This is an open access article under the CC BY-NC-ND license (<http://creativecommons.org/licenses/by-nc-nd/4.0/>).

Contents

1. Introduction	106
2. Charge-transfer and energy level alignment at metal/organic interfaces	107
2.1. The Integer Charge-Transfer (ICT) model	108
2.2. The Induced Density of Interface States (IDIS) model	110
2.3. The "Electrostatic" model	110
2.4. Strong interacting systems	111
2.5. Some representative examples	112
3. Molecular conformations, substrate reconstructions and substrate-mediated interactions	114
4. Catalytic roles of charge-transfer at organic/inorganic interfaces	121

* Corresponding author at: Instituto de Ciencia de Materiales de Madrid-CSIC, Cantoblanco, 28049 Madrid, Spain.

E-mail address: roberto.otero@uam.es (R. Otero).

4.1. Isomerization reactions	122
4.2. Bond breaking and bond making	125
5. Intermolecular versus molecule-substrate charge transfer: charge-transfer complexes at solid surfaces	127
5.1. Structure of donor/acceptor mixtures on solid surfaces	128
5.2. Donor-acceptor versus molecule-substrate charge transfer: quantification and mechanisms	130
6. Electronic structure of organic adsorbates in the strong interaction limit: Delocalized electron states and molecular Kondo resonances	133
7. General conclusions	142
References	142

1. Introduction

Organic electronic and optoelectronic devices have been investigated in recent years as a potentially competitive alternative to the current inorganic semiconductor technology for applications such as Organic Light Emission Diodes (OLEDs) [1], Organic Field Effect Transistors (OFETs) [2], bulk-heterojunction [3] or dye-sensitized solar cells [4] or chemical sensors [5]. While some of these applications are already in the market (OLEDs, OFETs), some other are still far from real applications in spite of the enormous strides in efficiency registered in the last decades (bulk heterojunction solar cells) [6]. Improving the efficiency of such devices requires control over many parameters, such as the chemical nature and electronic structure of the molecular building blocks, the degree of order of the organic molecules in the active layer, the presence of dopants and impurities or the nanoscale morphology of the organic films [7].

In particular, the interface between the organic active layer and the metallic contacts is of paramount importance in determining the efficiency of the device: for example, the alignment of the molecular orbital levels of the organic layer with the vacuum and Fermi levels of the metallic leads determines the electron- and hole-injection barriers [8–10]. Alongside the purely electronic effects, the molecular organization at the interface will also determine the morphology and structure of the organic molecules in thicker films and, thus, will play an important role in steering the physical behavior of the device [11].

Thus, during the 90's and the first decade of the 21st century, research on the structure of organic monolayers deposited on metallic or passivated semiconductor surfaces progressed at a very fast pace [12–16], driven by the observation that, if the nature of the organic molecules and the substrate were properly chosen, many of the concepts that had been developed by Supramolecular Chemistry in solution phase [17] could be directly exported to the 2D organic adlayers. Thus, organic molecules were found to organize due to the formation of hydrogen bonds [18–21], coordination with metal adatoms [22–24] or van der Waals (vdW) interactions [25,26], following patterns that could be rationalized by assuming that the surface only acted as a support that would keep the molecules in a bidimensional arrangement. It can be argued that this enormous progress was the result of the cross-fertilization between Surface Science and Supramolecular Chemistry, and to a large extent was pushed further by the choice of molecules and substrates with a relatively weak interaction, so that the properties of the organic building blocks were mostly preserved upon adsorption. It is worth mentioning however that even in this limit of weak molecule-substrate interaction, small changes in the electronic structure and morphology of both adsorbates and substrate have been reported [12–16].

Regardless of the success of this approach, the application of such concepts to cases of interest for the development of electronic and optoelectronic applications is limited by the nature of organic molecules commonly used in these devices. If we consider the functions that these devices must perform, we often find that

molecules with a strong donor or acceptor electronic character, or mixtures of them both, are required in order to separate regions with opposite sign of the charge carriers, electrons and holes. This requirement must be met, for example, by OLEDs [1], since the light emission mechanism is ultimately related to the recombination of electrons and holes in the active layer. Similarly, the working principle underlying bulk-heterojunction solar cells requires the splitting of the tightly bound excitons formed by light absorption on the organic molecules, into electrons and holes that can be later on driven to different metallic electrodes [6]. The interesting physical properties of charge-transfer compounds must also be mentioned here: Solids composed of strong organic acceptors and donors display a large variety of exotic electronic behavior, ranging from metallic conduction in different dimensionalities, superconductivity, Charge and Spin Density Wave states, etc. [27,28], which are ultimately related to the transfer of electron charge from the donor to the acceptor species, thereby creating holes in the valence band of the donors and electrons in the conduction band of the acceptors. Since those molecules that are interesting for electronic and optoelectronic applications turn out to be strong donors or acceptors, charge transfer between the substrate and the adsorbate is to be expected, especially when the substrates are metallic. The properties of such charged adsorbates in terms of molecule-molecule or molecule-substrate interactions cannot be expected to be the same as when they are neutral in solution.

For this reason, during the last few years many groups have directed their attention to the adsorption and self-assembly of organic donor and acceptor species on metal surfaces [29–39] and, as it might be expected, their investigations have shown many new phenomena with no counterpart in the solution-based Supramolecular Chemistry of these compounds. Such effects have their origin in, but are not limited to, the charge-rearrangement at the interface and the concomitant realignment of the energy levels. These modifications have been related to conformational changes upon adsorption [38–43], substrate reconstructions [39,42], substrate-mediated interactions [39,44], changes in island morphologies [37], or novel chemical reaction pathways [38] for the adsorbed donors and acceptors on metal surfaces. Moreover, the transfer of electrons across the organic/inorganic interface leads to the formation of dispersive delocalized electron states [30] or may even confer magnetic properties to the organic adlayers [31,45–47].

This Review aims at offering a comprehensive overview of the different effects that have been observed for donor and acceptor organic monolayers on solid surfaces, related to charge-transfer between the substrate and the adlayer. In Section 2 we will discuss the process of charge-transfer by itself, paying attention to the different models (vacuum level pinning, Fermi level pinning) that have been proposed to understand the alignment of the electronic levels at the interface between metals and organic donors and acceptors. As a result of such realignment of the energy levels, a charge redistribution occurs which, in turn, affects the structural properties of the interface. Thus, in Section 3, we will review the changes in the molecular conformation due to charge transfer, the

atomic rearrangements of the substrate atoms, the modifications in the intermolecular interactions caused by these rearrangements, and the effects that these modified interactions have for the self-assembly of the donor and acceptors species on metallic surfaces. Of course, the charge-rearrangement also has an effect on the strength of the bonds between the constituent atoms and chemical groups within the adsorbates, and thereby, on the chemical stability of these bonds. New chemical reactions, not observed in solution, might thus take place on the surface due to charge-transfer between the surface and the donor or acceptor adsorbates, and this will be the subject of Section 4. A new degree of freedom is added to these systems when the organic adlayer consists of mixtures between donors and acceptor species: a delicate balance between intermolecular and molecule-substrate charge transfer is now established, whose details still need to be fully understood. Again, this balance of different charge-transfer processes has an effect in the structure of the overlayer. The electronic and structural effects of charge transfer in donor/acceptor mixtures on solid surfaces will be the subject of Section 5. Finally, charge-transfer will also have an effect on the electronic structure of the samples close to the Fermi level. The partial filling of the molecular orbitals leads to a number of interesting consequences, such as for example, the existence of delocalized electron states at the interface characterized by dispersive energy bands. Moreover, when the charge transfer is of an integer number of electrons, spin magnetic moment can be conferred to the organic adsorbates, which can display Kondo resonances observable by Scanning Tunneling Spectroscopy. These phenomena will be reviewed in Section 6.

In this Review we mostly show results obtained by STM or Photoelectron Spectroscopies, which allow for a very precise characterization of the molecular-scale morphology of the organic films and their electronic structure. Many studies have also addressed the investigation of the optical properties of organic thin films, including some recent reviews [48–50]. The results obtained by optical techniques such as FTIR, ellipsometry, Photoluminescence or Reflection Spectroscopies, include usually information both about the morphology of the film and its electronic structure, and in order to obtain a full picture of molecular adsorption, they are usually complemented with STM, Low Energy Electron Diffraction or other surface sensitive techniques.

2. Charge-transfer and energy level alignment at metal/organic interfaces

One of the main effects of charge transfer at the metal-organic interface is to fix the energy level alignment between the organic layer and the metal by modifying the surface dipole, thus causing a departure from the perfect Schottky-Mott limit. Although this is not the main topic of this paper, and very good reviews have already been writing about this subject [8–10], we will present here a summary of the basic ideas.

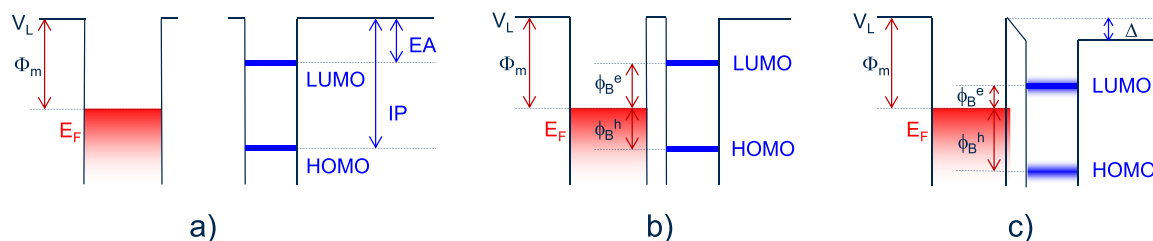


Fig. 1. Scheme of the energy levels of a metal (left) and an organic molecule (right): a) when they are far away from each other; b) in contact assuming vacuum level alignment; c) in contact after the formation of a surface dipole. EA=electron affinity; IP=ionization potential; Φ_m =work function of the clean metal surface; E_F =Fermi level of the metal; Φ_B^e =electron injection barrier; Φ_B^h =hole injection barrier; Δ =interface dipole.

Fig. 1 a shows a schematic of the energy levels of a metal and a typical semiconducting molecule when they are separated from each other. When the molecule comes into contact with the metal (Fig. 1.b), in the ideal case of no interaction between the organic layer and the metal, that is, if there is no rearrangement of the electronic density (the so-called Schottky-Mott limit), the organic layer is now in the potential of the surface dipole of the metal, and vacuum level alignment can be assumed. In this case, the injection barriers (that is, the energy necessary to inject an electron from the metal into the molecule, Φ_B^e , or from the molecule into the metal, Φ_B^h) are given by

$$\Phi_B^e = \Phi_m - EA, \quad (1)$$

$$\Phi_B^h = IP - \Phi_m. \quad (2)$$

As a consequence of Eqs. (1) and (2), when the metal changes, the injection barriers should change in the same amounts than the work function does, and the parameter S , defined as $S = d\Phi_B^e / d\Phi_m = -d\Phi_B^h / d\Phi_m$, is equal to 1. This limit is generally valid for systems prepared in ambient conditions, where the hybridization between the molecular orbitals and the metal wave functions is negligible, due to the formation of an oxide layer on the substrate or to presence of contaminants. An example is shown in Fig. 2, where poly(9,9-dioctylfluorene) (PFO) was spin coated onto Al_xO_y , SiO_2 and Au substrates [51].

In many cases, however, and even for weakly interacting systems, the Schottky-Mott limit is not obeyed, the experimentally determined hole and electron injection barriers are different from those calculated using vacuum-level alignment, and the parameter S is significantly smaller than 1 (see Fig. 3) [52–54]. As we shall see below, the origin of these differences must be found in the existence of an (additional) interface dipole Δ .

To understand the origin of this additional dipole it is convenient to notice that the work function Φ_m of a metal, that is, the energy needed to move an electron from the Fermi level inside the metal to just outside the solid, has two contributions. One comes from the bulk chemical potential inside the solid, while the other comes from the electrostatic potential across the interface. At the surface, the positive charge density, coming from the nuclei, drops abruptly to zero, but the negative charge density, coming from the electrons, “spills-out” into the vacuum [55,56]. This creates a negative charge density on the vacuum side of the interface and a positive charge density on the bulk side, giving rise to the so-called surface dipole. The potential created by this surface dipole adds to the bulk chemical potential to give the net work-function of the metal surface.

When a molecule is adsorbed on a metallic surface, many factors can modify the interface dipole and thus the work function of the metal [9,53]. Among them, we may mention:

- The “pillow” or “push-back” effect. When a molecule adsorbs onto the metal, there is necessarily a rearrangement of the electron cloud at the metal surface, since the electrons “spill-out” from

the metal are pushed-back by repulsion with the electron clouds from the adsorbate. This decreases the value of the surface dipole, and then also the work function of the metal. This is the so-called “push-back” or “pillow” effect [57–61].

- b) *Any molecular dipole, either permanent or induced by the substrate.* Also, the molecule may have a permanent dipole, in which case this dipole must be added (or subtracted, depending of its orientation) to the surface dipole [62,63]. In some cases, even if the molecule is non polar in gas phase, a dipole may be induced due to the interaction with the substrate [36].
- c) *Charge transfer between the metal and the organic molecule.* Any charge transfer from the substrate to the molecule, or the

other way around, will also contribute to the interface dipole, modifying the work function of the system [53,57].

While the pushback effect is present in all systems, the other contributions may or may not occur. In any case, the injection barriers now are given by

$$\phi_B^e = \phi_m - EA - \Delta, \quad (3)$$

$$\phi_B^h = IP - \phi_m + \Delta. \quad (4)$$

2.1. The Integer Charge-Transfer (ICT) model

This model is generally applied for systems prepared in ambient conditions, where the hybridization between the molecular orbitals and the metal wave functions is negligible, due to the formation of an oxide layer on the substrate or to the presence of contaminants. However, electron transfer can still take place by tunneling, a process that implies the transfer of an integer amount of charge. Even in these cases, however, the Schottky-Mott limit is observed only within a limited range of work function values; outside these limits, the work function of the system remains constant ($S=0$) (Fig. 4).

As shown in Fig. 5, in a very simple approximation, charge transfer should take place if

- the work function of the metal is larger than the ionization energy of the molecule, or
- the work function of the metal is smaller than the electron affinity of the molecule.

In the first case (Fig. 5.a), electrons would be transferred from the molecule to the substrate, which then becomes negatively charged. This creates a dipole at the interface that shifts downwards the vacuum level. The charge transfer process continues

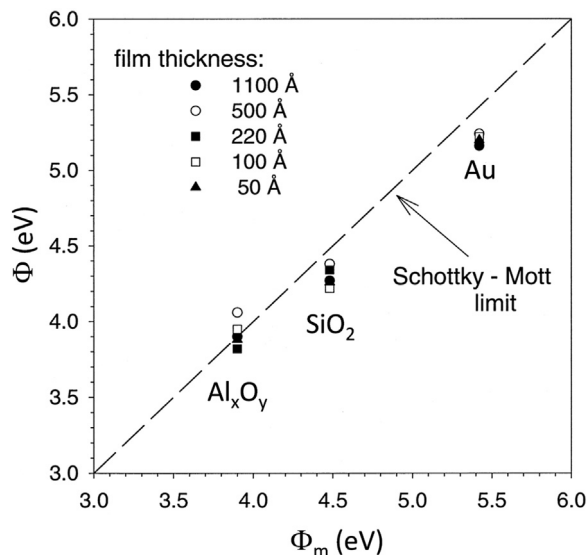


Fig. 2. Dependence of the final work function on the clean metal work function for PFO (poly(9–9-dioctylfluorene)) films of different thicknesses. Reprinted from Ref. [51], Copyright (2000), with permission from Elsevier.

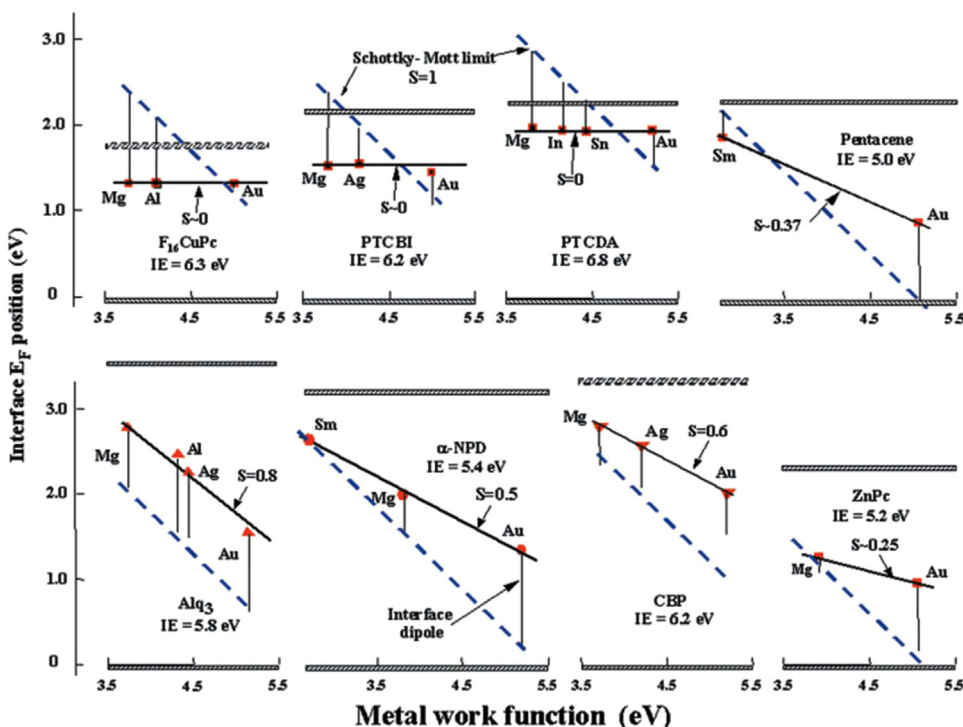


Fig. 3. Position of the final Fermi level with respect to the HOMO of the organic molecule as a function of the metal work function for eight different molecular materials. The dashed line correspond to the Schottky-Mott limit. Adapted with permission from Ref. [53], © (2003) Wiley Periodicals, Inc.

- a) the work function of the metal is larger than the ionization energy of the molecule, or
 b) the work function of the metal is smaller than the electron affinity of the molecule.

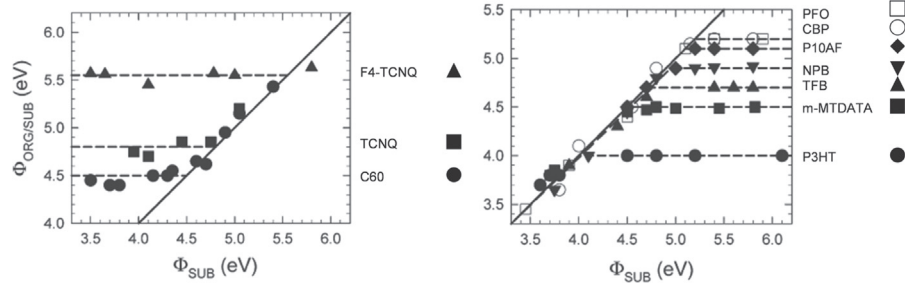


Fig. 4. Dependence of the final work function on the clean metal work function for different molecule/metal systems. Adapted with permission from Ref. [10,53]. Copyright © 2009 WILEY-VCH Verlag GmbH & Co. KGaA, Weinheim.

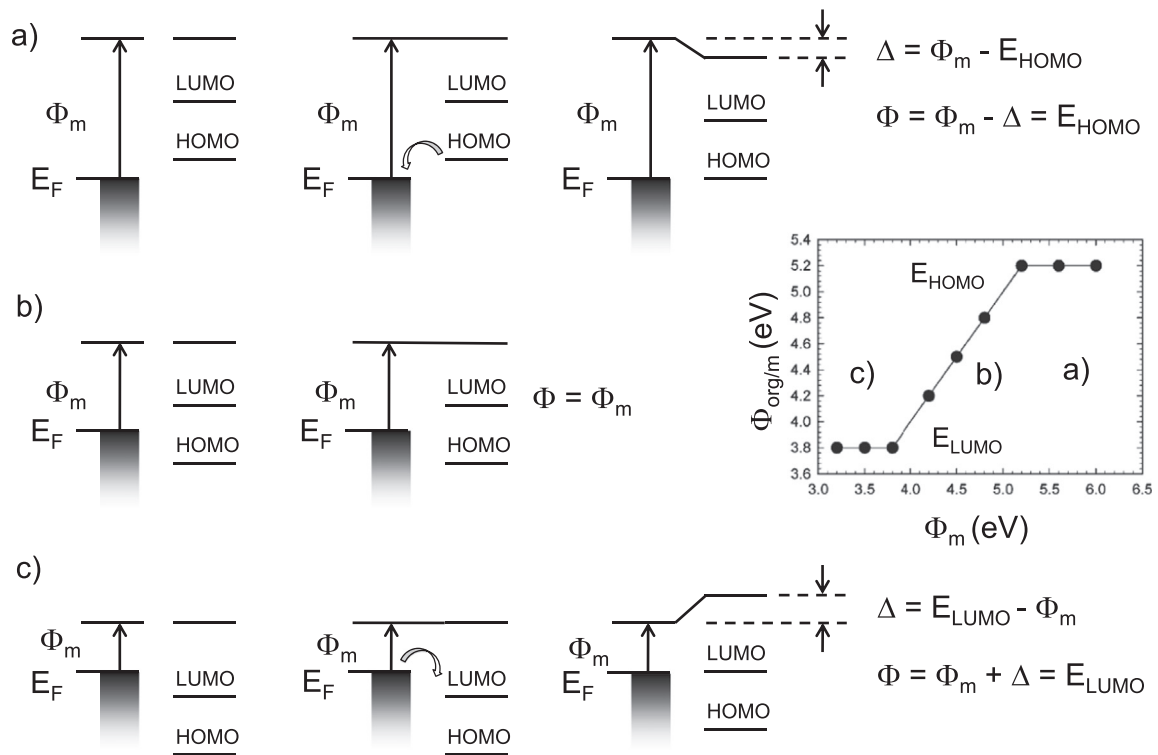


Fig. 5. Schematic illustration of the energy level alignment when an organic molecule is adsorbed on a metal surface for three different cases: a) $\Phi_m > E_{\text{HOMO}}$; b) $E_{\text{HOMO}} > \Phi_m > E_{\text{LUMO}}$; c) $E_{\text{LUMO}} > \Phi_m$. The graph shows the expected dependence of the final work function on the clean metal work function for the three different cases. Adapted with permission from Ref. [10]. Copyright © 2009 WILEY-VCH Verlag GmbH & Co. KGaA, Weinheim.

until the value of the HOMO level of the molecule aligns with the Fermi level of the metal. At this moment

$$\Delta = \Phi_m - E_{\text{HOMO}} \quad (5)$$

And the final work function of the system is given by

$$\Phi = \Phi_m - \Delta = E_{\text{HOMO}}. \quad (6)$$

In the second case, when the work function of the sample is smaller than the electron affinity of the sample (Fig. 5.c), electrons will be transferred from the metal to the molecule. Again, this creates a dipole at the interface that grows until equilibrium is reached. Then,

$$\Delta = E_{\text{LUMO}} - \Phi_m, \quad (7)$$

$$\Phi = \Phi_m + \Delta = E_{\text{LUMO}}. \quad (8)$$

These two situations, when $S=0$, are known as Fermi level alignment, since the molecular energetics levels are pinned to the Fermi level of the metal.

In the last case, when the work function of the substrate is larger than the HOMO level of the molecule, Fig. 5.b, but smaller than the LUMO value, there is no charge transfer across the interface, no dipole formation, and the vacuum levels of the sample and molecule remain aligned. This is the Schottky-Mott limit, where the final work function is equal to the work function of the metal.

In many cases, especially for π -conjugated molecules and polymers, the limits of the Schottky-Mott limit do not correspond exactly to the values of the HOMO and LUMO of the molecule, but to the values of the so-called positive integer charge-transfer state, EICT+, and the negative integer charge-transfer state, EICT-, which correspond to the energy required to take away one electron from the molecule/organic layer system producing a fully relaxed state, and the energy gained when one electron is added to the molecule/organic layer, respectively. These are states situated above the HOMO (EICT+) and below the LUMO (EICT-) levels that appear in the HOMO-LUMO gap of the neutral molecule due to the

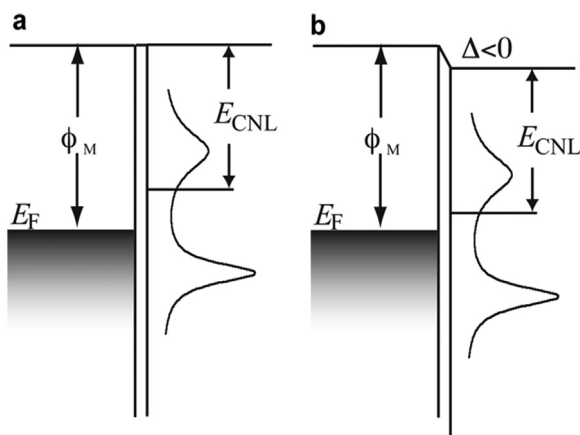


Fig. 6. Schematic energy level alignment for a metal/organic interface according to the IDIS model; a) before charge transfer; b) after charge transfer. Reprinted from Ref. [65], Copyright (2012), with permission from Elsevier.

geometrical and electronic distortions of the original system when the amount of charge changes by the addition or removal of one electron [10].

2.2. The Induced Density of Interface States (IDIS) model

This model applies to weakly interacting systems, but where the hybridization of the metal states with the molecular states is not negligible. This causes a broadening of the molecular levels, creating a local density of states between the HOMO and LUMO levels (Fig. 6). Thus, charge transfer for any value of the metal work function is possible [64].

According to the model, charge transfer will take place until the Fermi level of the metal aligns with the so-called charge-neutrality level (CNL) of the organic molecule when adsorbed on the metal surface. For each molecule, the CNL is calculated by imposing charge neutrality conditions: the total electronic charge below the CNL integrates to the number of occupied molecular states [66]. The relative position of the substrate Fermi level and the molecule CNL will determine the direction and amount of the charge transfer. (Note that the position of CNL does not describe the molecular charge transfer after contact. Rather, it is the Fermi level of the molecule in proximity of the metal, but before charge transfer is considered). Charge transfer will induce a dipole Δ at the interface that will screen the difference $(\Phi_m - \text{CNL})$ to $S(\Phi_m - \text{CNL})$, where S is the parameter defined above, $S = d\Phi_B^e/d\Phi_m$, and that, within the IDIS model, can be written as

$$S = \frac{1}{1 + 4\pi e^2 D(E_F) \delta / A}, \quad (9)$$

where $D(E_F)$ is the density of states at the Fermi level, δ the metal-organic distance, and A the area associated with one organic molecule. The resulting work function for the combined metal/organic interface, Φ , and the induced dipole, Δ , are given by

$$\Phi - \text{CNL} = S(\Phi_m - \text{CNL}). \quad (10)$$

$$\Delta = (1 - S)(\Phi_m - \text{CNL}). \quad (11)$$

Thus, the extent to which the Fermi level aligns with CNL depends on the parameter S and, in particular, on the density of states around CNL. As the density increases, the amount of charge transfer is enough to align E_F and CNL (Fermi level pinning, $S=0$), and the work function and associated injection barriers become increasingly independent of the metal work function. On the other hand, if the density of states is very small or null, no charge may

flow to align E_F and CNL, and any change in the work function of the metal will shift the work function of the system in the same amount (vacuum level pinning, $S=1$). In many cases S takes an intermediate value, meaning that there is some IDIS available, but not enough to completely align E_F and the CNL. The IDIS model has been also extended to include the pillow effect and any permanent molecular dipole [67], and has been applied successfully to a number of non-reactive systems, especially those including Au as the substrate [66,68–70].

Fig. 7 shows the results obtained for a monolayer of TTF (tetrathiafulvalene) on Au(111) [69]. In this case the alignment between the metal and the organic levels is mainly controlled by the charge transfer between the two materials, as determined by the difference between the CNL, which is close to the LUMO level, and the Fermi level of the clean metal surface, as shown in Fig. 7.c, which displays the density of states projected on the TTF orbitals along with the energy levels of the isolated molecule. The figure also shows the work function of the clean metal surface (5.3 eV), the interface Fermi energy, E_F , (that is, the final work function, Φ), the HOMO and LUMO levels, and the CNL. The CNL is located around 0.1 eV from the LUMO level of the interacting molecule, which is 0.8 eV from vacuum, and thus describes a molecule having a strong donor character. It can be seen that the adsorption on the surface creates an induced density of states within the original molecular gap and thus a charge transfer between the molecule and the metal. This gives rise to a potential that tries to align the initial Fermi level Φ_m and the organic CNL. The charge transfer, from the molecule to the gold substrate, turns out to be 0.37 eV. By changing artificially Φ_m , (Fig. 7.c) the parameter $S=0.47$ can be obtained.

Fig. 8 shows similar results for the system TCNQ/Au(111) [68]. In this case, however, the Fermi level coincides with the CNL, and the charge transfer turns out to be very close to zero, in accordance with the experimental results [71].

2.3. The “Electrostatic” model

Very recently a different model relying heavily in the density of states of the organic film has been proposed [72]. To quantify the amount of transferred charge, the organic film is partitioned in individual layers, and the charge density $\rho(z)$ in each of these layers is determined by the Fermi-Dirac statistics according to (Fig. 9)

$$\rho(z) = e \cdot n \cdot \left\{ \int_{-\infty}^{+\infty} dE f_H(E) \cdot D_H[E + eV(z)] - \int_{-\infty}^{+\infty} dE f_L(E) \cdot D_L[E + eV(z)] \right\}, \quad (12)$$

where e is the elementary charge, and n the number of molecules per unit area in each layer. D_H and D_L are the HOMO and LUMO energy distributions. $f_H(E)$ and $f_L(E)$ are the modified Fermi functions

$$f_H(E) = \frac{1}{\frac{1}{g_H} e^{-\beta(E-E_F)} + 1}, \quad f_L(E) = \frac{1}{\frac{1}{g_L} e^{-\beta(E-E_F)} + 1}, \quad (13)$$

where g_H and g_L are the HOMO and LUMO spin degeneracies. The first integral in Eq. (12) is the number of holes in the occupied DOS of the organic film, and the second integral is the number of electrons in the unoccupied DOS. Starting with vacuum level alignment, that is, by initially setting $V(z)$ to equal zero, an initial guess for the charge density $\rho(z)$ is obtained through Eq. (12). The obtained charge density is then used to solve the one-dimensional Poisson equation

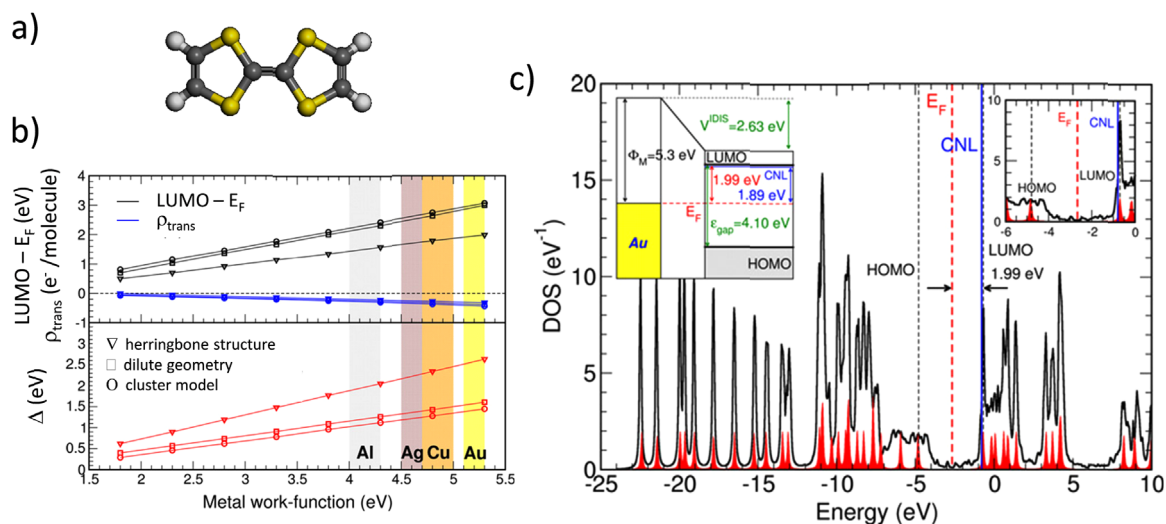


Fig. 7. a) Chemical structure of TTF (grey: C, yellow: S, white H). b) $(LUMO - E_F)$ (top, black line) and transfer of charge (top, blue line), and the interface dipole Δ (V^{DIS}) (bottom, red line) for TTF adsorbed on different metals as a function of the metal work function. c) DFT calculated DOS for a TTF monolayer on Au(111). The red shaded region shows the initial molecular levels. The inset on the left shows the energy level diagram for the system. Reprinted from Ref. [69], Copyright (2011), with permission from Elsevier. (For interpretation of the references to color in this figure legend, the reader is referred to the web version of this article.)

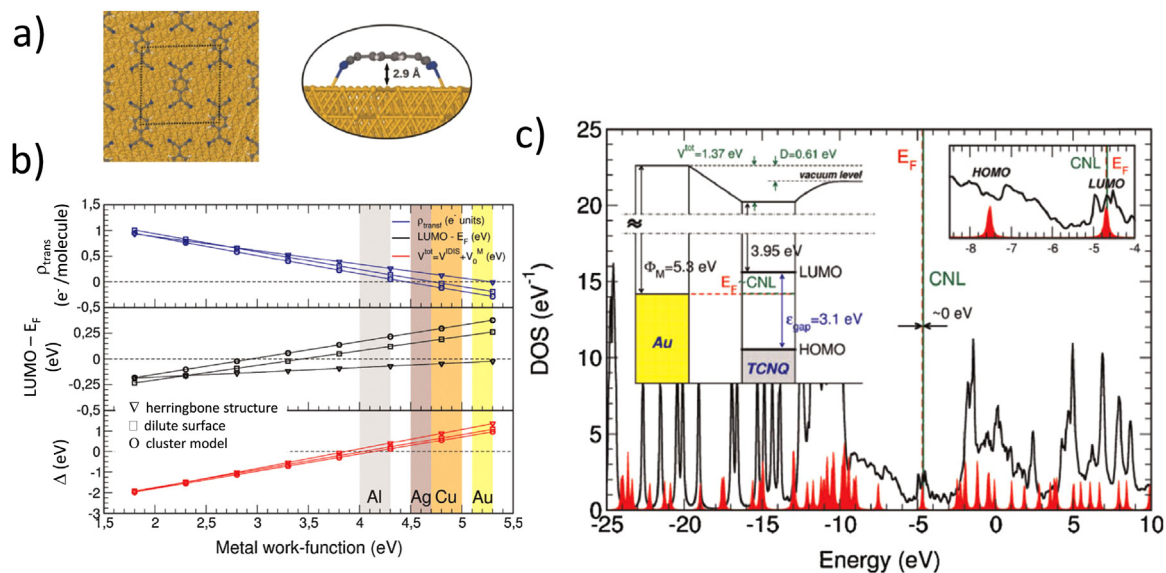


Fig. 8. a) Schematic illustration of the structure of a TCNQ monolayer on Au(111). b) Charge transfer (top), $(LUMO - E_F)$ (middle) and interface dipole (Δ) (bottom) as a function of the metal work function. c) DFT calculated DOS for a TCNQ monolayer on Au(111). The red shaded region shows the initial molecular levels. The inset on the left shows the energy level diagram for the system. Adapted with permission from Ref. [68], © 2011 WILEY-VCH Verlag GmbH & Co. KGaA, Weinheim. (For interpretation of the references to color in this figure legend, the reader is referred to the web version of this article.)

$$\nabla[\epsilon \nabla V(z)] = -\frac{\rho(z)}{\epsilon_0}, \quad (14)$$

where ϵ and ϵ_0 are the dielectric constants of the organic material and the vacuum, and thus to obtain the new electrostatic potential, which is then substituted in Eq. (12). This process is then repeated in an iterative way until stationary solutions for the charge density and the electrostatic potential are obtained.

Fig. 10 shows the calculated charge injection barriers Φ_B^e and Φ_B^h as a function of the substrate work function for a 10 nm film of pentacene [73]. For a Gaussian DOS, the results are very similar to the expected result (as in the inset in Fig. 5), with a region with $S=1$ between two regions where $S=0$. If a Lorentzian contribution is added to the DOS of the first organic monolayer, a larger amount of molecular DOS overlaps with the Fermi level, and fractional values of S can be obtained. For the case of pentacene, $S \approx 0.4$, in agreement with experimental results.

2.4. Strong interacting systems

For chemisorbed systems, the above models cannot be applied, and the systems must be treated in a one-by-one basis. In principle, a chemical bond implies a charge rearrangement that will produce a dipole at the interface and will shift the vacuum level. In a simple approximation, charge will be transferred from the species of higher chemical potential to the one with lower chemical potential, where the chemical potential of the metal, μ_m , and of the organic molecule, μ_{org} , are defined as

$$\mu_m = -\Phi_m \quad (15)$$

$$\mu_{org} = -(IP + EA)/2 \quad (16)$$

The amount of transferred charge, ΔN (where N is the number of electrons), is given by

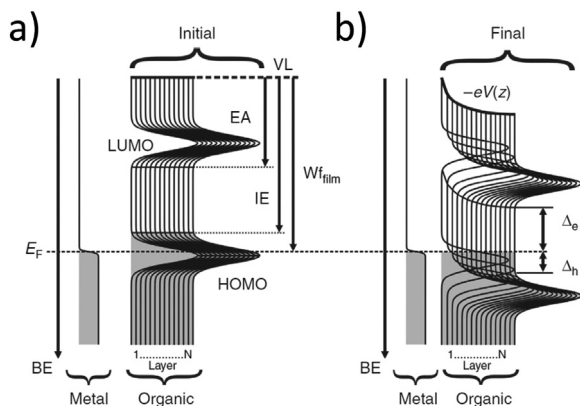


Fig. 9. a) A possible initial situation for the iterative electrostatic model. b) Final energy level alignment. Adapted by permission from Macmillan Publishers LTD: Ref. [72], copyright (2014).

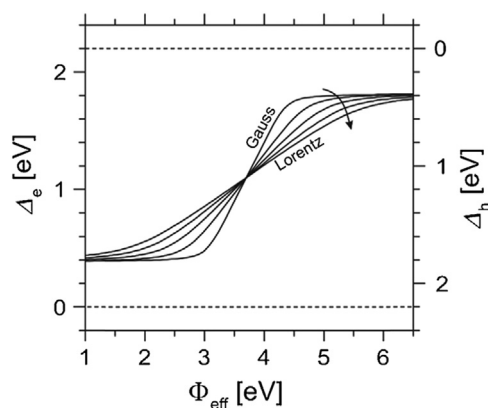


Fig. 10. Calculated charge injection barrier of a pentacene film on a metallic substrate as a function of the metal work-function for increasing lorentzian contributions to the initially gaussian distribution of the molecular DOS. Adapted by permission from Macmillan Publishers LTD: Ref. [72], copyright (2014).

$$\Delta N = \frac{1}{2} \frac{\mu_m - \mu_{org}}{\eta_m + \eta_{org}}, \quad (17)$$

where η is the absolute hardness, defined as the derivative of the chemical potential with respect to N , and which is found to be inversely proportional to the density of states at the Fermi level [74]. Thus, in this case, not only the initial position of the Fermi level of the metal is important, but also the density of states at the Fermi level. This makes possible that adsorption of the same molecule onto different metals with similar work functions may give raise to different injection barriers.

A nice example is provided by the adsorption of acrylonitrile on different metallic surfaces [57]. As measured by XPS, the binding energy of the N1s and C1s core levels decreases upon adsorption on Ni, Fe and Cu surfaces with respect to the gas phase value, indicating charge transfer from the substrate to the molecule. However, the amount of the shift, related to the amount of charge transferred, is significantly lower for Cu than for the other two metals (Fig. 11.a). The explanation can be traced back to the position of the Fermi level. While for Ni and Fe it is located in the 3d band, for Cu is located in the 4s band, where the density of states $D(E_F)$ is much lower, as can be seen in the UPS spectra of the bare metals (Fig. 11.b). Thus, the hardness of Cu is greater than for Fe and Ni, and then, according to Eq. (3), the amount of charge transfer is smaller. (Note, however, that in all three cases the work function decreases upon adsorption due to the predominance of the “pillow effect” [57]).

2.5. Some representative examples

Let us consider the case of PTCDA (perylene-tetracarboxylicacid-dianhydride) on three metal surfaces, Au(111), Ag(111) and Cu(111). PTCDA can be considered a prototype of a large π -conjugated molecule, and its adsorption on different metal surfaces has been extensively studied [77]. In these three cases PTCDA forms different versions of a herringbone structure, which seems to be commensurate on Ag(111) [76,78] and Cu(111) [79], but incommensurate on Au(111) [75,80] (see Fig. 12). The interaction with the surface, however, is very different in the three cases.

Fig. 13 shows some series of UPS spectra taken on Au(111), Ag(111) and Cu(111) as a function of the PTCDA layer thickness [81]. From the cut-off region of the spectra, the changes in the work function can be monitored. For coverages close to 1 Å of PTCDA, the work function decreases in all cases: for Au(111) it decreases 0.20 eV from 5.15 eV (although it decreases further 0.25 eV as the film thickness increases to 48 Å); for Ag(111) 0.10 eV from 4.90; and for Cu(111), 0.15 from 4.90. At monolayer coverage, the work function is 4.75 eV on all three substrates.

In the UPS spectra (see Fig. 14, Ref. [82]), for PTCDA on Au(111) there is no evidence of any peak within the energy gap signaling a metal-molecule reaction, and the peak at 1.80 eV must be related to the molecular HOMO. The PTCDA/Ag(111) system is more reactive, with charge transfer from Ag to PTCDA, and the submonolayer peaks in the energy gap of PTCDA, not present in the clean metal surface and in the multilayer spectra, can be assigned to hybrid states of the Ag 4d bands and the LUMO (now partially filled L'), and HOMO (now H') states of neutral PTCDA [83]. In a similar way, for PTCDA on Cu(111) interface states related to the former molecular HOMO and LUMO can be identified in the photoemission spectra. Their binding energy, however, is higher than for Ag(111), indicating a greater hybridization with the copper d states and a stronger bonding [83]. A scheme of the energy level alignment is shown in Fig. 15.

In order to understand the changes in the work function and the origin of the interface dipole, a plot of the theoretically calculated charge redistribution upon adsorption on the three different surfaces is shown in Fig. 16a [84]. In the case of Ag(111), on the metal side, there is a decrease of electron density right above the topmost metal layer, accompanied by a weak increase on the topmost layer, that can be attributed to the push-back effect. On the molecular side, right on the plane of the C atoms there is decrease of electrons, while in the regions above and below there is a gain in electron density. These features are due to a gain of electrons in the π system and a loss of electrons in the σ system. For Cu(111) the plot is very similar, although the push-back effect is stronger since the molecule is closer to the substrate. For Au(111) the situation is different, with no increase of electron density close to the molecular plane, and only the push-back effect can be recognized. The calculated density of states is plotted in Fig. 16.b. In accordance with the experimental results, for both Ag and Cu the LUMO is almost completely occupied (although the peaks are broadened, the maximum is located below the Fermi level), corresponding to a charge transfer from the metal to the LUMO of 1.4 electrons in the case of Ag and 1.50 for Cu. (The net charge transfer, however, is much smaller (0.47 and 0.50 electrons, respectively), due to the loss of charge from other deeper, previously occupied orbitals). For Au, on the other hand, the LUMO seems almost completely empty. It is remarkable, however, that despite these differences, the three systems show the same work function at submonolayer coverage. Actually, the non-reactive PTCDA/Au(111) system can be understood using the IDIS model [85], and although it can qualitatively describe the PTCDA/Ag(111) system, it cannot account, for example, for the behavior of PTCDA on the different silver surfaces [86].

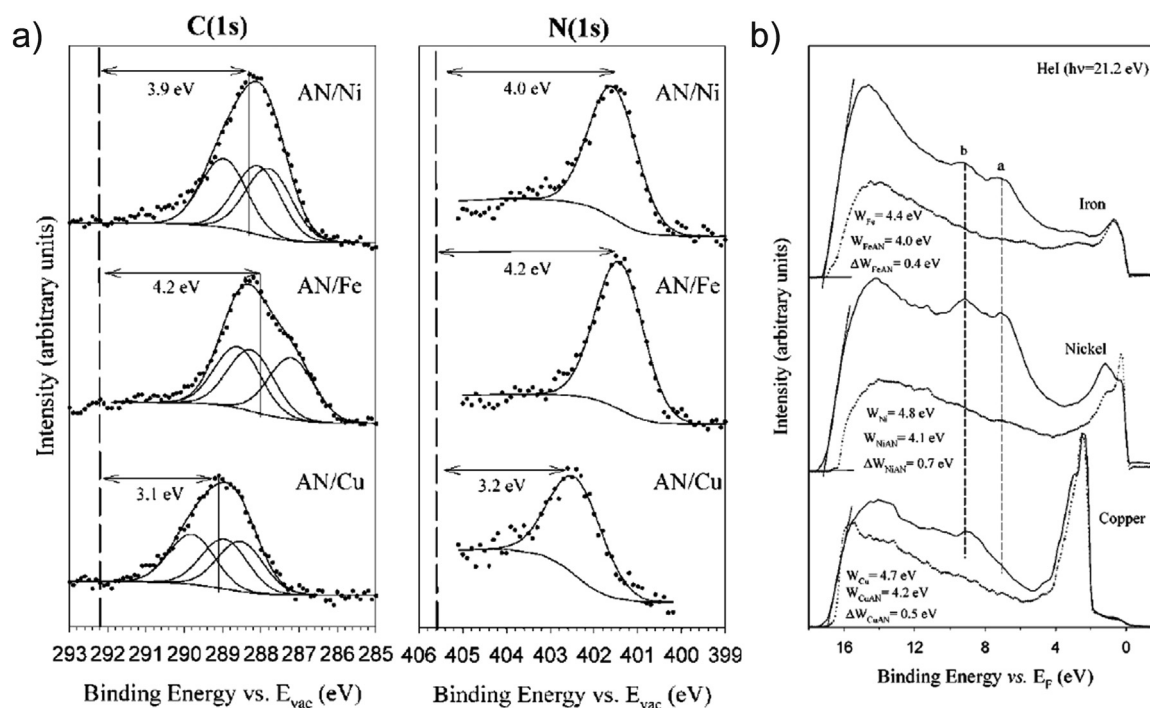


Fig. 11. a) C1s and N1s core levels of AN monolayers adsorbed on Ni, Fe and Cu. The vertical dashed lines indicated the position for the molecules in gas-phase. Binding energies are referred to the vacuum level. b) UPS spectra of the clean metal surface (dotted line) and after adsorption of an AN monolayer on iron, nickel and copper (full line). Adapted with permission from Ref. [57]. Copyright (2002) American Chemical Society.

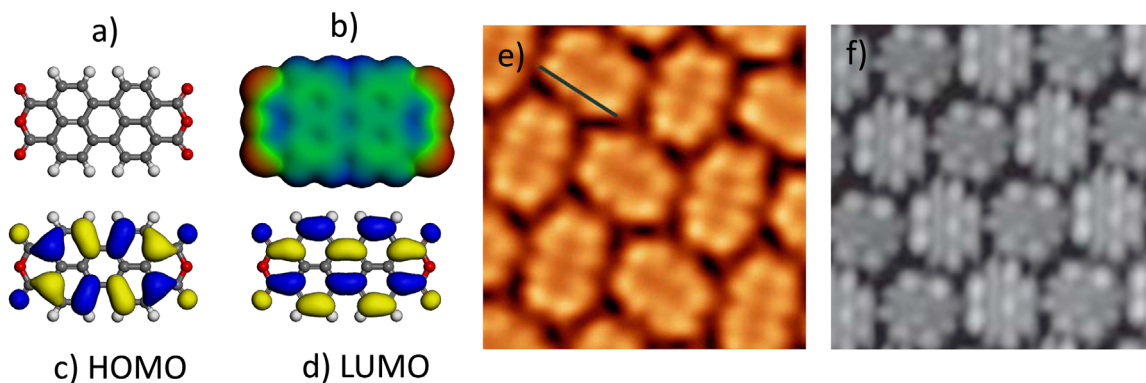


Fig. 12. PTCDA: a) Chemical structure; b) Electronic density isosurface colored according to the value of the electrostatic potential (from red, more negative, to blue, more positive; c,d) HOMO and LUMO orbitals of the gas-phase molecule. e) STM image of PTCDA on Au(111). Reprinted from Ref. [75], Copyright (2006), with permission from Elsevier. f) STM image of PTCDA on Ag(111). Reprinted with permission from Ref. [76], Copyright (2006) by the American Physical Society. <http://dx.doi.org/10.1103/PhysRevB.74.041402>. (For interpretation of the references to color in this figure legend, the reader is referred to the web version of this article.)

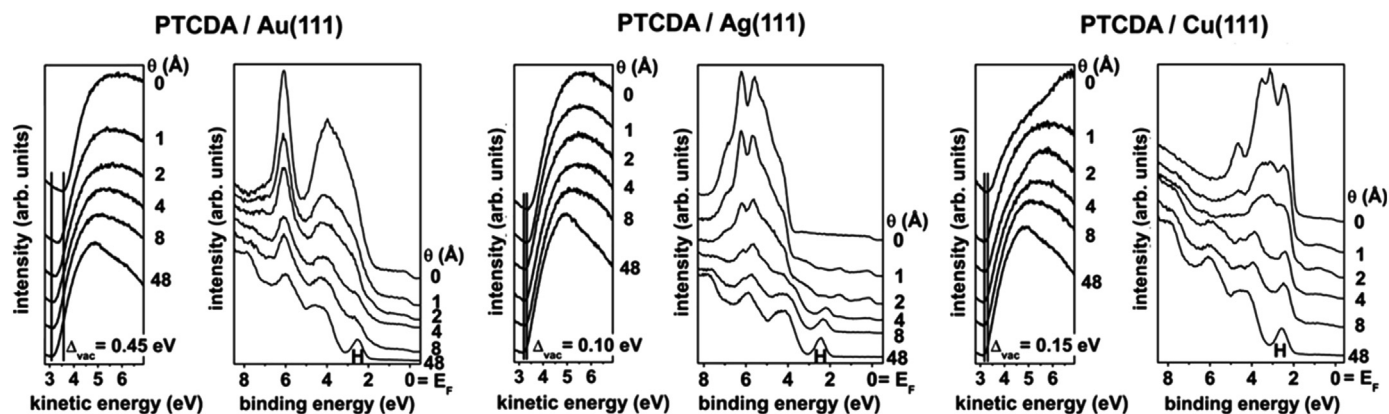


Fig. 13. UPS spectra of PTCDA on Au(111), Ag(111) and Cu(111) for different layer thicknesses. In every case, the left panel shows the secondary electron cut-off spectra. Reprinted from Ref. [81], Copyright (2007), with permission from Elsevier.

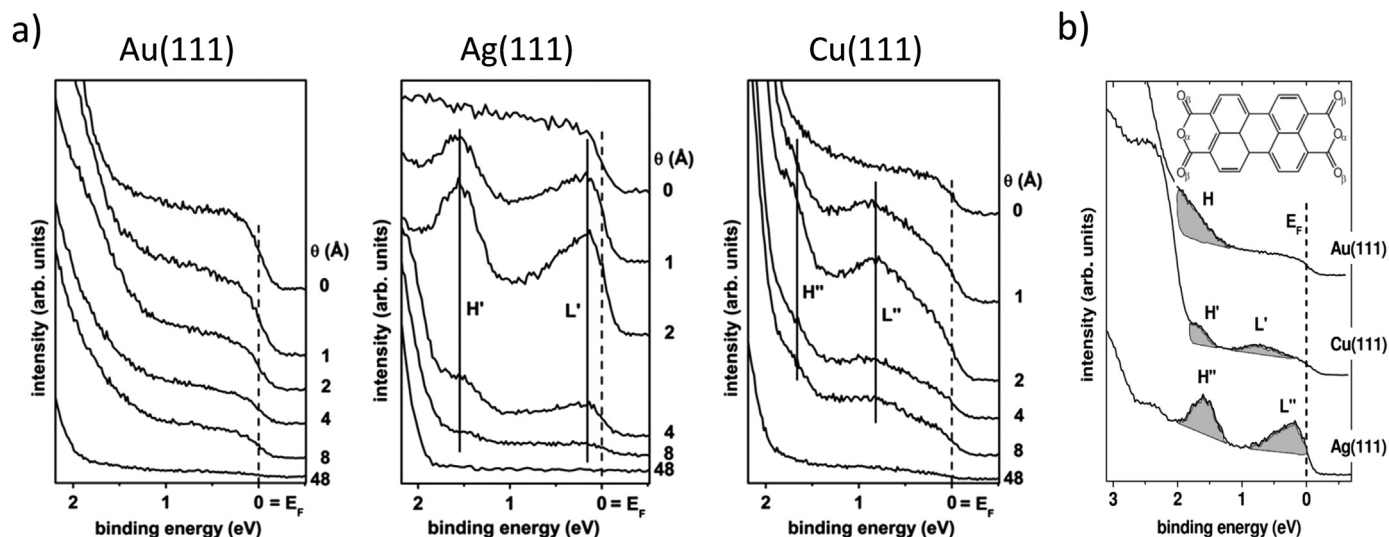


Fig. 14. a) Close-up of the region close to the Fermi level for the UPS spectra for Au, Ag and Cu shown in Fig. 13. Reprinted from Ref. [78] with permission. Copyright (2007), with permission from Elsevier. b) The UPS spectra taken for a coverage of ~ 1 ML of PTCDA. Reprinted from ref. [82]. © IOP Publishing & Deutsche Physikalische Gesellschaft. CC BY-NC-SA. <http://iopscience.iop.org/article/10.1088/0953-8984/20/18/184008>.

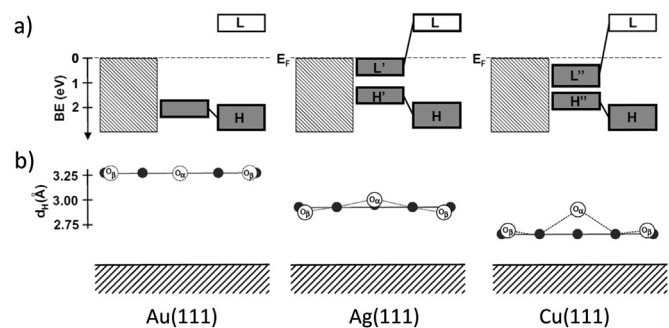


Fig. 15. a) Schematic energy level diagram for the adsorption of PTCDA on Au(111), Ag(111) and Cu(111). In every case, the left part represents the metal electronic density, the right part the HOMO and LUMO orbitals for the PTCDA molecule in gas phase, and the middle part the positions of HOMO and LUMO derived interface states after adsorption. b) Schematic geometric structure of the PTCDA molecule after adsorption. Reprinted from Ref. [81]. Copyright (2007), with permission from Elsevier.

These differences in the electronic structure are correlated with the different adsorption geometry and bonding distance, as deduced from X-ray standing wave experiments [87–89] (see Fig. 15. b, Ref. [81]). Thus, the weak interaction between PTCDA and Au(111) is reflected in a relatively high adsorption distance (3.27 Å), with the molecule keeping basically a planar geometry. For Ag(111) the average C distance is 2.86 Å, while for Cu(111) it is 2.66 Å. In addition, in the last two cases the molecule is distorted with respect to the gas phase configuration. While on Ag(111) the carboxylic oxygens bent towards the surface and the anhydride oxygens bent away from the surface, on Cu(111) all the oxygen atoms are bent away from the surface. These experiments show the intimate connection between the adsorption geometry and the strength of the metal-molecule interaction. (How the adsorption may affect both the molecular and substrate geometrical structure will be discussed in more detail in the next section).

Fig. 17 shows the calculated work functions for PTCDA on another series of metals for different metal to molecule distances [90]. Adsorption on Au(111) lowers the work function, but it increases in all the other cases. Surprisingly, however, the work function seems to be pinned at 4.7 eV for a number of metal substrates and distances, which is in agreement with the previous results and with other experimental data [52]. Fig. 18 show the

calculated PDOS for two different distances. They are very similar, although the spectra at 3.0 Å are shifted towards lower binding energy. For PTCDA on Au the LUMO is empty, but already for Ag it is partially occupied, the amount of charge transfer increasing along the series Ag, Al, Mg and Ca. By comparing Figs. 17 and 18 it can be noticed that work-function pinning occurs when the Fermi level crosses the level of the LUMO. As long as the Fermi level is inside the LUMO peak, the work function is pinned. Unpinning takes place for Ca and $d = 3.0$ Å, when the Fermi level jumps to the next peak, the LUMO + 1.

The changes in the work function are then a result of two competing effects. If the metal-molecule interaction is weak, the “pillow” effect dominates, lowering the work-function. On the other hand, if the work function of the metal is low with respect to the molecular LUMO, electrons are transferred to the molecule, increasing the work function.

3. Molecular conformations, substrate reconstructions and substrate-mediated interactions

Although many times ignored, it has long been known that the metal/organic interface is rarely a passive, inert system where both the metal and the organic molecule can be treated as fixed reproductions of the bulk materials. On the contrary, both the metal and the organic molecule often experience modifications both in their geometric and electronic structure. Molecular adsorbates, like the atomic ones [91,92], can induce structural rearrangements on metallic surfaces. Although the first observations were related to the disappearance of the reconstruction of the clean metal surface [93], it soon became clear that surface reconstructions could also be induced [94], and, in some cases, this surface rearrangement can lead to step edge alignment or even surface faceting [95].

Very recently, the detailed structure of the metal/organic interface has been the subject of a number of studies due to the role they play in the efficiency of optoelectronic devices. However these systems are usually composed of strong electron acceptors and/or donors materials, and to control their electronic properties, a thorough understanding of their electronic and geometric properties is required. In this chapter we will see some examples of how charge transfer in metal/organic interfaces, where the

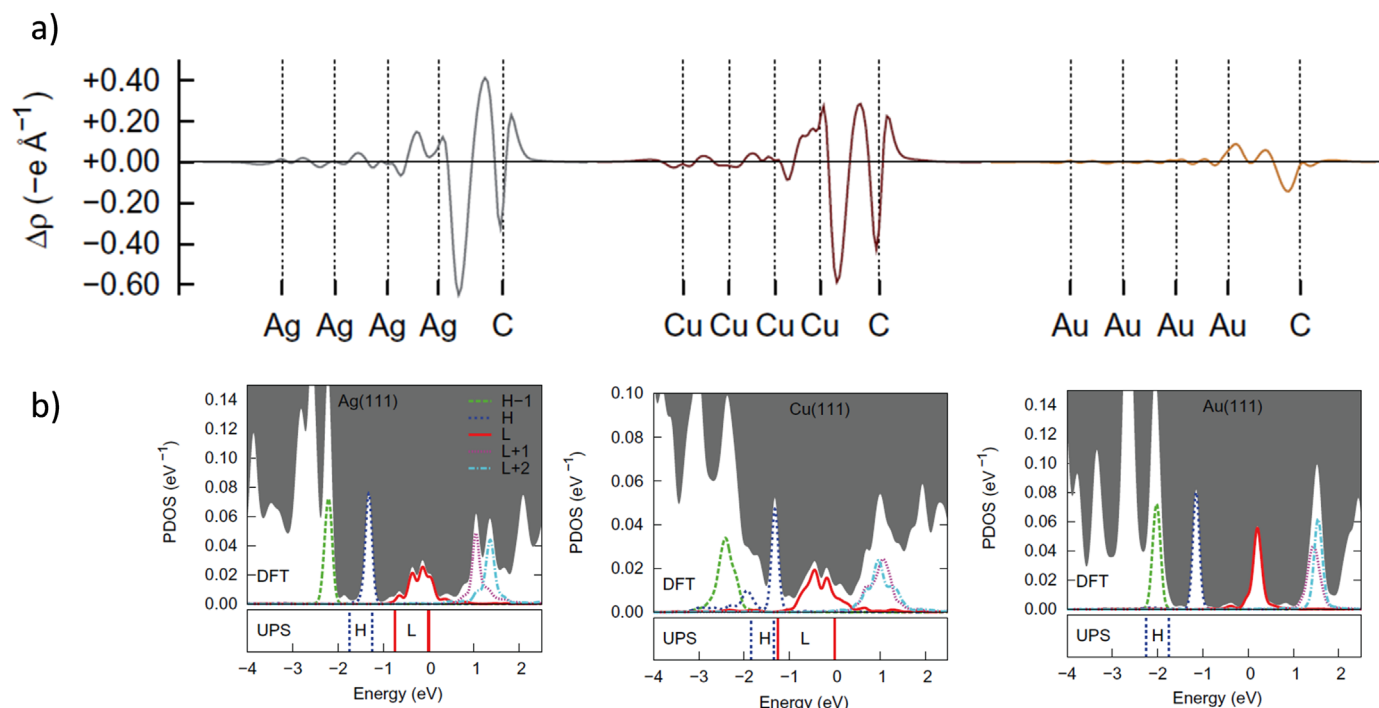


Fig. 16. a) Electron density difference after adsorption of PTCDA on Ag(111), Cu(111) and Au(111). b) Density of states projected onto the molecule and selected molecular orbitals (colored lines). The bottom panels indicate the experimentally measured positions of the HOMO and LUMO orbitals. Reprinted from ref. [84]. © IOP Publishing & Deutsche Physikalische Gesellschaft. CC BY-NC-SA. <http://iopscience.iop.org/article/10.1088/1367-2630/11/5/053010>. (For interpretation of the references to color in this figure legend, the reader is referred to the web version of this article.)

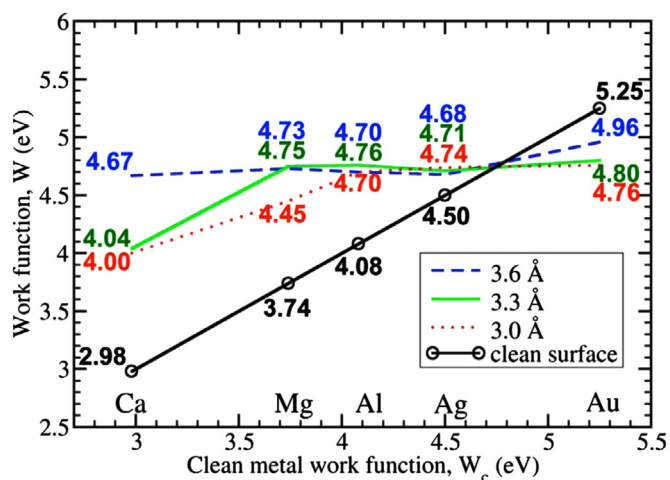


Fig. 17. Calculated work-functions for a monolayer of PTCDA on the (111) faces of different metals for different distances between the molecule and the surface. Reprinted with permission from Ref. [90]. Copyright (2010) by the American Physical Society. <http://dx.doi.org/10.1103/PhysRevB.81.125403>.

organic layer is composed of strong electron donors and/or electron acceptors, may produce modifications of the electronic and geometric structure in both the metal and the organic layer.

Fig. 19 shows the chemical structure, along with their frontier orbitals, of some of the molecules that we will be dealing with in this section: TCNQ (tetracyanoquinodimethane), F4-TCNQ, and TCNE (tetracyanoethylene) along with their frontier orbitals. TCNQ is a prototype of a number of electron acceptor species, and is one of the most studied molecular organic acceptors, along with its derivatives. It has been shown to accept charge from the substrate when adsorbed on Cu(111) [96,97], Ni(111) [98], Cu(100) [39], Ag(111) [99], and Ag(100) [100]. It is important to notice that, in this context, the acceptor or donor character of an organic molecule

depends upon the surface on top of which it is adsorbed. For example, TCNQ on Cu(100) takes almost two electrons from the copper surface [39], but there is no charge transfer when adsorbed on Au(111) [68,71].

One of the first examples to demonstrate that charge transfer can actually induce substantial modifications on the geometric structure of a metallic substrate is the case of TCNE on Cu(100) [42]. TCNE is another strong electron acceptor, and charge transfer has been reported when deposited on polycrystalline silver [101], polycrystalline copper [102], Cu(111) [47,103], Ag(100) [104,105]. Previous STM studies [104] had shown that TCNE self-assembles on the Cu(100) surface by forming islands with square symmetry or 1D chains (see Fig. 20.a).

Based on geometrical considerations, two different structural models were proposed to explain the chain assembly (Fig. 20.b and Fig. 20.c). In the first one, the TCNE molecules were placed in high symmetric sites on the surface separated by a distance compatible with the experimental results, while the second one involved the presence of Cu adatoms between the cyano groups of neighboring molecules. DFT calculations showed that, in the first case, the Cu surface was severely distorted, especially close to the cyano groups, where one copper atom was lifted 1.3 Å out of the surface plane. In the second case the surface remained unreconstructed, the Cu adatoms covalently bonded to the cyano groups and acting like bridges between the molecules. By comparing simulated STM images and the experimental STM measurements, it was concluded that the reconstructed model fitted better the results, and that was indeed the buckling of the copper surface the driving force for the TCNE self-assembly into chains. The results also showed that TCNE was significantly distorted with respect to the gas phase structure, although no details of the geometric structure were given. It seems that the formation energy of the TCNE/Cu(100) complex compensated more than enough the energy required to distort the substrate and the

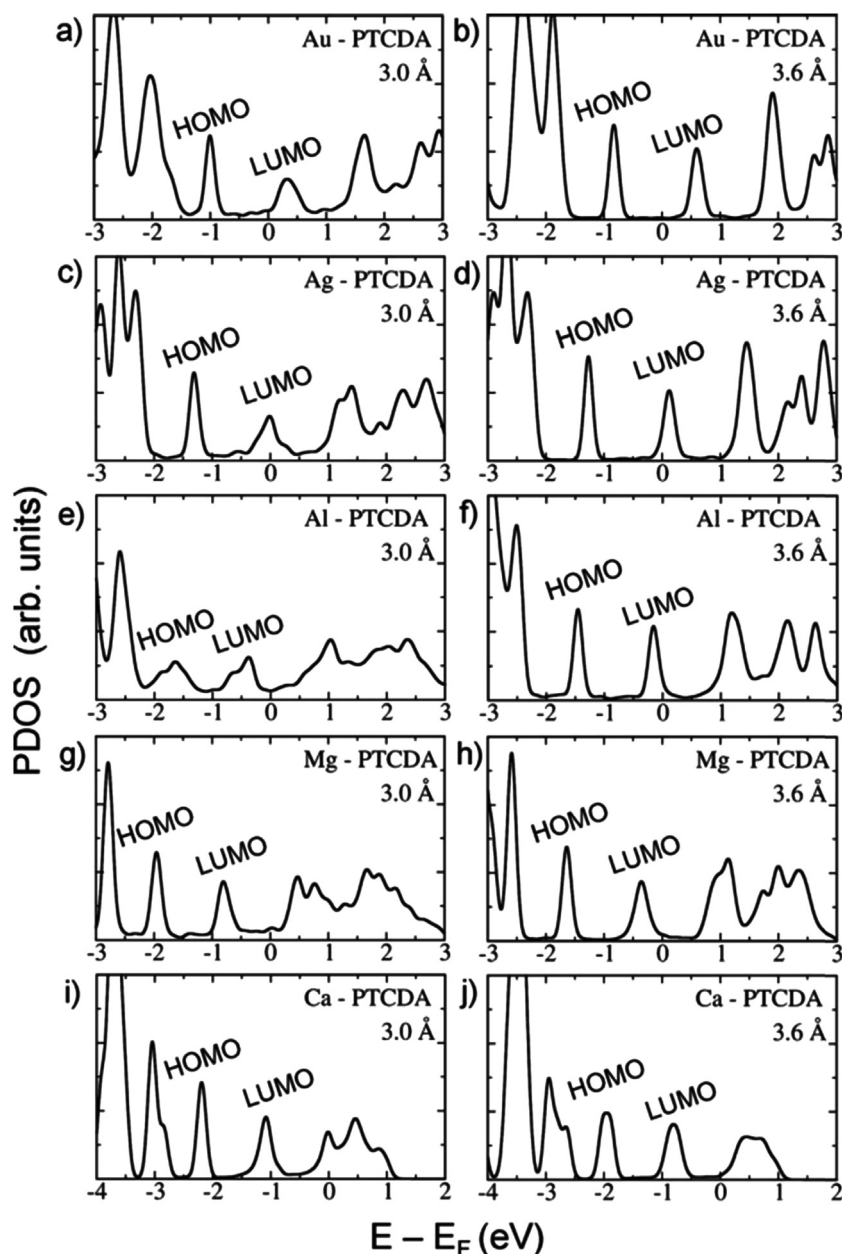


Fig. 18. Projected Density of States for a PTCDA molecule adsorbed on different metal surfaces and for two metal-molecule separations. Reprinted with permission from Ref. [90]. Copyright (2010) by the American Physical Society. <http://dx.doi.org/10.1103/PhysRevB.81.125403>.

molecule. Additionally, the DFT results showed that there is a substantial amount of charge transfer between the metal and the molecule: TCNE accepts $1.8e^-$ from the copper surface. However, like for most transition metals, there is also a strong back donation, and Cu receives $1.5e^-$ from the molecule. Thus, a Mulliken population analysis gives a net charge of $0.30e^-$ on TCNE.

On the other hand, it is known that some organic molecules can significantly alter their conformation when adsorbed on a metal surface [39,41,88,106]. The distortion can be due to van der Waals attraction, but also to charge transfer from the substrate, as has been reported for the F4-TCNQ/Cu(111) system [41]. Using a combination of experimental (UPS, XSW) and theoretical (DFT) techniques, it was concluded that the strong molecule-metal interaction produces several modifications in the molecular geometry: the molecule was no longer planar, but is significantly bent (Fig. 21.a), with the N atoms much closer to the Cu surface than the C ring and the F atoms; at the same time, the C ring was no longer

quinoid, but almost aromatic; and the two C atoms carrying the cyano groups showed a markedly sp^3 character, thus allowing the strong bending of the molecule. This geometric structure is similar to the one reported for reduced TCNQ. As a result of the bending, the molecule acquires a dipolar moment perpendicular to the surface that goes from the more negative N atoms (closer to the surface) to the (more positive) C ring and then decreases the metal work function by 0.8 eV.

Additionally, both UPS and DFT results showed that there is an appreciable charge transfer from the substrate to the molecule. Fig. 21.b shows the projection of the calculated DOS onto the molecular orbitals of the isolated molecule. The former LUMO level is almost completely filled, receiving $1.8e^-$ from the copper surface; at the same time, there is a strong back donation from the molecule to the surface. Actually, these back-donated electrons do not come from the molecular HOMO, but from the σ levels localized at the cyano groups of the molecule, that participate more strongly in the

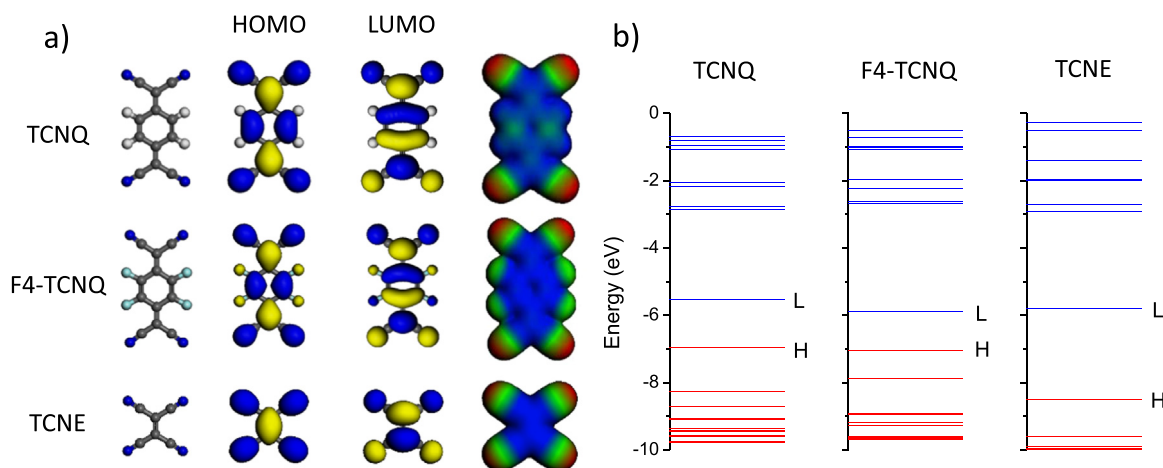


Fig. 19. a) Chemical structure of TCNQ, F4-TCNQ and TCNE along with their frontier orbitals. The last column shows a charge density isosurface where every point of the isosurface is colored according to the value of the electrostatic potential at that point (from more negative, red, to more positive, blue). b) DFT calculated energy level diagram for the three molecules. (For interpretation of the references to color in this figure legend, the reader is referred to the web version of this article.)

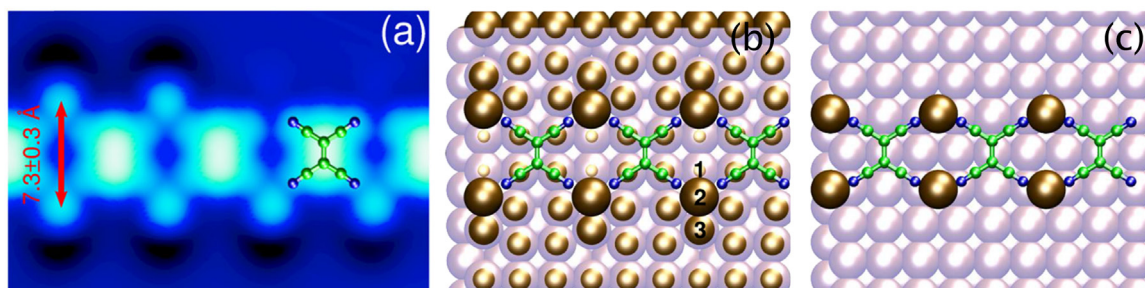


Fig. 20. a) STM image of a chain of TCNE molecules on Cu(100). b,c) The two DFT optimized models for the adsorption of TCNE on Cu(111) (b) without and (c) with copper adatoms. A transparent plane has been used to emphasize the magnitude of the reconstruction of the topmost layer Reprinted with permission from Ref. [42]. Copyright (2008) by the American Physical Society. <http://dx.doi.org/10.1103/PhysRevLett.101.216105>.

bonding with the Cu atoms (from the HOMO – 9 to HOMO – 12, which are only 80% to 90% occupied after adsorption). As a result, there is a net charge of $0.6 e^-$ per molecule that translates into a bond dipole that goes from the (more negative) molecule to the copper surface and increases the work function by 1.0 eV. On the other hand, the bending of the molecule creates a molecular dipole pointing in the opposite direction and which contributes to decreasing the work function by 0.8 eV. Thus, the net work-function increase is around +0.2 eV (the experimental value is +0.6 eV).

A similar, and more clear connexion between charge transfer, substrate reconstruction, and molecular distortion was reported for the related system TCNQ/Cu(100) [39]. In this case the molecules self-assemble on the copper surface in the shape of elongated islands, with a rhombohedral unit cell and the average molecular plane parallel to the surface (see Fig. 22a). The assembly along the short side of the cell can be understood simply as due to the electrostatic interaction between the negatively charge cyano groups and the hydrogen atoms of the neighbouring molecule (Fig. 19). However, the interaction along the long side cannot be understood without the presence of the substrate due to the otherwise repulsive interaction between the cyano groups.

The answer to this problem came from the results of DFT calculations, which showed that, like in the TCNE/Cu(100) case, the copper surface is strongly distorted (Fig. 23a). The copper atoms closer to the N atoms (the average Cu-N distance is 2.0 Å) are lifted by 0.3 Å from their equilibrium position. Note that, unlike the TCNE/Cu(100) case, the N atoms from neighbour TCNQ molecules are not bonded to the same Cu atom; thus, there is not a direct N-Cu-N interaction, but a more indirect N-Cu-Cu-N interaction. Rather, it is the stress field created by the lifted Cu atoms what

directs the self-assembly, not the possible formation of a metal-organic coordination bond.

Also, as in the previous F4-TCNQ/Cu(111) case, the molecular structure is strongly distorted. The table in Fig. 23b shows the bond lengths for the gas phase of neutral TCNQ, TCNQ¹⁻, TCNQ²⁻ and TCNQ adsorbed on Cu(100). It can be seen that upon adsorption, the C ring becomes almost aromatic (the difference between B4 and B5 decreases from $\sim 0.08 \text{ \AA}$ to $\sim 0.01 \text{ \AA}$), and bond B3 increases appreciably its length, acquiring a marked single-bond character that facilitates the bending of the cyano groups. All these changes are very similar to those arising from charging the TCNQ molecule in the gas phase with two electrons [107], which can be rationalized in terms of the rearrangement of bonds to accommodate the extra electrons at the dicyanomethylene ends (Fig. 23c). Actually, a Bader analysis of the electronic charge for the TCNQ/Cu(100) system gives a transfer from the Cu(100) surface to the molecule of $\sim 1.5e^-$. This electronic charge is almost entirely located in the former LUMO of the molecule, as can be seen in the electron density difference graph of Fig. 23d. Accordingly the projected density of states shows the former LUMO related orbital to be almost entirely occupied (Fig. 23e). The charged state of TCNQ on the Cu surface was experimentally confirmed by X-Ray photoelectron spectroscopy (Fig. 22b) and X-ray absorption fine structure spectroscopy (NEXAFS). First, the binding energy of the N1s core level is 398.7 eV, very similar to that measured in TCNQ salts [108], and almost 1 eV lower than for solid, neutral TCNQ [109]. In addition, NEXAFS measurements proved the molecular LUMO to be populated upon adsorption on the surface [39].

These results show how charge transfer processes may modify the structural and electronic properties of both the organic

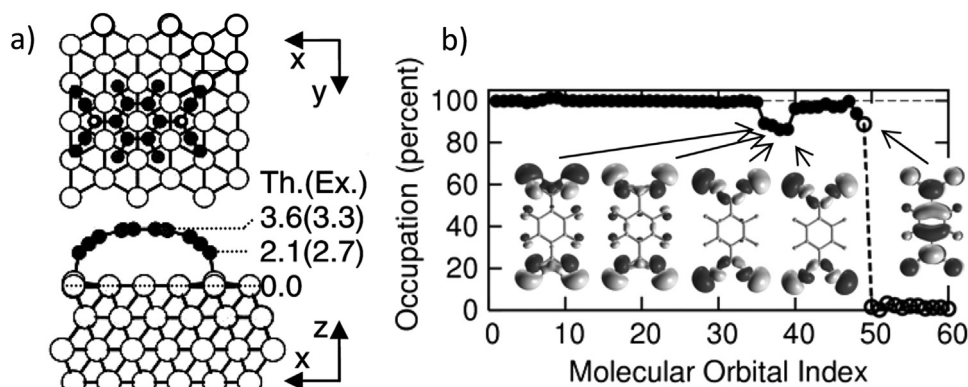


Fig. 21. a) Geometric structure of a F4-TCNQ molecule adsorbed on Cu(111). b) Theoretically calculated occupation of the lowest 60 molecular orbitals after adsorption. The full (open) circles and solid (dashed) lines correspond to the orbitals which are occupied (unoccupied) in the isolated molecule. Reprinted with permission from Ref. [41]. Copyright (2007) by the American Physical Society. <http://dx.doi.org/10.1103/PhysRevLett.99.256801>.

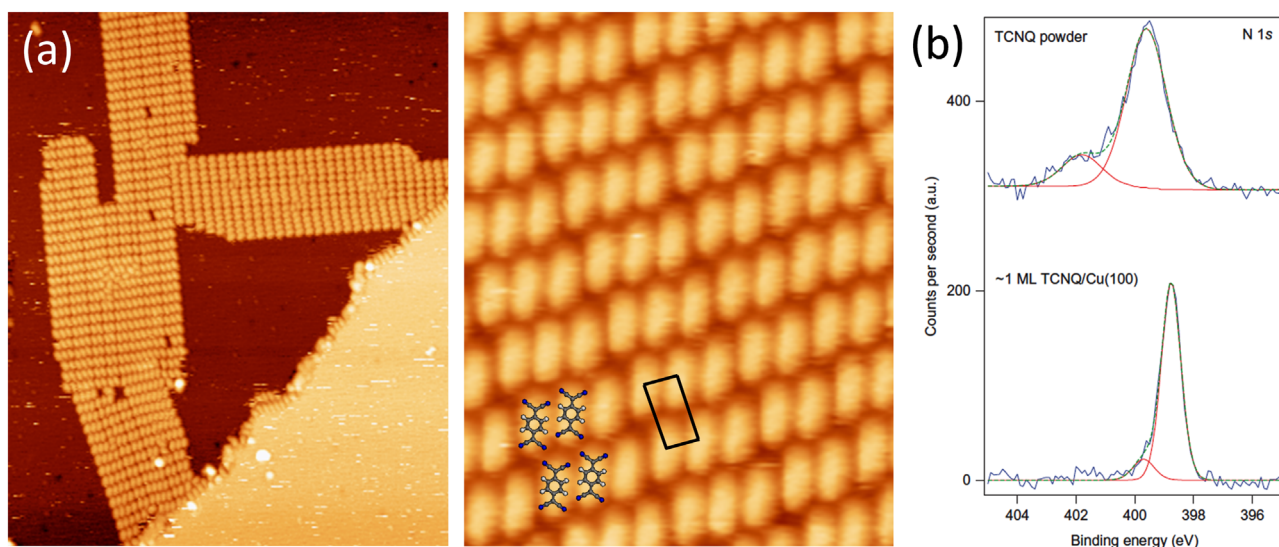


Fig. 22. a) STM images taken after depositing submonolayer amount of TCNQ on Cu(100). b) N1s core level XPS spectra taken for bulk TCNQ (top), and a monolayer of TCNQ on Cu(100) (bottom). Adapted by permission from Macmillan Publishers LTD: Ref. [39], copyright (2010).

molecule and the metal substrate, creating new intermolecular interactions, and then new molecular assemblies, that could not have been predicted from the gas-phase conformation.

Strong electron acceptors do not only modify the substrate surface on flat terraces, they can also cause step edge alignment and step etching [110]. Fig. 24.b and Fig. 24.c show details of a Cu(100) surface close to a step edge after depositing a small amount of F4-TCNQ. The F4-TCNQ molecules adsorb preferentially at the lower part of the steps, with the long axis perpendicular to the step edge, rearranging the copper atoms there and creating a periodic array of kinks. In general, the orientation of the steps change from the [110] direction characteristic of the clean Cu(100) surface (Fig. 24.a) to the [120] direction. A model of the adsorption configuration is shown in Fig. 24.d. In this geometry, the cyano groups closer to the steps are not only interact with the terrace copper atoms, but also with the copper atoms at the steps. This interaction can be maximized by etching the steps in the form of trenches like those shown in Fig. 24c: in here, all the cyano atoms are interacting with steps copper atoms.

As TCNQ, F4-TCNQ is a strong electron acceptor. It even reacts with a polycrystalline gold surface, with a significant charge transfer [111]. There is also charge transfer when adsorbed on Cu(111) ($\sim 0.6 e^-$) [41], Ag(111) ($\sim 0.5 e^-$) or Au(111) ($\sim 0.4 e^-$) [40]. Upon adsorption on the Cu(100) surface there is charge transfer

from the substrate to the molecule, and the LUMO becomes fully occupied, as proven by photoelectron spectroscopy [112]. However, for the molecules adsorbed at the steps the occupation of the LUMO is asymmetrical. Fig. 25 shows two close-up STM images of the molecules at the steps taken at two different voltages. At a bias voltage $V_s = +0.2 V$ (Fig. 25a) the molecular shape is rather symmetric, but at $V_s = -1.2 V$ it becomes very asymmetric. Fig. 25c shows STS dI/dV curves taken at different points of the molecular axis. For the cyano group closer to the steps (green curve) there are two distinctive peaks at $-1.2 eV$ and $-2.0 eV$ that correspond, respectively, to the LUMO and HOMO of the gas-phase molecule. The intensity of these peaks, however, is much smaller for the cyano groups farther away from the steps, indicating a different electronic population. Actually, a closer look at the STM image shows that the electronic structure is also asymmetric along the short molecular axis, due to the different configuration of the two cyano groups closer to the steps (see Fig. 24d).

Similar step etching has been observed for TCNE on Ag(111) [113]. In this case, step etching occurs even at low temperature. Fig. 26a shows a STM image of the silver surface closer to a step after depositing $\sim 0.4 ML$ at 150 K. Far from the steps the molecules self-assemble into islands with a Kagomé structure. A closer look to the STM images seems to suggest that the molecules are connected by silver atoms, forming a metal-organic coordination

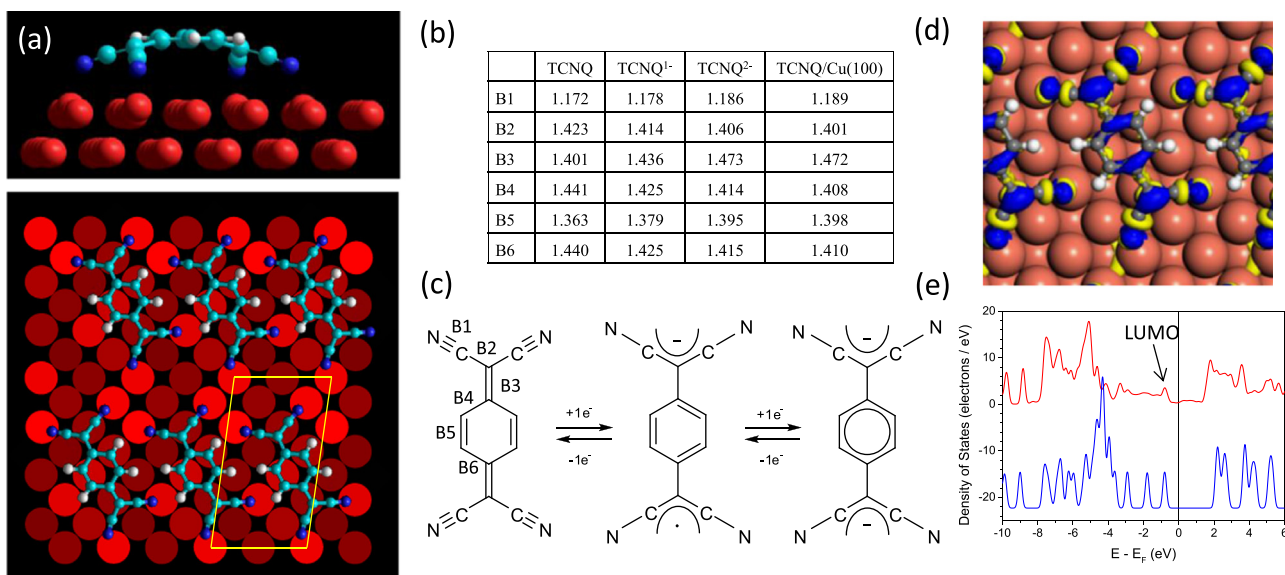


Fig. 23. a) Side and top views of the calculated optimized conformation for a TCNQ molecule on Cu(100). The different shades of red in the bottom panel represent different heights with respect to the clean copper topmost surface layer. b) Bond lengths for TCNQ in the neutral, anion and dianion gas-phase conformation, and when adsorbed on the Cu(100) surface. c) Schematic illustration of the changes in gas-phase TCNQ upon reduction [107]. d) Calculated electron density difference for TCNQ on Cu(100) (blue = electron gain regions; yellow = electron loss regions). e) Calculated density of states projected on the TCNQ molecule (red line). The LUMO derived orbital is indicated in the graph. The blue line shows the density of states of the molecular layer in the absence of the copper substrate (it has been horizontally shifted to make the LUMO levels to coincide in the two cases). Adapted by permission from Macmillan Publishers LTD: Ref. [39], copyright (2010). (For interpretation of the references to color in this figure legend, the reader is referred to the web version of this article.)

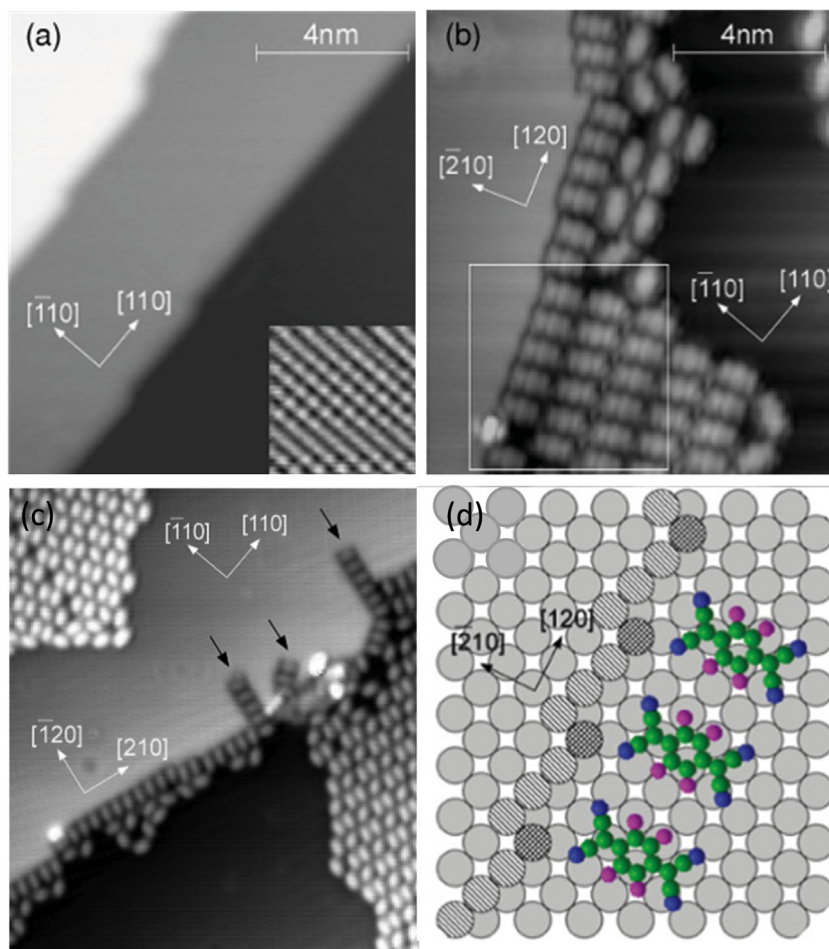


Fig. 24. a) An STM image of the clean Cu(100) surface, b, c) STM images of the Cu(100) close to a step edge after TCNQ adsorption, d) Proposed structural model of the adsorption geometry close to the step edge. Reprinted with permission from Ref. [110], Copyright (2011) by the American Physical Society. <http://dx.doi.org/10.1103/PhysRevB.83.153403>.

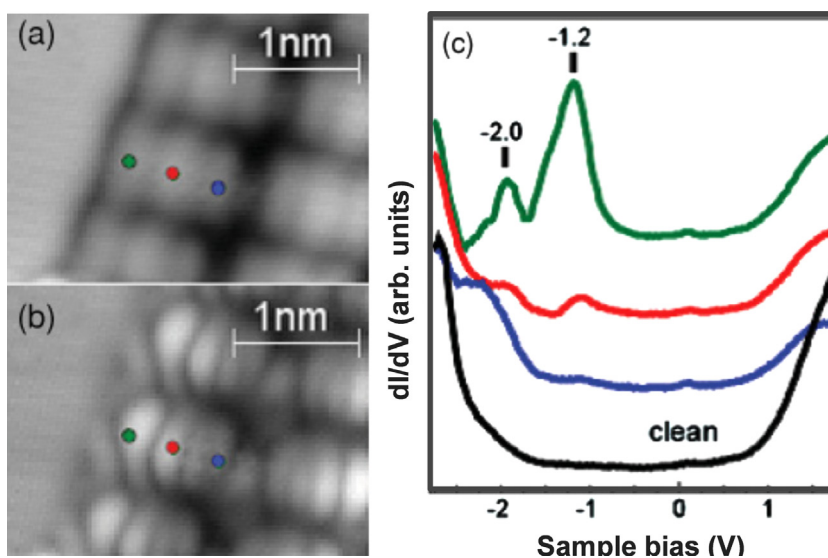


Fig. 25. a, b) Close-up STM image of F4-TCNQ at a lower step edge taken at a) 0.2 V (unoccupied states) and b) -1.2 V (occupied states). c) dI/dV spectra taken at different positions along the molecular axis of the TCNQ molecule. Reprinted with permission from Ref. [110], Copyright (2011) by the American Physical Society. <http://dx.doi.org/10.1103/PhysRevB.83.153403>.

network (see Ref. [113]), and with the silver adatoms coming from the surface steps. Contrary to what is observed for the clean surface (see the lower right inset), after TCNE adsorption the step looks very rough, with clear indication of loss of material. In this case, however, and contrary to the F4-TCNQ/Cu(111) case, no preferential direction is clearly observed after etching. But, like in the F4-TCNQ/Cu(111) case, the etching can also take place in the form of trenches perpendicular to the steps. In this case, however, no TCNQ molecules can be seen inside the trenches, which seems to indicate that the TCNE molecules have removed the silver atom from the upper terrace. Otherwise, the molecules would have to enter the trench all the way in and then diffuse out of it, which seems a very unlikely scenario. This assumption is further supported by the fact that in some occasions small vacancy islands can be observed inside the terraces far from the steps. Curiously enough, at room temperature the steps recover their original shape since there is a continuous atom diffusion along the steps [114], healing the damage caused by the molecular etching.

Another strong acceptor molecule is C_{60} (one of its derivatives, PCBM, is one of the materials most used in organic solar cells). On

most single-crystal metal surfaces C_{60} forms compact close-packed hexagonal overlayers, due to the predominance of the C_{60} - C_{60} van der Waals interaction over the C_{60} substrate-interaction, with the molecules separated by ~ 10 Å [115]. However, there is still a strong interaction with the metal substrates, which in some cases has been observed to lead to strong surface modifications. For example, on the more open Pt(110) and Au(110) surfaces, C_{60} adsorption leads to the disappearance of the (1×2) missing row reconstruction, while creating 2 atom vacancies [116,117]; on the other hand, on the more compact Ag(100) surface it creates 5 atoms holes [118]. It has been suggested that the degree of surface modification depends on the amount of charge transfer from the substrate. For example, C_{60} reconstructs the Ni(110) surface, but not the Cu(110) surface [119] (see Fig. 27). Although it has been shown that both in Cu(110) [120] and Ni(110) [121] there is charge transfer from the substrate to the molecule, in general C_{60} interacts more strongly with transition than with noble metals [121,122]. According to a simple model, the LUMO of the C_{60} molecule is closer in energy to the d band of Ni(110) than Cu(110), and thus the hybridization of the LUMO with the metal d states is stronger in this case [119].

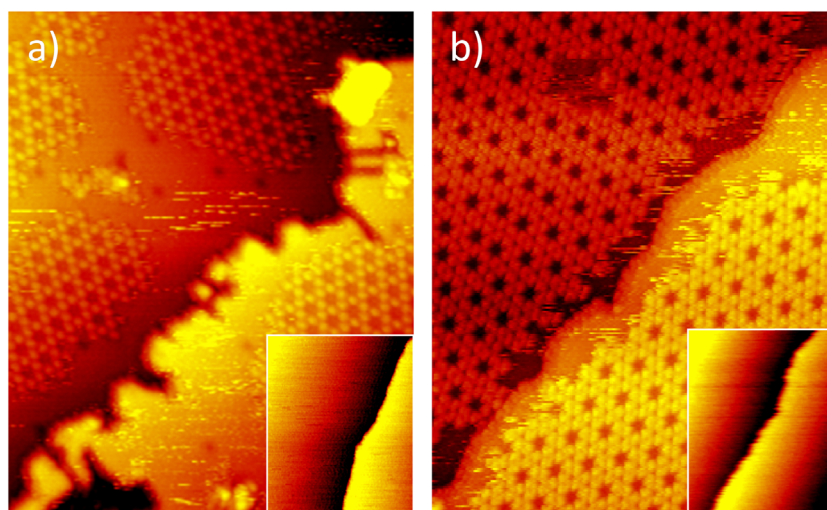


Fig. 26. STM images taken after depositing TCNE on Ag(111) a) at 150 K; b) 300 K. The STM images were taken at the deposition temperature. The insets show STM images of the clean Ag(111) surface taken a) at 130 K; b) 300 K. Reprinted from Ref. [108], with the permission of AIP Publishing.

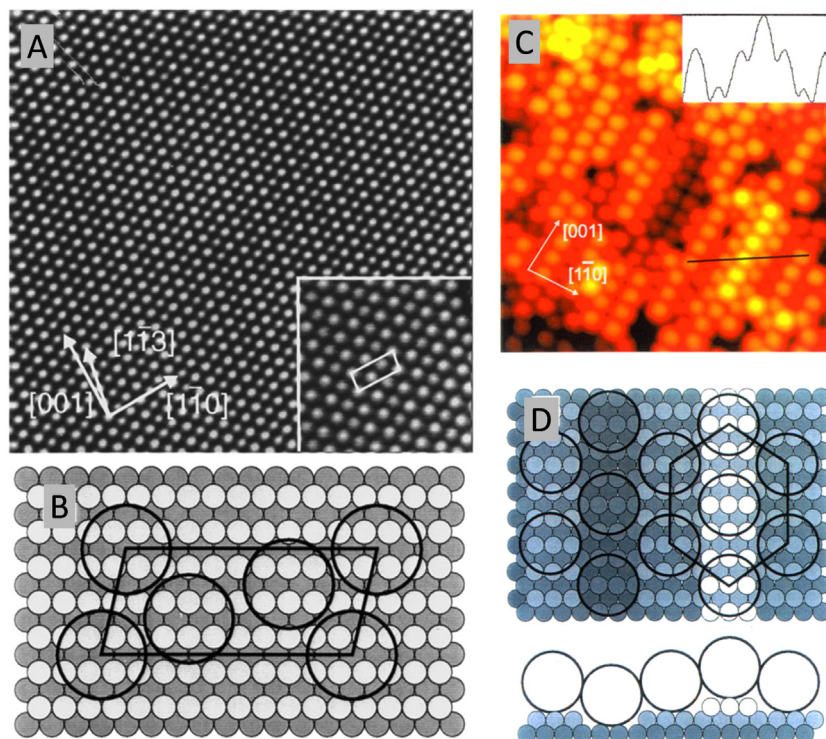


Fig. 27. a, b) STM image of C_{60} on Cu(110) after depositing at 470 K and the proposed geometric model. c, d) STM image of C_{60} on Ni(110) after depositing at 575 K and the proposed structural model. Reprinted with permission from Ref. [119]. Copyright (1997) by the American Physical Society. <http://dx.doi.org/10.1103/PhysRevB.55.9360>.

C_{60} even reconstructs close-packed metals surfaces, creating either 1 or 7 atoms holes: 1 atom hole for Pt(111) [123,124], Au(111) [125] and Ag(111) [126]; 7 atoms hole for Cu(111) [127]. This difference has been thought to depend on the lattice parameter of the substrate [128]: as the metal lattice constant increases, the 7-atom hole leaves a smaller number of metal atoms to participate in the metal-C bonding (see Fig. 28).

That charge transfer and surface reconstruction are intimately related was proved in Ref. [127]. Fig. 29 shows a C_{60} island on the Cu(111) surface created in a two steps process, by first depositing C_{60} at ~ 500 K, and then at ~ 250 K. The island created this way display core-shell structure, the core having a reconstructed interface and the shell an unreconstructed one. The surface reconstruction, as determined by LEED I-V analysis, consists of highly distorted top Cu layer, with 7 atoms holes in every (4×4) unit cell. STS spectra taken at 77 K on the unreconstructed surface showed that the LUMO was located ~ 0.75 eV above E_F , indicating a very small amount of charge transfer. However, in the core, reconstructed surface, the LUMO peak appears almost at the Fermi level, suggesting that $\sim 3 e^-$ are transferred from the substrate to the molecule.

In conclusion, we have described a few examples where charge transfer is responsible, or maybe better, goes hand in hand with both molecular and substrate distortions, but there is a increasing number of systems where these effects are being reported [29,129–133].

4. Catalytic roles of charge-transfer at organic/inorganic interfaces

The fact that the exchange of charge between the molecular orbitals of a molecular adsorbate and the band states of the substrate plays a major role in determining the chemical fate of the molecules upon adsorption has long been recognized in the field of Surface Science [134–137]. For example, while the adsorption of CO on early transition metals surfaces leads to molecular dissociation, the molecule adsorbs intact on late transition metals [136]. This fact can be rationalized as due to the different degrees of filling of the d bands. CO interacts with transition metal surfaces via the well-known Blyholder or donation/backdonation mechanism [137]. In this mechanism the bonding between the CO

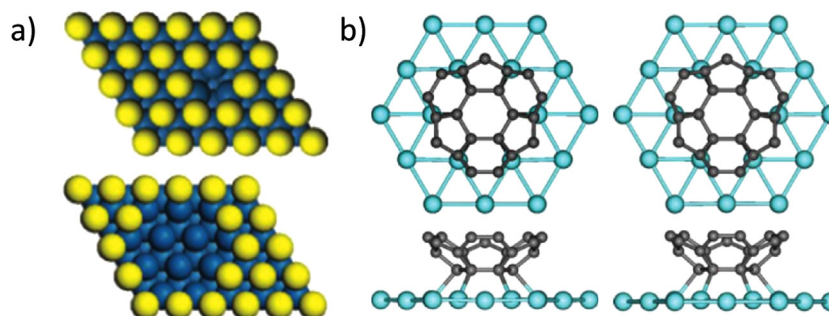


Fig. 28. a) Structural models of the 1- and 7-atoms holes. b) Calculated adsorption geometry of C_{60} on the 1-atom model of Pt(111) for two different unit cells. Reprinted with permission from Ref. [128]. Copyright (2012) by the American Physical Society. <http://dx.doi.org/10.1103/PhysRevB.85.075421>.

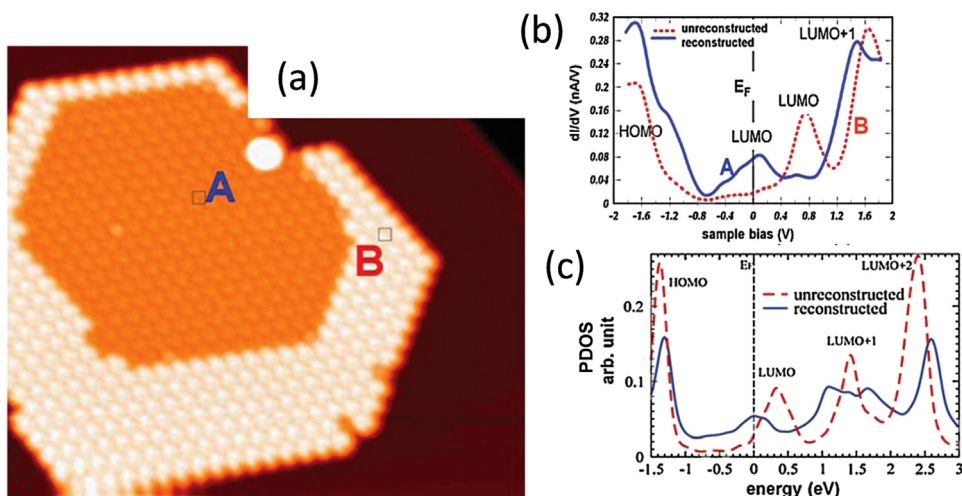


Fig. 29. a) A C₆₀ island on Cu(111) created in a two steps process. The core has a reconstructed interface, but the shell has not. The inset shows that there is no energy gap at T=5 K. b) dI/dV spectra taken on both regions of the island. On the unreconstructed area the LUMO seems completely empty, but in the reconstructed area it is partially occupied. c) Projected DOS calculated for both the reconstructed and the unreconstructed surface. Reprinted with permission from Ref. [127]. Copyright (2009) by the American Physical Society. <http://dx.doi.org/10.1103/PhysRevLett.104.036103>.

molecules and the metallic surface involves two different processes: first, the 3σ HOMO of CO interacts with empty d_{z^2} orbitals of the metal surface, thereby donating electrons from the molecule to the surface; second, the interaction between the filled d_{xy} and $d_{x^2-y^2}$ states of the sample and the $2\pi^*$ LUMO of the CO molecule leads to the backdonation of electrons from the surface to the molecule. Early transition metal surfaces have the center of the d-band quite high in energy, possibly higher than the Fermi level and, thus, at an energy quite close to that of the $2\pi^*$ LUMO of the CO molecule. The hybridization between the d-band of the surface and the $2\pi^*$ LUMO of the CO molecule, thus, leads to the formation of bonding and an antibonding states between the surface and the molecule, with a rather large energy splitting due to the similarity between the energies of the original states at the surface and the molecule. Such large splitting pushes the metal-molecule hybrid bonding state below the Fermi level of the metal surface, which is thus populated. The population of the bonding state between the surface and the CO molecule leads thus to a population of the intramolecular $2\pi^*$ LUMO state, which facilitates dissociation. On the other hand, moving to the right in the d-block of the periodic table makes the d-band center move lower in energy. The interaction is weak and hybrid metal-molecule states do not form. Thus population of the $2\pi^*$ LUMO of the CO molecule does not occur and the molecule adsorbs intact, without dissociation [136].

The interest in chemical reactions at solid surfaces has been recently renewed due to the realization that relatively complex organic molecules can actually be covalently interconnected on solid surfaces, leading to relatively well-ordered 2D polymers and oligomers [138–141]. Such products are very challenging to obtain by standard synthetic procedures without the templating role of a solid surface and, thus, expectations of scalable methods of production based on this novel “on-surface synthesis” procedures have been rising over the last decade. Most of the available literature discusses chemical reactions which are relatively well-known from solution phase [139,140,142–147]. However, an increasing number of examples of reactions taking place on solid surface without a known solution counterpart is appearing [38,148,149]. Moreover, investigations on the mechanisms of even those reactions which are not exclusive from solid surfaces reveal that they may be fundamentally different when occurring on a solid surface [138,150]. Given the previous knowledge on the chemical reactions of small molecules on surfaces, it might be expected that electronic effects could play a major role to

understand the chemistry of more complex organic adsorbates. Moreover, as we discussed in the previous sections, charge-transfer during the adsorption of donor or acceptor molecules on solid surfaces leads to important structural changes which might also affect the reactivity of the adsorbates. However, the electronic factors determining the reactivity of organic molecules have not been considered in depth so far. In this Section we will study some examples in which a relation between charge-transfer and chemical reactivity has been claimed or suggested.

4.1. Isomerization reactions

A chemical process by means of which a molecule in an initially stable state changes to a final stable state characterized only by a different geometrical distribution of the atoms or functional groups of the molecule, is known as an isomerization reaction, and each one of the stable states is an isomer of the molecule. Isomerization reactions have attracted much attention in the last 20 years, especially when they can be triggered by external stimuli (light, voltage pulse, etc.), since they could eventually act as a switch for molecular electronic devices [151].

Isomerization reactions have been observed to take place in molecules adsorbed on solid surfaces [151], whether the reactions have been externally triggered by light [152–154] or by the tip of the STM [155–157], or just thermally induced [43,158,159]. For example, inelastic tunneling current was used to induce tautomerization reactions on substituted chlorobenzene adsorbates, where the relative position of halogen atoms around the periphery of the benzene ring could be successfully modified [160].

However, the most studied isomerization reaction for molecules adsorbed on solid surfaces is the cis-trans isomerization of azobenzene derivatives [153,155,157,159]. Azobenzene molecules consist of two phenyl rings linked together via a double N=N bond (Fig. 30). The two phenyl rings could thus sit both at the same side of the N=N bond (cis-isomer), or in different sides (trans isomer). In general the trans isomer is energetically favorable compared to the cis isomer, among other reasons due to steric hindrance between the phenyl rings in the cis conformation, and the concomitant loss of planarity of the molecule. Two mechanisms have been proposed for the observed isomerization reaction, a rotation of the phenyl plane with respect to the N=N double bond, or an in-plane bending of the phenyl moiety (a process called inversion, see Fig. 30)). In both cases, the transition state can

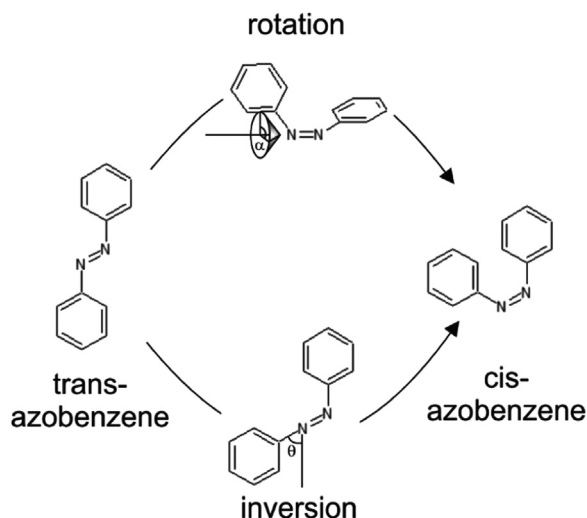


Fig. 30. Isomerization of azobenzene can proceed either by rotation around the N=N bond or by in-plane bending (inversion) of the phenyl bond.

only be reached by supplying a significant amount of energy (about 1.8 eV for the cis→trans reaction), which confers the bistability condition to azobenzene molecules. Azobenzene molecules have attracted much attention, since both the trans→cis and cis→trans reactions can be externally addressed by light with different wavelengths.

Cis-trans isomerization reactions in adsorbed azobenzene derivatives have been described in the literature [155–157,159] (see Fig. 31). The efficiencies found for these processes were however low: in particular, for those molecules excited by light, where direct comparison with solution-based photochemistry is possible, the efficiency was found to be about 50 times lower in adsorbed chemical species, even for azobenzene derivatives with bulky peripheral groups attached to the azobenzene core to separate it from the substrate, thereby minimizing molecule-substrate interactions [152]. The deactivation of the cis-trans isomerization activity for adsorbed molecules was attributed to three possible causes: a)

Steric hindrance from the surface, which would preclude rotations out of plane; b) Limited lifetime for the excited states, due to ultrafast deexcitation of the electron to the surface; c) Changes in the optical absorption of the molecules upon absorption, due to hybridization of the molecular orbitals and the electronic states at the surface. All three explanations assume that the structural change does not take place because of the existence of a rather large energy barrier between reactants and products (case a), because of a short lifetime of the excited state (case b) or because of an inadequate choice of the radiation wavelength (case c) [152].

An intriguing alternative model to explain the low efficiency of isomerization reactions was recently suggested based on state-of-the-art DFT calculations including dispersive interactions [161]. According to this work, the trans→cis reaction might actually not be suppressed for the adsorbed molecules, but if the energy barrier for the reverse cis→trans reaction is too low, the system would quickly relax to the low energy trans configuration, precluding the observation of the cis isomer as the stable reaction product. In a sense, the role of the surface would not be that of making the transition more difficult, but rather eliminating the bistability condition of the molecules to act as switches on the surface. More precisely, the calculations show that the energy barrier for the trans→cis reaction is about 0.6 eV lower for azobenzene molecules adsorbed on a Ag(111) surface than in the gas phase (see Fig. 32a). The lowering of the energy barrier, along with a destabilization of the high-energy cis isomer of about 0.2 eV renders the barrier for the cis→trans reaction of the order of 0.1 eV (compared with about 1 eV in the gas phase). That is, the cis isomer might actually be formed upon light irradiation, but it would not be stable enough to be observed after the excitation has been removed.

The change in the energy landscape described above can be rationalized in terms of charge-transfer between the azobenzene molecules and the Ag(111) surface in the transition state for a rotation mechanism. The relative rotation of the phenyl planes with respect to the N=N double bond can only occur by weakening this double bond, which is energetically costly in gas or solution phases. However, in the presence of the metallic surface, the breaking of the double bond can actually be compensated by

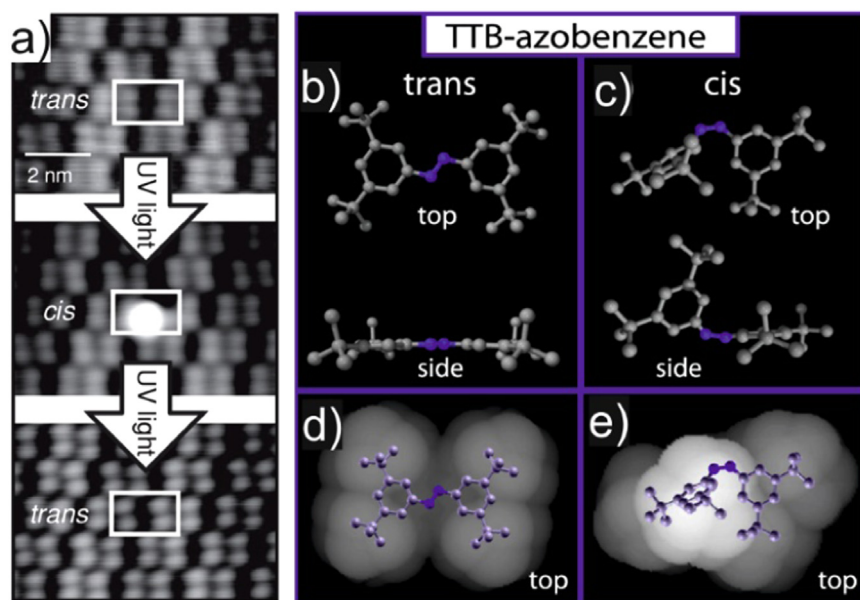


Fig. 31. Photoisomerization of tetrabutyl-azobenzene (TTB-azobenzene) on Au(111). a) STM images revealing the modifications in the shape of the TTB-azobenzene molecules upon UV irradiation. b) and c) top and side views of the relaxed molecular conformations for trans and cis isomers. d) and e) top view of the constant LDOS isosurfaces for trans and cis isomers [152]. Reprinted with permission from [152]. Copyright 2007 by the American Physical Society. <http://dx.doi.org/10.1103/PhysRevLett.99.038301>.

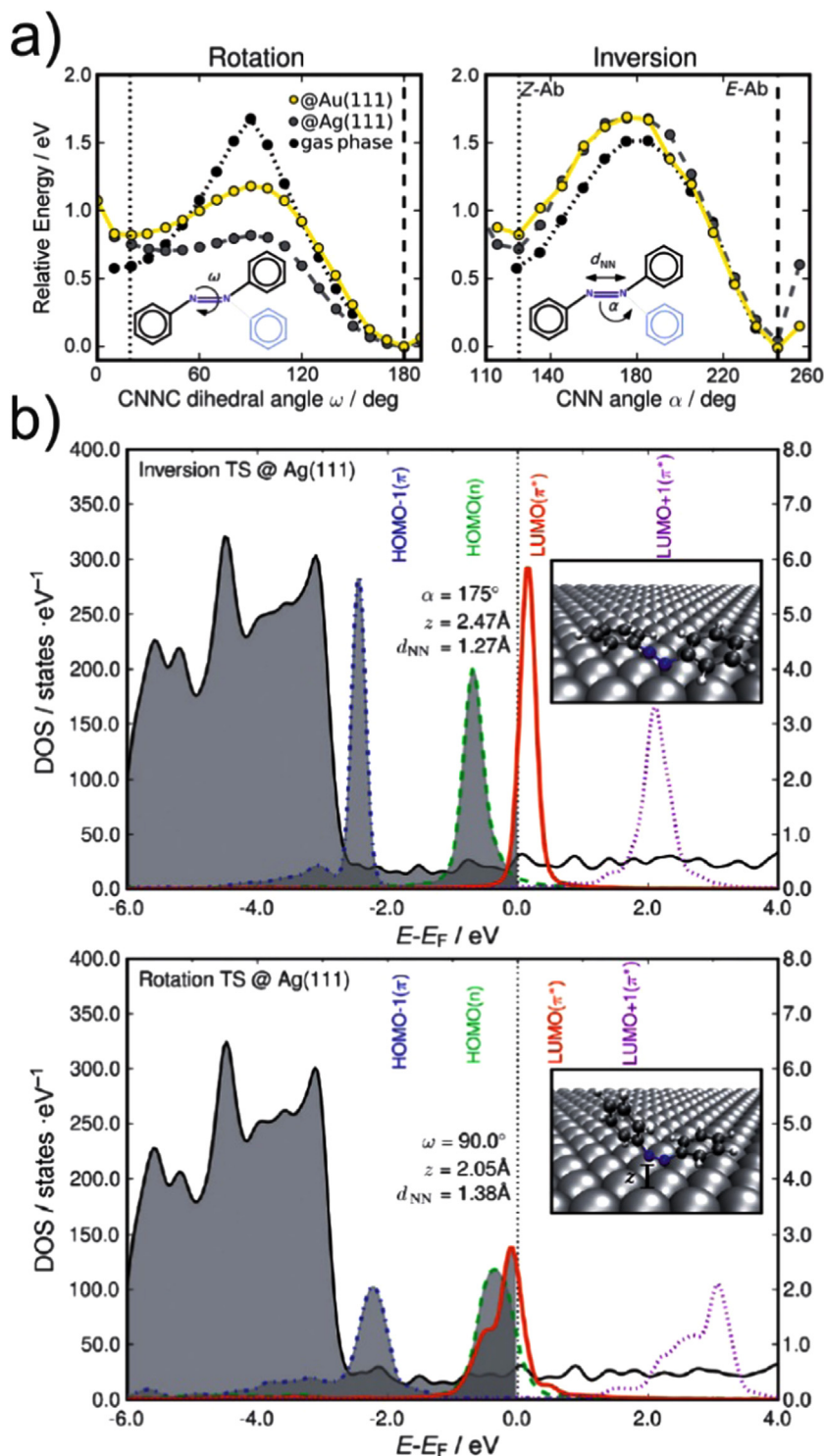


Fig. 32. a) Potential energy landscapes for the isomerization of azobenzene in the gas phase (black dots), adsorbed on Au(111) (yellow dots) and Ag(111) (grey dots), through a rotation (left panel) or an inversion (right panel) mechanism. b) Calculated LDOS for a molecule in the inversion (upper panel) or rotation (lower panel) transition states on Ag(111), showing that the LUMO is completely occupied for the molecule in the transition state of the rotation mechanism [161]. Reprinted with permission from [161]. Copyright 2012 by John Wiley and Sons. <http://dx.doi.org/10.1002/anie.201205718>. (For interpretation of the references to color in this figure legend, the reader is referred to the web version of this article).

forming new covalent bonds to the Ag(111) surface. The formation of such bond implies the transfer of electrons from the surface to the N atoms in the azo group, so that the LUMO of the molecule is now almost completely occupied (see Fig. 32b). Charge transfer is thus ultimately responsible for the stabilization of the transition state and the concomitant destabilization of the cis final product. This interpretation is also supported by comparison with the

situation in which azobenzene molecules are adsorbed on a Au (111) surface. The higher work function of the Au(111) surface makes it more difficult to transfer electrons to the nitrogen atoms of the azo group, which again destabilizes the transition state and, thus stabilizes the cis isomer. This might be the reason why cis-trans isomerizations have been reported for azobenzene molecules adsorbed on Au but not on Ag.

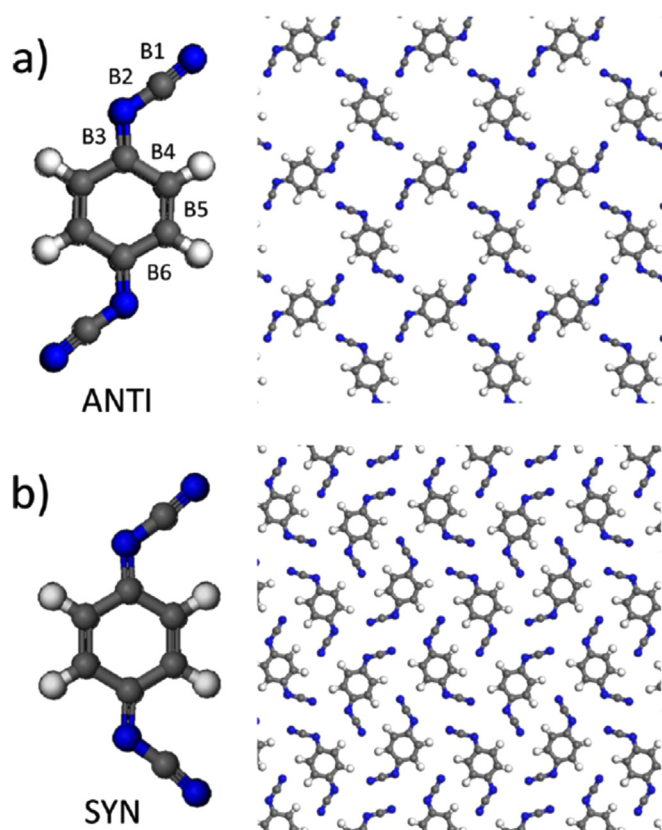


Fig. 33. Chemical structure and DFT calculated minimum energy self-assembly of free-standing monolayers of (a) anti- and (b) syn- DCNQI. Reprinted with permission from [43]. Copyright 2014 American Chemical Society. <http://dx.doi.org/10.1021/jp508458y>.

These results suggest that isomerization reactions could actually be not only not hindered but even promoted by charge-transfer upon adsorption on metal surfaces. In this framework, the key issue would be the choice of a molecule with two very symmetric isomeric states, especially on the surface. This was recently described in the system dicyano-*p*-quinodiimine (DCNQI) adsorbed on a Cu(100) surface [43]. DCNQI consists of a quinoid ring with two imine groups at both ends attached to cyano groups [162]. As shown in Fig. 33, the cyano groups can sit both of them at the same side of the quinoid symmetry axis (syn isomer) or on opposite sides of such axis (anti isomer). The anti isomer is slightly more stable than the syn isomer due to electrostatic repulsion between the electronegative cyano groups, but the molecule does not lose planarity, which might be expected to facilitate a similar binding between the substrate and both isomers [163,164]. Moreover, well-ordered 2D structures can be constructed for both isomers, with slightly different aggregation energies and a symmetry that reflects the different symmetries of both isomers: while the network of the anti isomer would have a C₂ symmetry axis, this would be absent for the syn isomeric form (See Fig. 33).

The mechanisms proposed for the anti-syn isomerization reaction in solution or gas phase are very similar to the ones described above for the cis-trans isomerization of azobenzenes: the lowest energy transition state (0.6 eV) is achieved by an inversion of the cyano group, but a rotation of the cyano with respect to the quinoid axis is also possible [163]. The charge state of the molecule should also be important for the isomerization barrier. DCNQI is a very strong organic acceptor, due to the strong electronegativity of the imine and cyano nitrogen atoms, but also due to the aromatization of the quinoid ring upon electron capture. This aromatization leads also to the weakening of the B3 double bond to

the iminic nitrogen which, in turn, facilitates the rotation of the cyano group.

Upon deposition of DCNQI on Cu(100), two different networks can be observed on the surface depending on whether the deposition is carried out with the substrate held below 100 K or at RT [43] (see Fig. 34). Whereas the low temperature phase has the expected symmetry for the assembly of the anti isomer, deposition at RT leads to more compact network consistent with the syn isomeric form. STM images also reveal different shapes for the individual molecules in the LT and RT phases, being more symmetric for LT, while they have a “croissant” shape in the RT phase. If the deposition is carried out at LT and the sample is later heated to about 250 K, the LT phase islands can be observed to disappear from the surface, while RT islands nucleate and grow. This implies that the isomerization reaction takes place only when the molecules are in the form of diffusing monomers, while intermolecular interactions prevent isomerization in the ordered islands. Thus, the isomerization process should be fast enough to occur at least once during the diffusion and nucleation process of the RT phase. This diffusion time can be estimated from the statistical analysis of island density and size as a function of the coverage, yielding $(4 \pm 3) \times 10^{-2}$ s. If the isomerization barrier were unaffected by the presence of the surface, the average time in between two isomerization events would be about 1000 times longer than this value and, thus, the molecules would be unable to change their isomeric form before attaching to the RT phase islands. This observation demonstrates that the surface not only does not hinder the isomerization reaction, but actually promotes it, as suggested by the previous theoretical calculations.

The theoretical analysis helps in finding the reasons for the observed promotion of the isomerization process upon adsorption. As we had anticipated based on the molecular architectures, both anti and syn isomers adsorb on Cu(100) with very similar geometries: the cyano bonds rotate slightly towards the surface to enable the bonding to copper atoms of the substrate. The quinoid ring is however kept planar by dispersive interactions. The transition state for the rotation of the cyano group is thus stabilized by bonding with the surface, and the transfer of electrons from the surface to the molecule.

4.2. Bond breaking and bond making

While isomerization reactions are important to implement the switching functionality of adsorbed organic molecules, most of the interest in the chemical reactions that organic adsorbates undergo on solid surfaces is related to the possibility to synthesize well-ordered 2D polymers, that is, to replace the relatively weak and labile non-bonding interactions in self-assembled monolayers for more robust covalent bonds [138–141]. Many different reactions have been successfully explored to covalently link organic adsorbates, such as for example the Ullmann coupling reaction [165,166], boronic acid condensation [142,145], polyester condensation [167], Glaser coupling [147], Huisgen cycloadditions [168], imine [146,169] and Schiff base [170] formation, etc. Moreover, a number of novel reactions, with no definite counterpart in solution or gas phases have found to occur at solid surfaces, such as the dehydrogenation and direct coupling of porphyrins [149] or alkanes [148].

The precise mechanisms for these reactions depend of course on the nature of the organic adsorbate and the solid surface, and in many cases are still not fully understood. In any case, all of them share at least two steps: one in which an internal bond in the adsorbate is cleaved, yielding radical intermediates which may be stabilized by bonding to the surface or to metal adatoms, and a second step in which the radicals can meet and recombine to form a new molecular species resulting from the covalent linkage of the

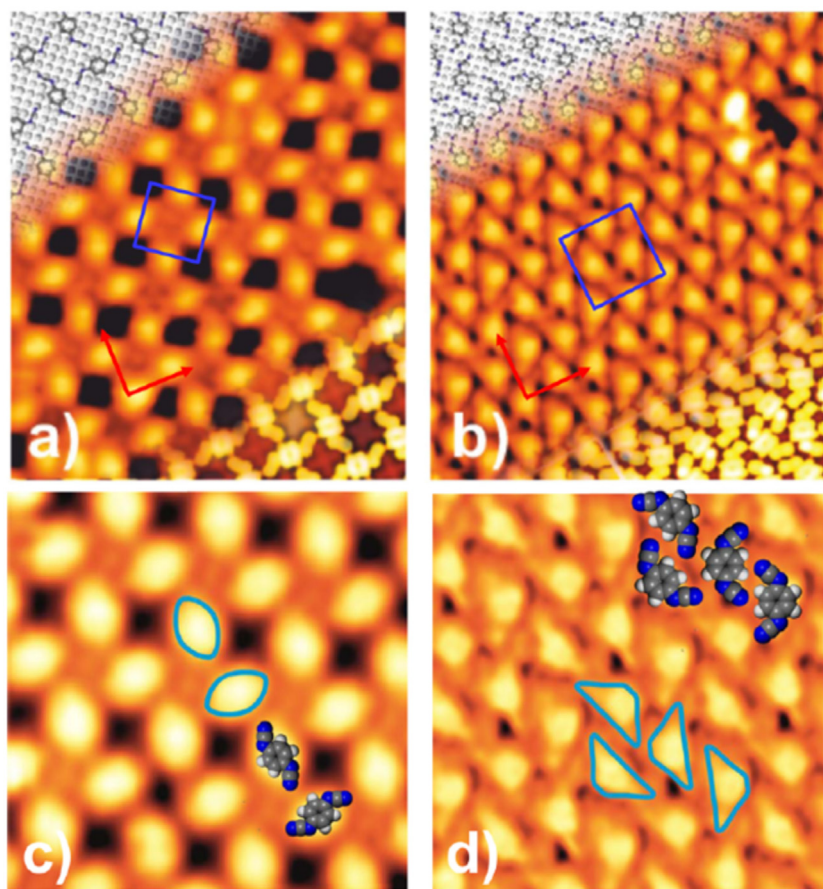


Fig. 34. (a,b) STM images ($90 \text{ \AA} \times 100 \text{ \AA}$) taken after depositing DCNQI on Cu(100) (a) with the substrate at 145 K ($V_b = -1.0 \text{ V}$, $I_t = -0.21 \text{ nA}$; the image was taken at 235 K); (b) with the substrate at room temperature ($V_b = -1.24 \text{ V}$, $I_t = -0.48 \text{ nA}$; the image was taken at room temperature). Top left corners show the calculated optimized structures of a monolayer of DCNQI molecules in the (a) anti and (b) syn configuration on the Cu(100) surface. Bottom right corners show the corresponding simulated STM images. The blue squares indicate the respective unit cells, while the red arrows show the high symmetry directions of the copper surface. (c, d) Higher resolution images showing the difference in the apparent shape of the molecules. The shapes (marked with a light blue line) strongly resemble the (c) anti isomer for the LT phase and (d) the syn isomer for the RT phase. Some CPK molecular models have also been added for clarity. Reprinted with permission from [43]. Copyright 2014 American Chemical Society. <http://dx.doi.org/10.1021/jp508458y>. (For interpretation of the references to color in this figure legend, the reader is referred to the web version of this article.)

reactants [150]. Obviously, the weakening of the intramolecular bonds and the stabilization of the resulting radicals are related to the hybridization of the molecular orbitals in the reactant and intermediate radical with the electronic states of the surface. This line of research, however, has not been fully explored so far, and most of the theoretical approaches aim at calculating energy barriers and transition states without a rationalization in terms of electronic structure considerations [150]. We expect that achieving full control over the polymerization processes taking place at solid surfaces requires that these considerations are properly accounted for.

Recently, more complex roles for charge-transfer in steering the chemistry of adsorbed organic molecules on metal surfaces have been described [38]. 15,15,16,16-tetracyano-6,13-pentacene-*p*-quinodimethane (TCPQ) is a strong organic acceptor from the TCNQ family, consisting basically of a TCNQ moiety with two naphthalene units fused at both sides of the quinoid ring [171–173]. In the gas phase, steric repulsion between the naphthalene units and the cyano groups leads to a saddle conformation in which the dicyanomethylene groups and the aromatic rings fold in opposite directions. Upon adsorption on the Cu(100) surface the molecules accept about one electron from the surface (judging by XPS experiments and DFT calculations), which has important consequences for their conformation. As in the TCNQ case, the extra electron is delocalized in the dicyanomethylene ends, changing the character of the bond to the quinoid ring (B3) from

double to single, and aromatizing the central ring (see Fig. 35a). The aromatization of the central ring leads to the formation of a rather rigid and flat pentacene moiety along the long symmetry axis of the molecule, and the stress due to steric hindrance is relieved not by folding the dicyanomethylene ends away, but rather by twisting them with respect to the short axis of the molecule (which is also facilitated by the new single character of the B3 bond). In this conformation, bonding to the surface occurs only via two of the cyano groups, whereas the other two cyano groups point away from the surface. This picture is supported by DFT calculations including vdW corrections, and the good agreement of the calculated STM images with the experimentally obtained ones (Fig. 35 b and c). Such images consist of an elongated dim protrusion corresponding to the pentacene moiety, with two bright lobes on the side corresponding to the dicyanomethylene groups. Notice that, while the four cyano groups are perfectly equivalent in the gas phase configuration, upon adsorption on Cu(100) the two cyano groups in contact with the surface will behave differently as those pointing away.

Annealing of the sample to relatively moderate temperatures (above 380 K) leads to important modification of the STM images (Fig. 36): While the pentacene moiety does not change significantly before and after annealing, the bright protrusions corresponding to the dicyanomethylene ends are suppressed, and only a relatively small lateral feature can be identified. Annealing to 490 K shows that the reaction is now complete: all the

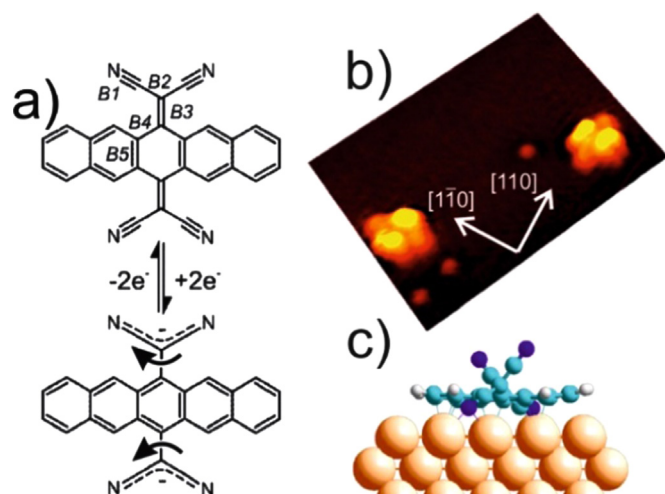


Fig. 35. a) Chemical structure and bond distribution for neutral and charged TCPQ. b) STM ($6.3 \times 4.4 \text{ nm}^2$) images of isolated TCPQ molecules on the Cu(100) surface ($V_b = -0.83 \text{ V}$, $I = 0.64 \text{ nA}$). c) Side view of the relaxed conformation of TCAQ on Cu(100) showing that the dicyanomethylene end groups are rotated around bond B3, consistent with charge-transfer from the metallic substrate. Reproduced from Ref. [38] with permission from The Royal Society of Chemistry.

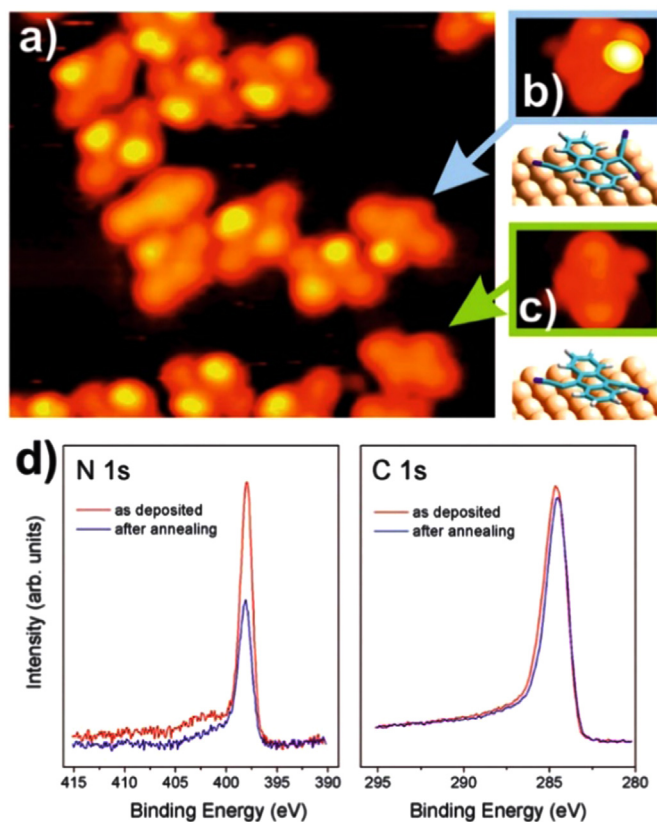


Fig. 36. (a) STM image ($9.5 \times 6.8 \text{ nm}^2$) of 0.5 ML of TCPQ deposited at room temperature on a Cu(100) surface followed by annealing to 380 K. Molecules can now be found which have lost either one (blue arrow) or two (green arrow) bright lobes. (b, c) Calculated relaxed geometries for the surface-stabilized radicals resulting from the elimination of one (b) or two (c) cyano groups from the TCAQ molecule, and the corresponding calculated STM images. (d) X-Ray photoemission spectra ($h\nu = 1468 \text{ eV}$) of the N1s (left) and C1s (right) core levels before (red line) and after (blue line) the annealing to 490 K. Reproduced from Ref. [38] with permission from The Royal Society of Chemistry. (For interpretation of the references to color in this figure legend, the reader is referred to the web version of this article.)

molecules have lost their two bright protrusions and complementary measurements with XPS reveal that half of the nitrogen is lost, together with about 10% of the C1s signal intensity.

These results show that the molecules are undergoing a selective decyanation reaction, where half of the cyano groups are lost while the other two cyano groups remain on the surface. Moreover, annealing at temperatures in excess of 490 K leads to the formation of covalently bonded oligomers, whose nature is not fully clear.

Notice that the fact that only two cyano groups are lost is related to the asymmetry between the up- and down-cyano groups which, in turn, is the result of the charge transfer between the adsorbate and the molecule. We expect this kind of situation to be common for relatively complex organic donors and acceptors deposited on metal surfaces, and progress in the field of “on-surface synthesis” to be coupled with our understanding of the fine details of the electronic interactions between organic adsorbates and solid surfaces.

5. Intermolecular versus molecule-substrate charge transfer: charge-transfer complexes at solid surfaces

As described in the Introduction, blends of organic acceptors and donors have been in the spotlight for a few years due to their key role as active elements in optoelectronic organic devices [1,3,6]. For example, in Bulk Heterojunction Solar Cells, the interfaces between electron donating areas and electron accepting areas are the active sites for exciton dissociation, a necessary process to generate electrical currents by light irradiation [3,6]. The fact that excitons can only travel a finite distance before electron-hole recombination (the exciton diffusion length), implies that the donor and acceptor domains must be generally smaller than the average exciton diffusion length, i.e. of the order of about 10 nm, and in order to avoid charge-carrier trapping, they must be connected to the electrical leads. The importance of the nanoscale morphology of donor/acceptor blends has been highlighted in many different publications, and the search for new growth methods that would optimize the morphology of the organic layer for photovoltaic performance is a very active topic of research [6].

Most of the works addressing the issue of nanoscale morphology of donor/acceptor blends have used solution-based processing to fabricate the organic films, as a scalable and cheap production method. While significant progress has been achieved in this field, the degree of control over the film morphology is limited, and in most cases globular donor and acceptor domains are obtained, without electrical connectivity to the leads, which limits significantly the device efficiency [6]. In a more traditional Surface Science approach, the fabrication of mixed donor-acceptor blends by vacuum sublimation of the organic material was also shown to be a powerful method to fabricate efficient photovoltaic devices [174]. Moreover, the submonolayer-thick films that can be obtained by the method are well suited for investigations using traditional analysis techniques such as STM or XPS. In this section we will describe some important aspects of the structure of such films, including recent reports on the variations in adsorption heights upon coadsorption of donors and acceptors (Section 5.1).

On the other hand, the coexistence of electron donating and accepting species on a metal surface that can act as an electron reservoir, naturally raises the question of the balance between intermolecular versus molecule-substrate charge transfer. This question has been addressed by using spectroscopic techniques to characterize the electronic structure close to the Fermi level (UPS, STS) [30,32,33,35,175–177], but the multiplicity of the states, the broad character of the peaks and the possibility for hybridization of the orbitals hinders a direct interpretation of the results [33]. Core-level Spectroscopy (XPS), and in particular the evolution of the chemical shifts with the donor/acceptor ratios, has also been exploited to characterize the charge state of the organic

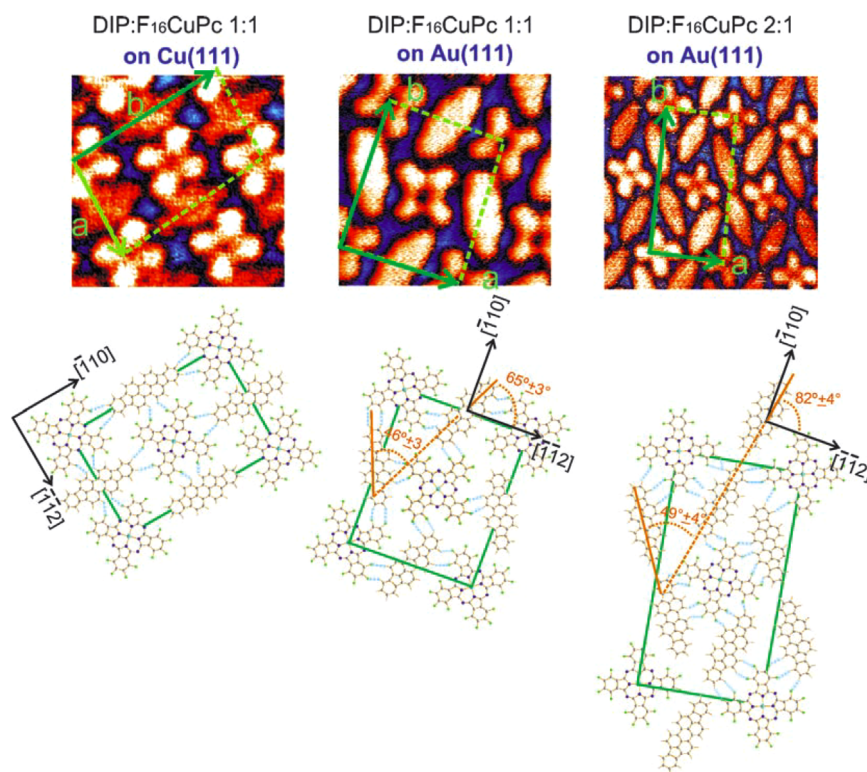


Fig. 37. STM images (upper row) and molecular models (lower row) for the self-assembled monolayer formed by codeposition of di-indenoperylene (DIP) and perfluorinated copper phthalocyanine (F_{16} -CuPc) on Au(111). Reprinted with permission from [178]. Copyright 2007 by John Wiley and Sons. <http://dx.doi.org/10.1002/cphc.200700494>.

adsorbates, although some care is required to correctly interpret these results [32,33]. These issues will be thoroughly discussed in Section 5.2.

5.1. Structure of donor/acceptor mixtures on solid surfaces

Codeposition of organic donor and acceptor molecules on solid surfaces leads very often (especially for planar molecules) to the existence of ordered networks including both species. It is common to find ordered domains with different stoichiometric donor/acceptor ratios depending on the relative amounts of donor and acceptor molecules deposited on the surface [8,30,178–181] (see Fig. 37). In these cases, it has been reported that the order of deposition does not significantly affect the final structures, suggesting that the assembly is driven mainly by thermodynamic rather than kinetic factors. It is interesting to notice that there are very few examples in which segregation of pure donor and acceptor domains occur [182], even for molecules without complementary functional groups in the periphery of the molecular backbone which could make energetically favorable the formation of hydrogen bonds between different molecular species. The tendency to mix could be related to electrostatic dipole-dipole interactions. Charge transfer from the donor to the surface or from the surface to the acceptor should lead to dipoles with opposite orientations, and the electrostatic energy would be thus minimized by arranging both dipoles in a common network rather than separate domains of dipole up and down regimes. This mechanism would actually explain some interesting observations about the adsorption and self-assembly of TTF and TCNQ on Au(111) surfaces [30,44,71]. TTF alone does not form islands on the surface, but the molecules adsorb as isolated entities in the fcc areas of the reconstruction, separated by rather large distances (of the order of 2–3 nm depending on the coverage) [44]. In line with our previous discussion, this was explained as intermolecular repulsion due to transfer of about $0.6e^-$ from the molecule to the metal surface,

corresponding to the donating character of TTF [44]. However, when deposited together with the acceptor TCNQ, well ordered 1:1 mixed domains could be found, with intermolecular distances of about 1 nm, even though the total coverage was far from the monolayer, and bare Au(111) areas were abundant [30]. A word of caution is however necessary in applying this argument, since other specific intermolecular or substrate-mediated interactions could play a more important role in determining the final structure of the mixed layer. Actually, for a 1:1 TTF:TCNQ network on Au(111), the structure revealed in STM images is that of alternated rows of TTF and TCNQ molecules. If dipole-dipole interactions were the only driving force in this assembly, one should rather expect a checkerboard configuration, which is not observed.

Segregation between donor and acceptor regions has been observed, for example, in the case of the non-planar organic donor 2-[9-(1,3-dithiol-2-ylidene)anthracen-10(9H)-ylidene]-1,3-dithiole (exTTF) mixed with phenyl-C61-butyric acid methyl ester (PCBM) on a Au(111) surface [182] (see Fig. 38). exTTF self-assembles into molecular rows along specific directions of the surface, forming a well-defined angle (about 10°) with the reconstruction lines [62]. exTTF islands have the shape of strips elongated in the direction of the reconstruction elbow sites, and as they grow, they push the elbows away to make room for their assembly. This adsorption-induced surface reconstruction, along with the lack of strong direct intermolecular interactions that could explain the formation of molecular rows, suggest that the surface deformation is playing an active role in mediating the interactions between the exTTF adsorbates. PCBM, on the other hand, forms different self-assembled structures depending on the coverage, which can be explained as the joint effect of vdW interactions between the fullerene moieties, the formation of weak hydrogen-bonds between the ester chains, and the templating effect of the Au(111) surface reconstruction, revealing a much weaker interaction with the metal surface [20]. When exTTF and PCBM are codeposited on the Au(111) surface, exTTF is observed to form stripped islands, identical in structure and

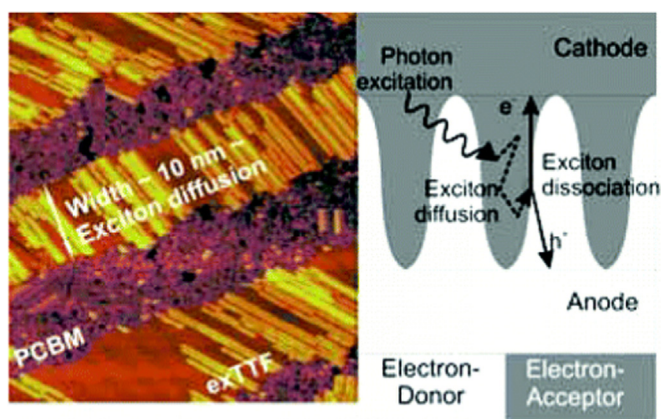


Fig. 38. STM image (left panel) showing the segregation of exTTF and PCBM on Au (111). The final morphology is similar to that identified as ideal for the efficiency of bulk heterojunction solar cells (right panel). Reprinted with permission from [182]. Copyright 2007 American Chemical Society. <http://dx.doi.org/10.1021/nl070897z>.

morphology to those found in the absence of PCBM. PCBM, on the other hand, forms disordered arrays similar to those found for coverages close to the full monolayer in the absence of exTTF, but constrained to the stripes that are not occupied by exTTF (see Fig. 38). It would thus appear that the segregation of exTTF and PCBM is related to the strong reshaping that the adsorption of exTTF produces when in contact to the Au(111) surface, thereby creating a substrate-mediated intermolecular interaction which is attractive for other exTTF molecules but not for PCBM. Notice, however, that the final morphology of the film can be described as a lateral superlattice of electron donor and acceptor species, which was previously identified as optimal for the performance of Bulk Heterojunction Solar Cells [182].

Interestingly, the adsorption geometry of the individual donor and acceptor species has been reported to change when the mixed layers are formed. In the example of TTF-TCNQ on Au(111), individual TTF molecules were shown to adsorb with an angle of 8° between the molecular plane and the surface, in order to maximize the covalent interactions between the lone pair electrons at the sulfur atoms and the gold atoms at the surface, and the distance between the molecule and the substrate was calculated to be 2.76 \AA [44]. However, when TTF molecules are embedded in mixed layers with TCNQ, their molecular backbone sits parallel to the Au (111) plane, at a larger distance of 3.1 \AA [30].

The variation in adsorption height with the formation of mixed donor-acceptor layers has been recently demonstrated by Normal Incidence X-ray Standing Wave (NIXSW) experiments (see Fig. 39) [35,177]. The investigated molecules were copper phthalocyanine (CuPc, donor) and 3,4,9,10-perylene tetracarboxylic dianhydride (PTCDA, acceptor) deposited on Ag(111). Individual PTCDA molecules are adsorbed in a non-planar geometry, with the carbonyl oxygen atoms bent towards the surface at a distance of 2.66 \AA , and the central aromatic moiety being planar and parallel to the surface, at a distance of 2.86 \AA . CuPc is naturally a non-planar molecule due to the mismatch between the size of the Cu atom coordinated at the central position, and the size of the cavity left by the central isoindole nitrogens, which leads to a conical shape with the copper atom not in the same plane as the phthalocyanine plane. The distance between the copper atoms and the surface (3.02 \AA) is thus shorter than the average distance between the carbon atoms and the surface (3.08 \AA). Notice that PTCDA molecules sit closer to the surface than CuPc, revealing a stronger interaction between PTCDA and Ag(111). Codeposition of PTCDA and CuPc on Ag(111) leads to ordered mixed arrangements which significantly different adsorption heights: the aromatic moiety of PTCDA is now farther apart from the surface (3 \AA) but the average

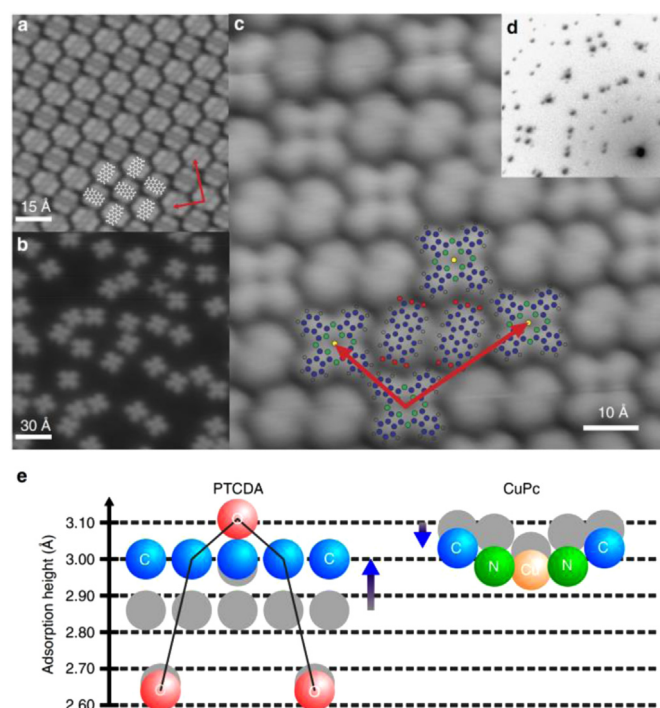


Fig. 39. STM images displaying the structure of PTCDA (a), CuPc (b) and a 2 PTCDA:1CuPc mixture (c). The mixed layer shows long range order, as evidenced by the LEED pattern (d). (e) Adsorption heights for C (blue spheres), oxygen (red spheres), nitrogen (green spheres) and copper (orange spheres) for a mixture of PTCDA and CuPc obtained by NIXSW. The heights obtained for the same atoms for molecular layers consisting in only one of the two components in the mixture are marked as grey spheres. Notice that, upon mixing, the average molecular heights equalize. Reprinted by permission from Macmillan Publishers Ltd: Nature Communications, Ref. [35], copyright 2014. (For interpretation of the references to color in this figure legend, the reader is referred to the web version of this article.)

separation between the carbon atoms at CuPc and the Ag(111) substrate is slightly shorter (3.04 \AA). Notice that, as a result of such variation in adsorption heights, the aromatic moieties are almost at the same distance with respect the metal surface.

The equalization of adsorption heights upon coadsorption does not however seem general. On the contrary, similar NIXSW experiments carried out with perfluorinated pentacene (PFP) and CuPc seem to indicate the opposite effect [180]. The adsorption height measured for the PFP and CuPc molecules separately adsorbed on Ag(111) surfaces is of 3.16 \AA and $3.04\text{--}3.08 \text{ \AA}$ respectively, i.e. their adsorption heights are very close before mixing. Upon the formation of a mixed monolayer, however, the adsorption height of CuPc slightly increases to $3.16\text{--}3.08 \text{ \AA}$ (which also becomes slightly more conical in shape), but the adsorption height of PFP increases much more, going to a final value of $3.48\text{--}3.52 \text{ \AA}$. Thus, contrary to the PTCDA-CuPc case studied above, the formation of the mixed monolayer makes the height difference between donors and acceptors actually increase. Similar results were also found for Cu(111) [180].

Interestingly, at least for the last example, this effect does not seem to be driven by intermolecular interactions, since one should expect these interactions to be maximal in the coplanar geometry. If we try to find a common explanation for the differences in adsorption height due to the formation of mixed donor/acceptor lattices at metal surfaces, we should focus our attention on the fact that, for both experiments, the adsorption height of the acceptor increases significantly, whereas the one of the donor stays almost unchanged. This can be rationalized if we assume that electron charge is accumulated at the acceptor/metal interface, corresponding with the high electron affinity of the acceptor species. As

suggested in Ref. [35,177], such accumulation of electron density would lead to a larger binding distance due to stronger Pauli repulsion. This is also in line with the changes in the work function measured in Ref. [180] due to the adsorption of the acceptor PFP on top of bare Ag or Cu(111) surfaces, and on top of those surfaces covered by about 0.5 ML of the donor (CuPc): the reduction in the work function caused by the adsorption of PFP is actually larger for the bare surfaces than for the surfaces precovered with the donor species, demonstrating that the “push-back” effect is more efficient on bare surfaces due to the shorter PFP-surface distances. More work is needed in the future in order to test the generality of these ideas.

5.2. Donor-acceptor versus molecule-substrate charge transfer: quantification and mechanisms

When considering the electronic structure of donor-acceptor mixtures adsorbed on metal surfaces, we need to take into account both molecule-molecule and molecule substrate charge-transfer processes. As discussed in Section 2, the adsorption of molecules with a large electron affinity (acceptors) or low ionization potential (donors) on metal surfaces leads to the transfer of electrons from the surface to the molecules (in the case of acceptors) or from the molecules to the surface (in the case of donors). The charge state of the resulting adsorbates is thus generally different from that of the gas phase molecules and so will be their electron affinity and ionization potential. The extent to which such adsorbates will behave as donors and acceptors needs to be carefully considered and, as we will discuss in the following, very often they will not exchange charge when brought into proximity.

The analysis of the density of states close to the Fermi level can offer important insights into the charge-transfer processes between the adsorbed donors and acceptors or between both species and the solid surface. Usually, charge transfer between organic donors and acceptors occurs by depopulation of occupied valence states (usually the HOMO) in the donor and the concomitant population of the unoccupied levels (usually the LUMO) of the acceptor. In the absence of the surface, the intermolecular interactions are usually too weak to change significantly the shape and width of the DOS peaks corresponding to the molecular orbitals (MO): thus the transfer of electrons involves a near-equalization of the energy levels involved in charge transfer. On the other hand, in the presence of a surface, the possible covalent interaction between the MOs and the substrate electrons will lead to important modifications in the shape and width of the MOs upon adsorption, and the alignment of the MOs is no longer guaranteed. For example, comparison of the pDOS over the HOMO and LUMO levels of TCNQ molecules in freestanding 1D chains and in the TTF-TCNQ/Au(111) system (see Fig. 40a) reveals that the shape and width of the peaks are almost equal, due to the weak interaction between TCNQ and the Au(111) surface, but, for the mixed system, the LUMO level shifts towards the Fermi level and becomes half-occupied [30]. A naïve picture of the charge transfer process for the TTF lines might lead to the expectation that the HOMO level should shift towards lower binding energies, in order to get depopulated. The analysis for TTF, however, also reveals a small shift of both HOMO and LUMO levels towards higher binding energies, but in this case the interaction with the surface substantially broadens the HOMO, decreasing thereby the occupancy of this level [30]. Similar calculations for the system perfluorinated copper phthalocyanine ($F_{16}CuPc$, donor) and pentacene (acceptor) show similar results (see Fig. 40b): while the electronic structure of pentacene is almost the same when it is directly adsorbed on the surface than in the mixed layer, all the levels from the donor shift towards lower binding energies by about 0.07 eV. It is interesting to notice that, in this case, the HOMO level also narrows, in

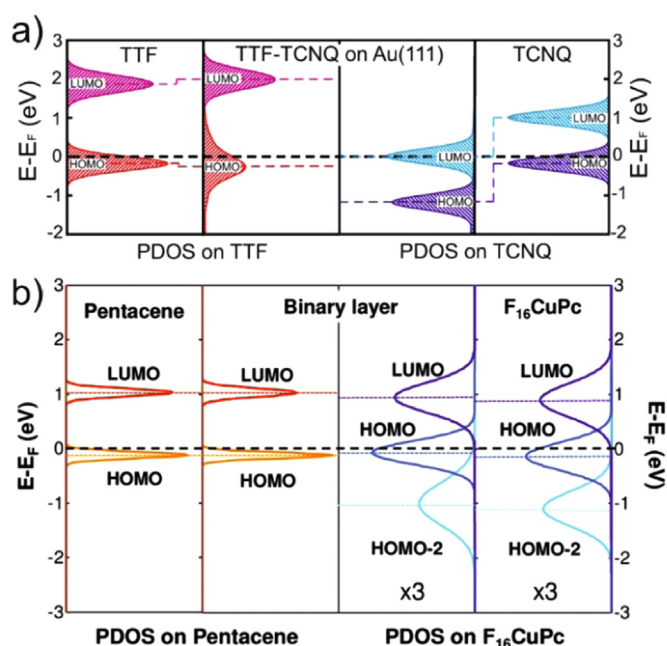


Fig. 40. DOS projected over HOMO and LUMO MOs for the systems TTF-TCNQ (a, reprinted with permission from [30]. Copyright 2008 by the American Physical Society. <http://dx.doi.org/10.1103/PhysRevLett.100.156805>) and pentacene- $F_{16}CuPc$ (b, Reprinted with permission from [176]. Copyright 2012 American Chemical Society. <http://dx.doi.org/10.1021/jp211749g>).

such a way that its population remain constant. A net increase of electron charge is however obtained from $0.32 e^-$ to $0.44 e^-$, but this is attributed to the broadening of the deeper energy levels (HOMO-2, HOMO-3), which leads to an increase in the DOS tails for these states above the Fermi level. It is therefore important to notice that the naïve picture in which the MO levels align in order to enable charge redistribution does not necessarily holds when donors and acceptors are supported on a solid surface.

Shifts in the MOs without a clear indication of broadening have been reported when non-metallic surfaces are used as substrates. For example, the electronic structure of binary mixtures of $F_{16}CuPc$ and CuPc on HOPG have been recently investigated [175]. In this binary mixture, $F_{16}CuPc$ will act as an acceptor, due to high electronegativity of fluorine. The HOMO levels of $F_{16}CuPc$ and CuPc are easy to identify in the UPS spectra, being resolved as peaks at 1.56 eV and 1.21 eV respectively (see Fig. 41). Upon formation of the well-ordered 1:1 binary mixture, two peaks are also visible at 1.65 eV and 0.91 eV. This result is rationalized by assuming that the HOMO level of the acceptor has shifted to higher binding energies by about 0.09 eV (increasing thus the filling of this level), whereas that of CuPc has shifted 0.3 eV towards the Fermi level, thereby becoming more unoccupied.

The experimental investigation of the degree of filling of HOMOs and LUMOs is complicated by the presence of interface states, arising from the hybridization of MOs with surface and bulk states of the substrate. Such states might actually be strongly localized between the outer atoms of the surface and the molecule, and have a low amplitude at the molecular positions. These states will thus not show in MO-projected DOS, but they can dominate the experimental spectra. This is the case, for example, for TTF-TCNQ/Au(111): whereas theoretical calculations show the LUMO of TCNQ exactly at the Fermi level, the experimental STS spectra is dominated by a very intense and narrow peak at about 0.3 eV above the Fermi level [30]. The origin of this peak can be traced to the formation of hybrid interface states between the HOMO of the TTF molecules and the surface and bulk states of Au(111), back folded because of the superimposed molecular periodicity, and does not correspond to the

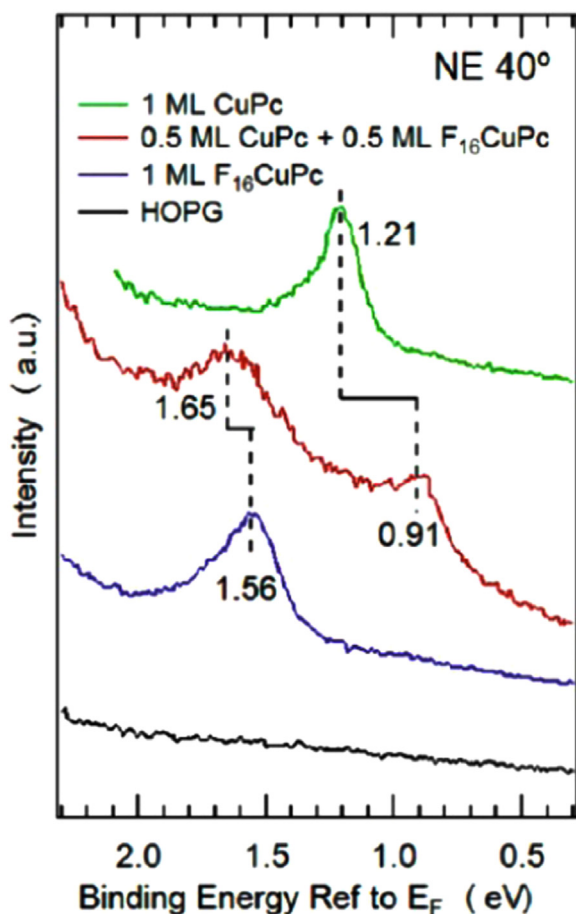


Fig. 41. UPS spectra corresponding to a film composed only of acceptor molecules (CuPc, green curve), only the donor molecule (blue curve) of a 1:1 donor-acceptor mixture (red curve), deposited on HOPG [175]. Reprinted with permission from [175]. Copyright 2014 American Chemical Society. <http://dx.doi.org/10.1021/nn406050e>. (For interpretation of the references to color in this figure legend, the reader is referred to the web version of this article.)

LUMO of the TCNQ molecules (see Fig. 42).

Generally speaking, the presence of interface states, the broadening of the MOs upon adsorption, and the existence of several MO derived states close to the Fermi level, hinders a straightforward interpretation of valence band spectra from donor/acceptor mixtures at metallic surfaces. In this respect, the technique of Orbital Tomography has been recently revealed as a powerful tool to distinguish the origin of the different features observed in UPS spectra [35,183]. In this technique, the UPS intensity of a particular feature is mapped in a cubic grid of k -values. The results are then compared with the Fourier transform of the MO orbitals of the gas phase molecules, allowing for a quantification of the contribution of the different MOs to a particular feature in the UPS spectra. The power of this technique is clearly shown in the example of CuPc and PTCDA on Ag(111) [35]. The UPS spectra of 1 ML CuPc/Ag(111) reveals one peak at about 1.2 eV below the Fermi level, and a slight increase in the intensity close to the Fermi level, analyzed by the authors as a broad peak at a binding energy of 0.1 eV, which are attributed to the HOMO and a partially occupied LUMO respectively (see Fig. 43a). Similarly, the spectra of PTCDA shows a HOMO feature at about 1.58 eV and a clearer LUMO signature at a binding energy of 0.2 eV. When the binary mixture is formed, the recorded spectra show a double peak in the region of the HOMOs, and a featureless peak at the Fermi level, whose nature cannot be disentangled by direct inspection and analysis of the spectrum. Orbital tomography (see

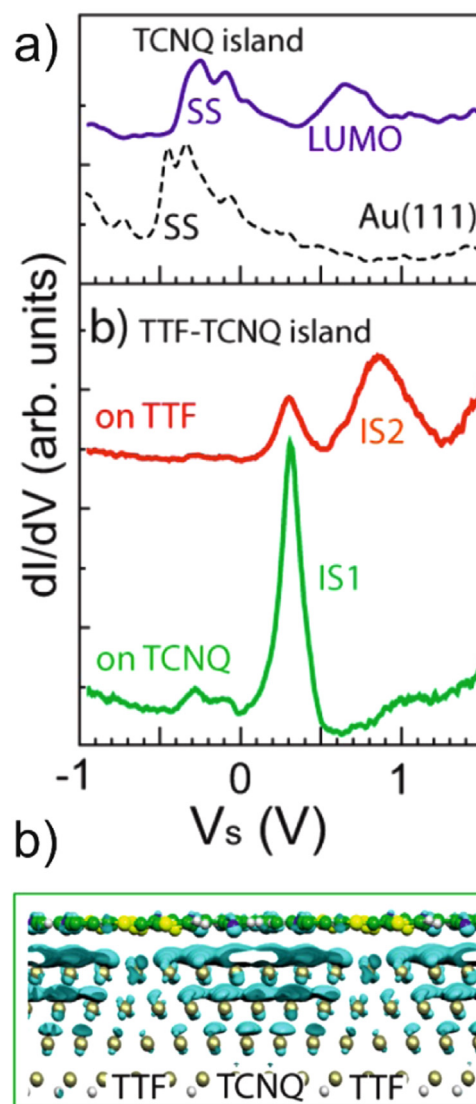


Fig. 42. a) dI/dV spectra corresponding to a pure TCNQ island (upper panel, blue curve), the bare Au(111) surface (upper panel, dashed black line) and the mixed 1 TCNQ:1 TTF phase on TCNQ positions (green curve) and TTF positions (red curve). The spectra in TCNQ molecules of the mixture is dominated by an intense peak 0.3 eV above the Fermi level, but this state corresponds to an interface state originated from the hybridization of TTF MOs and the electron bands at the surface (b). Reprinted with permission from [30]. Copyright 2008 by the American Physical Society. <http://dx.doi.org/10.1103/PhysRevLett.100.156805>. (For interpretation of the references to color in this figure legend, the reader is referred to the web version of this article.)

Fig. 43b), however allows for a clear ascription of this peak as arising from PTCDA LUMO, shifted to higher binding energies due to the presence of the donor CuPc. The CuPc LUMO has no contribution at all to the Fermi level peak, thus showing that this level is now placed above the Fermi level and it is thus completely unoccupied (see Fig. 43c). Since complementary NIXSW measurements revealed the equalization of molecular heights upon binary mixture formation (described in Section 5.1), the authors proposed a substrate-mediated push-pull mechanism for the charge transfer, according to which the decrease in the bonding distance between the donor (CuPc) and the surface actually pushes away electron charge from the metallic substrate, which moves towards the acceptor (PTCDA), filling up the LUMO of this molecule and shifting it to higher binding energies.

A word of caution is however required at this point. The LUMO of the CuPc film was actually a weak feature even in the UPS

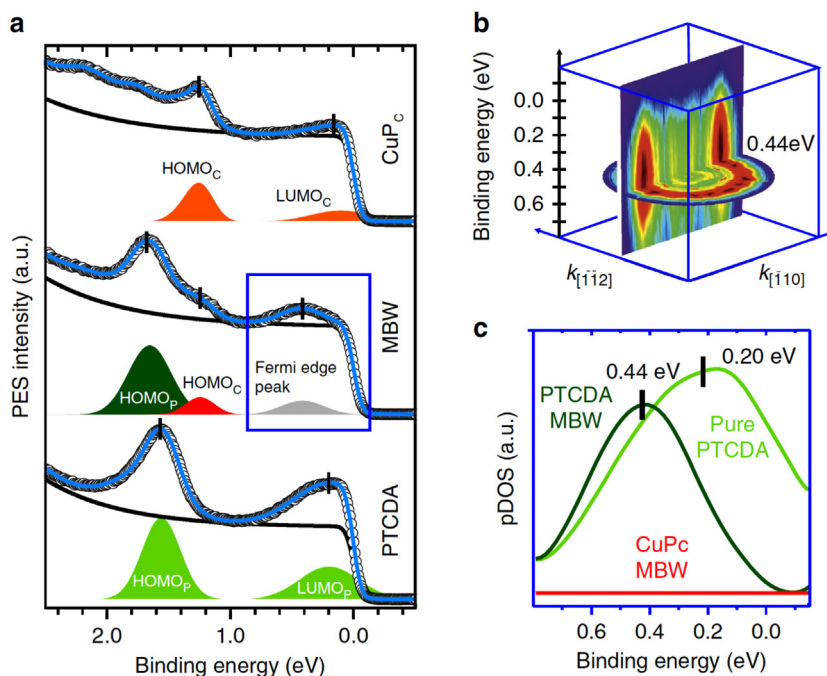


Fig. 43. a) UPS spectra of PTCDA/Ag(111) (acceptor, lower curve), the CuPc/Ag(111) (donor, upper line) and the adsorbed binary mixture (middle curve). b) UPS intensity in a cubic *k*-grid. c) DOS of the mixture projected over the LUMO level of PTCDA (dark green curve) and the LUMO level of CuPc (red curve). The results for PTCDA/Ag(111) are shown for comparison. Reprinted by permission from Macmillan Publishers Ltd: Nature Communications, Ref. [35], copyright 2014. (For interpretation of the references to color in this figure legend, the reader is referred to the web version of this article.)

spectrum corresponding to homomolecular films. The authors fit this spectrum by using a broad peak centered slightly below the Fermi level, which implies a relatively large population of the level. On the other hand, their own DFT calculations show that the LUMO peak in the projected DOS is placed at about 0.2 eV above the Fermi level [35], corresponding to a much lower population of this state than that suggested by the fit (notice that the agreement between the theoretically calculated energy level of CuPc HOMO and the experimental value is excellent). Upon formation of the binary mixture, this LUMO shifts to lower binding energies, thereby decreasing the population of the level. However, judging by the small variation in the pDOS and the charge density profiles, the net charge that is being transferred from the donor to the acceptor is small.

The analysis of core-level shifts in XPS experiments has been suggested to be more straightforward than the investigation of the electronic structure close to the Fermi level [8,33]. The general idea of these experiments is that, if charge transfer from the donor to the acceptor takes place for the adsorbed species, the partial charge in the donor will be less positive in the homomolecular donor film than in the binary mixture, and the partial charge in the acceptor will be more negative in the binary mixture than in the homomolecular acceptor film. Thus, increasing the donor/acceptor stoichiometric ratio should shift the core-levels of both the donor and the acceptor atoms to lower binding energies. Interestingly, the experimental observations reported so far seem to contradict this simplistic view. Experiments carried out with perfluorinated pentacene as the acceptor and CuPc as the donor or with perfluorinated copper phthalocyanine as the acceptor and pentacene as the donor show a shift of the core levels from both the donor and the acceptor towards higher binding energies for increasing D:A ratios [32,33] (see Fig. 44). These results have been rationalized by taking into account the different potential experienced at the atomic positions depending on the stoichiometry of the environment. The adsorption of donors will lead to the transfer of electrons from the donor to the substrate, and will thus

create an environment with a positive electrostatic potential on the average. Similarly, the adsorption of acceptors will have a negative contribution to the electrostatic potential at the position of the film. Increasing the D:A ratio will thus lead to an increase of the absolute value of the electrostatic potential at the atomic sites within both donor and acceptor molecules and, thus, to a shift towards higher binding energies of the core levels, in good agreement with the experimental results. This effect has been termed by the authors as “screening” [32,33], but this term might be misleading in the context of photoemission spectroscopy, as it can easily be confused with the dynamic screening of the core-hole, a final state effect. On the contrary, the relevant “screening” here results from the electrostatic screening of the organic molecules by substrate electrons, and it is an initial state effect. Actually, since all the films are investigated for coverages below the monolayer, final state effects arising from the screening of the core-hole by substrate electrons are expected to be similar regardless of the D:A ratio [32], and thus the experimentally observed shifts in the XPS spectra can be attributed exclusively to initial state effects due to charge redistribution.

Generally speaking, thus, two opposite contributions can be identified in the dependence of the core-level shifts with the D:A ratio. Intermolecular charge-transfer, leading to a shift towards lower binding energies with increasing D:A ratio, and the change in the electrostatic potential due to molecule-substrate charge-transfer, leading to a shift towards higher binding energies with increasing D:A ratios. Since the transfer between the organic adsorbates and the substrate can be expected to be stronger than between the molecules, it is understandable that the second effect dominates. Actually, the effect of the electrostatic potential due to molecule-substrate charge transfer can be gauged by measuring the change in the work function upon adsorption of the films. For the cases studied in the previous example, it is found that the shift in the work function corresponds quite precisely with the core-level shifts [32,33], suggesting that the contribution of the intermolecular charge transfer to the measured core-level shifts is

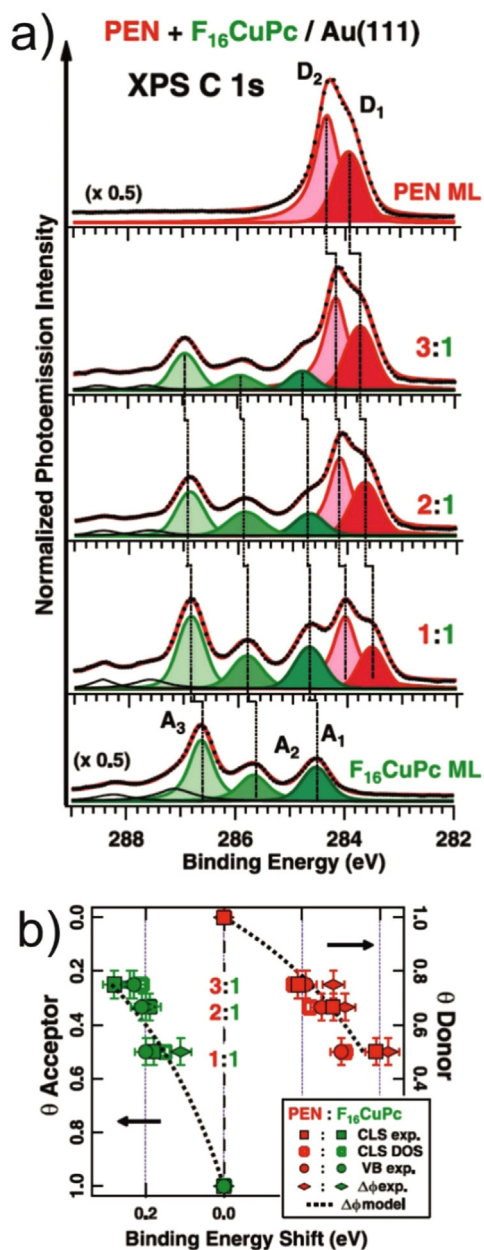


Fig. 44. a) C1s XP spectra corresponding to mixtures of PEN (donor) and F₁₆CuPc (acceptor) on Au(111) for different D:A ratios. b) Core-level shifts for donor and acceptor levels as a function of the D:A ratio demonstrating that both shift to higher binding energies [33]. Reprinted with permission from [33]. Copyright 2013 American Chemical Society. <http://dx.doi.org/10.1021/nn4020888>.

negligible. This is in line with the Bader analysis of the charges on the atomic positions of pentacene in the homomolecular film and the binary mixtures, which turn out to be indistinguishable within the accuracy of the calculation [32]. It might be argued that none of the species investigated are very strong donors and acceptors, and thus intermolecular charge transfer is basically suppressed by the stronger charge transfer with the substrate.

From the examination of the literature on this topic it thus appears that when the chemical species under investigation are weak donors and acceptors, evidence from XPS spectroscopy and work-function measurements rule out a very significant change in the partial charges at the molecules [32,33]. Moreover, although the HOMO and LUMO states show shifts in the sense expected for intermolecular charge transfer processes, the total amount of charge transferred (possibly via the substrate) seems to be small

[35,177]. On the other hand, for the case of TTF-TCNQ/Au(111), where the adsorbates are strong donors and acceptors and the binding of the substrate is very asymmetric (strong binding for TTF, weak binding for TCNQ), it seems that forming the binary mixtures leads to the occupancy of the TCNQ LUMO by one electron [31], but the occupancy of the TTF HOMO does not decrease accordingly [30], suggesting that the presence of TTF is facilitating the transfer of electrons from the gold substrate to TCNQ, rather than providing the electrons. It seems fair to say, thus, that the phenomenology of charge-transfer between organic donors and acceptors on metal surfaces is rather rich, and is only starting to be understood. In particular, no system with a measurably large charge transfer between the adsorbed acceptors and donors has been clearly identified so far, and it remains work for the future to find if such a system is possible at all.

6. Electronic structure of organic adsorbates in the strong interaction limit: Delocalized electron states and molecular Kondo resonances

The production of ordered arrays of magnetic objects in two dimensions is a topic that has attracted sustained interest for years [184]. The ultimate limit of miniaturization and identical size of the magnetic objects imply the use of magnetic molecules and their self-organization on surfaces [14]. Molecular spintronics is an emerging field of research that combines spintronics and molecular electronics [185]. The goal is to achieve a long-range structural ordering of magnetic molecules in two dimensions and, possibly, their long-range magnetic ordering due to mutual interactions between these molecules. Many molecules that show magnetic moments in gas phase have been deposited on surfaces, where the interaction with the substrate often eliminates the magnetic moment and complicate their mutual interaction. The practical implementation of molecular spintronics lies in probing and controlling the spin state of molecules deposited on a surface. For this concept to become real devices a more fundamental understanding of substrate-supported magnetic molecules is necessary since the molecular levels, charge, spin and magnetic anisotropy can change as the molecules come in contact with a surface.

The developments in low temperature scanning tunneling microscopy (LT-STM) and spectroscopy (STS) have permitted the interrogation of the electronic structure of individual molecules on different substrates. The study of magnetic impurities at surfaces has attracted a widespread interest in recent years and in particular molecules that develop a sizeable net spin density upon adsorption on non-magnetic metallic surfaces. The Kondo effect was discovered originally in the 1930s [186], measuring the variations of the resistance versus temperature, in dilute magnetic alloys. In 1964, J. Kondo gave the first explanation for the anomalous increase of the resistivity of some, in principle pure, bulk materials at low temperatures [187]. The explanation was based on a spin-flip scattering process due to the presence of magnetic impurities in the metallic samples. In late 1990s, several groups performed the first experiments where single magnetic adatoms were deposited on non-magnetic surfaces, e.g., Ce on Ag(111) [188], Co on Au(111) [189] or Mn on Al₂O₃ [190]. The theoretical model by P.W. Anderson for a single magnetic impurity diluted in a metal can be applied [191,192]. The model considers the hybridization between the conduction electrons of the metal and the unpaired electron state in the impurity, dismissing all the others electronic states of the impurity. This interaction leads, at temperatures below a characteristic Kondo temperature (T_K), to the many-body antiferromagnetic screening of the impurity magnetic moment and results in a non-magnetic single ground state. When scanning tunneling spectroscopy experiments are performed, the

electrons tunneling from the STM tip have two possible channels to reach the sample. They can tunnel directly into the empty states of the sample or indirectly via a spin-flip process into the localized impurity state. Therefore, when Kondo screening exists, the STS spectrum presents a resonance at E_F spatially localized at the magnetic impurity. This resonance is the result of the quantum interference of the discrete state of the impurity and the continuum of the conduction electrons in the metal and can be described by the Fano equation [193], as was demonstrated by V. Madhavan et al. [189]. In this context, the tunneling conductance is given by: $dI/dV \propto (\varepsilon + q) / (1 + \varepsilon)$ where q is the so-called factor form, $\varepsilon = (eV - \varepsilon_0) / \Gamma$ is a reduced energy, ε_0 is the energy shift of the resonance from the Fermi level and Γ is the half-width at half-maximum of the resonance given by [194,195]: $2\Gamma = [(\alpha k_B T)^2 + (2k_B T_K)^2]^{1/2}$. Then, the half-width at half-maximum of the Kondo resonance presents a dependence of the temperature and defines the characteristic Kondo temperature, T_K . The Kondo temperature reflects the strength in the hybridization between the magnetic impurity and the substrate.

When molecules are deposited on surfaces several processes take place. As described in previous sections, the interaction between the molecules and the surfaces produces energy level realignment, splitting and broadening of molecular electronic states as a response to charge transfer, structural distortions and hybridization with metal states. All these processes have an impact in the Kondo physics of molecules with a net spin density adsorbed on non-magnetic metallic substrates. In recent years these problems have been explored with experimental systems that combine different molecules and substrates. In the following we will discuss different results addressing these issues.

The first example of the effects described above was the study of the Kondo effect on cobalt phthalocyanine (CoPc) deposited on Au(111) [196]. The Co atoms in the CoPc molecule do not interact strongly with conduction electrons and exhibit no Kondo effect in the differential tunnel spectroscopy measured on the CoPc molecules. Using the STM it is possible to cut away eight hydrogen atoms from the molecule with voltage pulses, as can be seen in

Fig. 45. Single CoPc molecules adsorbed on Au(111) surface exhibit a protruding four-lobed structure that is consistent with the molecular symmetry as can be seen in Fig. 45(a) and (b). When the STM tip is placed directly over the edge of a lobe, the feedback loop is disconnected, and a high positive voltage pulse is applied (Fig. 45(b)) the hydrogen atoms 2 and 3 on the lobe are detached. A typical current trace simultaneously measured during the application of a 3.6 V pulse on one of the four lobes of a CoPc molecule (Fig. 45(c)) shows two sudden drops in the current signal, indicating the sequential desorption of the two hydrogen atoms from the benzene ring. The topographic images show that the bright lobes disappear sequentially, see Fig. 45(e)–(h). The apparent height of the molecular center (the Co atom) increases $\sim 0.8 \text{ \AA}$, indicating a strong conformational change in the molecular structure and/or a redistribution of the molecular local density of states (LDOS). After the dehydrogenation process an intense resonance peak arises immediately below E_F ($-6 \pm 3 \text{ meV}$) with an asymmetric shape and a narrow width of $\sim 50 \text{ meV}$ (see Fig. 2 in Ref. [196]). The amplitude of this peak decreases continuously as the dI/dV spectrum was measured at an increasing distance from the Co center. The estimated Kondo temperature extracted from the width of the resonance is 208 K. Much higher than any reported temperature for individual magnetic atoms.

In order to understand the experimental results first principle calculations were carried out. In a free CoPc molecule, the Co atom has unpaired d electrons and the magnetic moment of the Co atom is 1.09 Bohr magnetons (μ_B). In the CoPc adsorption system, the magnet moment is completely quenched by the molecule-substrate interaction. The spin-polarized Partial Density Of States (PDOS) of the Co atom in the CoPc adsorption system and in a free CoPc molecule revealed that the spin-down states are filled more than the spin-up states for the free CoPc molecule. However, the filling difference disappeared for the CoPc adsorbed on Au(111).

Dehydrogenation induces a marked change of the molecular structure, so that the dehydrogenated-CoPc molecule on Au(111) is no longer planar. The smallest separation between the end C atoms of the benzene ring and the gold substrate is $\sim 1.9 \text{ \AA}$,

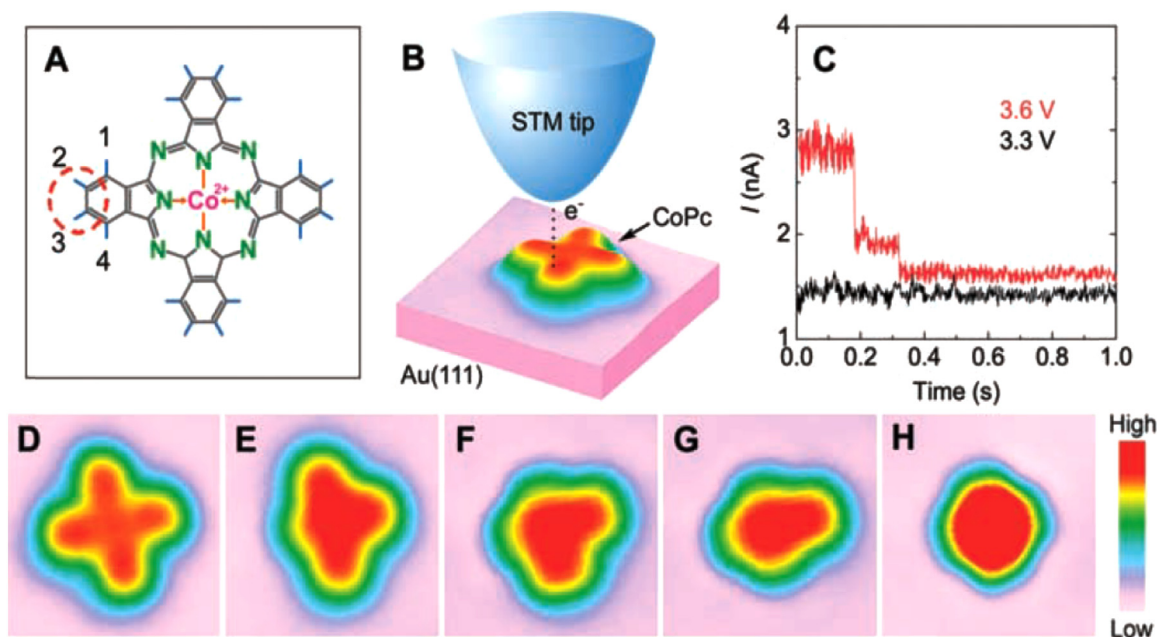


Fig. 45. (a) Structural formula of the CoPc. Hydrogen atoms 2 and 3 in every lobe were dissociated in the experiment. (b) Diagram of the dehydrogenation induced by the STM current. (c) Current versus time during two different voltage pulses on the brink of one lobe. (d)–(h) STM images of a single CoPc molecule during each step of the dehydrogenation process, from (d) an intact CoPc to (h) dehydrogenated-CoPc. Image area, 25 \AA by 25 \AA . The color scale represents apparent heights, ranging from 0 \AA (low) to 2.7 \AA (high). Adapted from [196] with permission. (For interpretation of the references to color in this figure legend, the reader is referred to the web version of this article.)

leading to a much stronger binding to the gold substrate. The central Co atom in the dehydrogenated CoPc molecule shifts upwards by ~ 0.8 Å, a similar value to the apparent change in the STM topographic images. More importantly, the magnetic moment is recovered for the dehydrogenated-CoPc adsorption system. The spin-polarized PDOS of the Co atom in the dehydrogenated -CoPc adsorption system near E_F has an empty minority spin peak. The magnetic moment of the dehydrogenated-CoPc molecule is now $1.03 \mu_B$, very close to the value of a free CoPc molecule.

The origin of the high Kondo temperature obtained for the CoPc compared with the one obtained for individual Co atoms on Au(111) relies on the fact that the on-site Coulomb repulsion is smaller on the dehydrogenated-CoPc on Au(111) compared with Co on Au(111) and the crystal field splitting of the Co d-level of the dehydrogenated-CoPc/Au(111) system is greater than that of the Co/Au(111) system, so the half-width of the hybridized d-level of the dehydrogenated-CoPc/Au(111) system is greater than that of the Co/Au(111) system.

Another study shows that the Kondo temperature measured on 5,10,15,20-tetrakis(4-bromophenyl)porphyrin-Co (TBrPP-Co) deposited on a Cu(111) surface can be changed by switching between different molecular conformation through the application of voltage pulses [197]. TBrPP-Co molecules anchor on the Cu(111) surface via the four bromine atoms positioned at the 3-fold hollow sites of the copper surface and can adopt two conformations, the saddle, 25% of them, and the planar, the remaining 75% (Fig. 46(a) and (b)). In the saddle conformation, the center of the molecule is bent by the elevation of two pyrrole units of the porphyrin macrocycle. STM images acquired at 4.6 K under ultra-high vacuum (UHV) conditions for the molecules on the saddle configuration show two central bright protrusions surrounded by four dimmer lobes forming a rectangular shape (Fig. 46(a)). The authors interpret this two central protrusions as the two pyrrole units lifted from the surface. On the other hand, the planar molecules have an approximately square shape, and the porphyrin plane is positioned parallel to the Cu(111) surface. In this

position, the four bromophenyl groups of the molecule can interact strongly with the surface via π -interactions. The STM images of planar TBrPP-Co reveal a set of four lobes (Fig. 46(b)). The saddling of the molecule can be removed by applying a series of voltage pulses with the STM tip, which supplies the necessary energy to switch the molecule from the saddle to the planar conformation.

The interaction between the Co atom on the TBrPP-Co molecule and the Cu(111) surface is studied measuring the differential conductance on the molecules on both conformations. The resultant dI/dV spectra of both saddle and planar molecules consistently reveal a small “dip” located around the substrate Fermi level, i.e., zero tunneling bias, which the authors attribute to the Kondo resonance (Fig. 46(f) i and ii). The authors found that the spectral feature corresponding to the Kondo resonance measured before and after the switching events was identical to the naturally adsorbed molecules on both configurations. Curve (i) in Fig. 46 (f) presents the dI/dV spectra measured on the saddle TBrPP-Co. The resultant Kondo temperature of saddle TBrPP-Co at 4.6 K is $130 \text{ K} \pm 15 \text{ K}$. The width of Kondo resonance increases for the planar TBrPP-Co, and the corresponding Kondo temperature is determined to be $170 \text{ K} \pm 10 \text{ K}$. In order to verify the origin of the observed resonance around the Fermi energy, the authors measured the dI/dV spectra of isolated TBrPP-Cu molecules on Cu(111). The TBrPP-Cu has a similar molecular structure as the TBrPP-Co except that the Co atom is replaced by a nonmagnetic copper atom. Since copper is nonmagnetic, the Kondo effect caused by spin-electron interaction should not occur because it was clear from the measurements performed on the TBrPP-Co molecules that the change in conformation does not alter the spin state of the molecules. The TBrPP-Cu molecules adsorb on Cu(111) with two different conformations as in the case of TBrPP-Co. The dI/dV spectra of both saddle and planar conformations of isolated TBrPP-Cu molecules are featureless around the substrate Fermi level (Fig. 46(f) bottom spectra). From this the authors conclude that the observed resonances in both conformations of TBrPP-Co originate

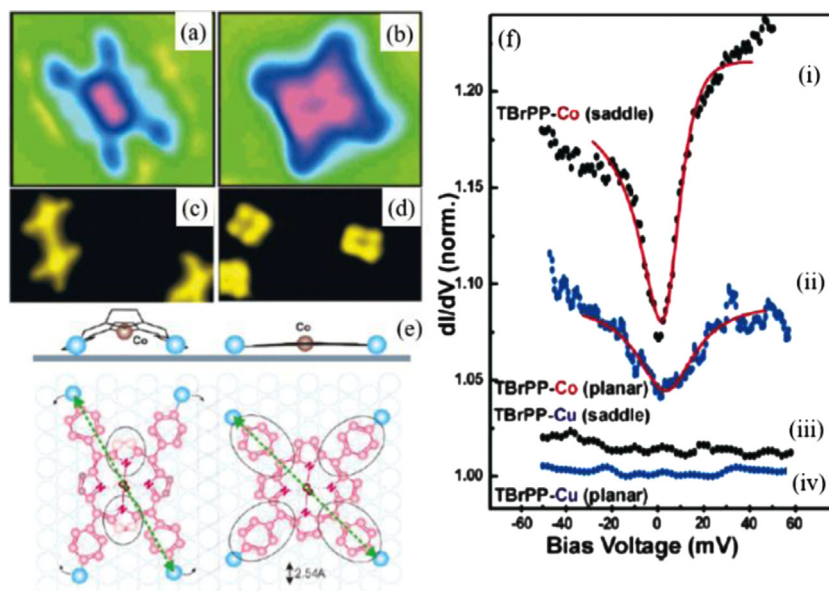


Fig. 46. (a) STM images recorded at 4.6 K of saddle conformation (width ~ 11 Å, length ~ 18 Å) and (b) planar conformation (length ~ 15.5 Å) of TBrPP-Co on Cu(111). Similar conformations are observed for the TBrPP-Cu on Cu(111), the saddle (c) and planar (d) conformations. (e) The corresponding models of saddle (left) and planar (right) conformation. Blue and pink color balls represent bromine and carbon atoms, respectively. The encircled regions of the molecule indicate the area providing higher current in the STM images. The length of the molecule along the diagonal (indicated with a dashed green arrow) is unchanged upon switching the two conformations. Kondo signatures. (f) dI/dV curves measured on TBrPP-Co and TBrPP-Cu molecules on both configurations. (i) The conductance spectrum on the saddle TBrPP-Co molecules show a dip (Kondo resonance) around surface Fermi level. The solid line represents the Fano line-shape fit to the data. The extracted Kondo temperature is $130 \text{ K} \pm 15 \text{ K}$. (ii) The width of the Kondo resonance increases in the dI/dV spectra on planar TBrPP-Co molecules, which corresponds to an increase in Kondo temperature. The solid line represents the Fano line-shape fit to the data. The extracted Kondo temperature is $170 \text{ K} \pm 10 \text{ K}$. (iii, iv) The dI/dV spectra on saddle and planar TBrPP-Cu molecules do not reveal any features around the surface Fermi level. The spectra have been shifted vertically for clarity. All the spectra are taken at the center of each molecule. Adapted from Ref. [197] with permission. (For interpretation of the references to color in this figure legend, the reader is referred to the web version of this article.)

from the spin-electron interactions, i.e., the Kondo effect.

As in the previous example the observed high Kondo temperature in TBrPP-Co molecules is caused by enhanced coupling of the magnetic impurity caged by the porphyrin molecule, to the conduction electrons of the surface through the molecular bonding. To explain the increased Kondo temperature after switching it is necessary to have a look to the electronic structure of both molecular conformations. In the saddle conformation the porphyrin plane is bent and the Co atom is lifted away from the surface. This effectively

reduces a direct spin-electron coupling between the Co atom and the surface state free electrons of Cu(111) resulting in the disappearance of the Co d_{z^2} associated peak from the spectrum of the saddle TBrPP-Co. As a result, the Kondo temperature is decreased in the case of the saddle as compared to the planar TBrPP-Co. The molecules bind to the substrate in both conformations via the bromine atoms and hence, spin-electron coupling through molecular bonding is still permitted in the saddle conformation, which provides the observed Kondo temperature of 130 K. In the case of

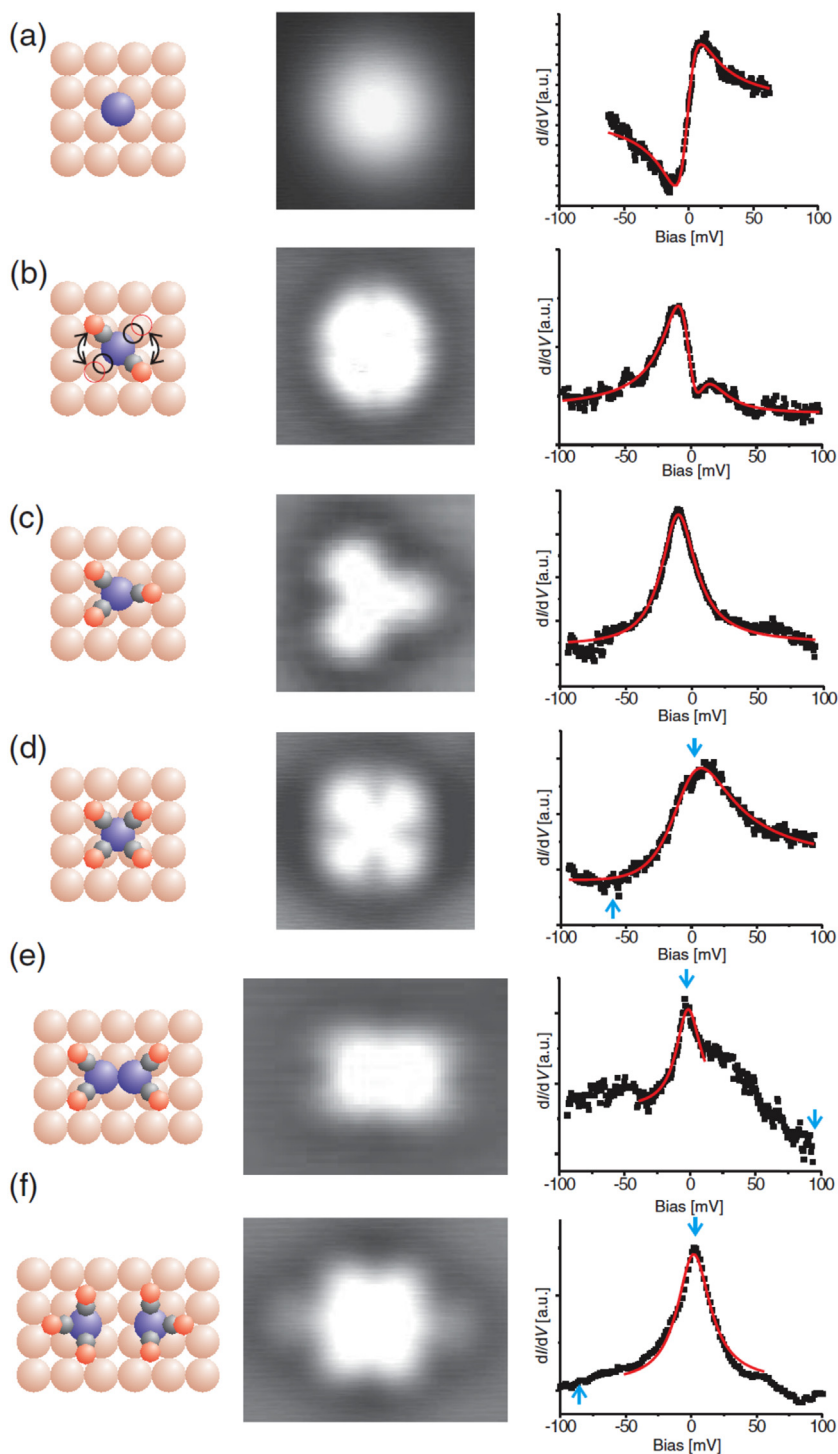


Fig. 47. Models, STM topographies, and STS spectra in the center of the Co adatoms and complexes under investigation: (a) Cobalt adatom, (b) $\text{Co}(\text{CO})_2$ (constantly flipping; from the spectrum a linear background has been removed), (c) $\text{Co}(\text{CO})_3$, (d) $\text{Co}(\text{CO})_4$, (e) $(\text{Co}(\text{CO})_2)_2$, (f) $(\text{Co}(\text{CO})_3)_2$. Models and topographies in (a)–(f) drawn to the same scale. The solid lines in the spectra are fits of a Fano function. Adapted from Ref. [199] with permission.

saddle conformation, the Kondo effect occurs most likely through a single path, coupling via molecular bonding, while the higher temperature Kondo effect in the planar case involves both paths.

Similar studies on the influence of the molecular conformation on the existence of a Kondo resonance have been carried out depositing tetracyanoethylene (TCNE) on Cu(111) [47]. Applying voltage pulses with the tip of a scanning tunneling microscope in UHV and at low temperatures it is possible to reversibly switch among five different configurations. A pronounced Kondo resonance in the tunneling spectroscopy data indicates that one of the conformations present a magnetic configuration. DFT calculations on the system show that molecular deformation changes the occupancy in the molecular orbitals of the TCNE deposited on Cu(111), producing in this way a magnetic state in a molecule that does not contain any magnetic atom.

The importance of the molecular conformation has also been tested using a double-decker bis(phthalocyaninato)terbium(III) complex (TbPc_2) adsorbed on Au(111) [198]. The dI/dV curves recorded onto TbPc_2 molecules as deposited show a sharp and pronounced peak at the Fermi level that is identified as a Kondo peak. The authors explained the existence of the Kondo resonance as the consequence of the interaction of an unpaired spin of the π -orbital of a phthalocyanine (Pc) ligand with the conduction electrons from the surface. By applying controlled current pulses it is possible to rotate the upper Pc ligand respect to the one in contact with the surface. The rotation shifts the molecular frontier-orbital energies, quenching the π -electron spin. Reversible switching between the two configurations is possible.

The coupling of the spin of a single magnetic adatom to the substrate can be controlled not only by changing the conformation of the organic ligands, as have been discussed previously, but also changing its local environment through organic ligand attachment. The first example was the controlled attachment of CO molecules to cobalt adatoms deposited on Cu(100) [199]. The left column of Fig. 47 shows the model for the carbonyl species together with the adsorption geometry of the individual Co atom. Middle column in Fig. 47 shows the corresponding STM images. The tunneling spectra acquired in the center of the carbonyl species show a pronounced feature near the Fermi energy in all cases and are shown in right column in Fig. 47. From the fit of the spectra to as a Fano function the widths of the resonances can be extracted and, from this value, an estimation of the corresponding Kondo temperature can be made. The Kondo temperature is found to increase with the number of ligands attached to the impurity from 88 K for a single Co adatom to 280 K for the cobalt tetracarbonyl complex. The behavior of the Kondo temperature of the complexes as a function of the number of ligands can be understood considering the interaction of the magnetic impurity with the sea of conduction electrons. The interaction is described by the exchange coupling J . An increase in the hybridization between the orbital that carries the spin and the conduction electrons from the host leads to an increase in J , while an increase in the on-site Coulomb repulsion produces a reduction in J . The bonding between CO molecules and transition metals is well known: When CO molecules bonds to cobalt adatoms, a donation of electrons from the σ orbital to the transition metal adatom takes place, and simultaneously a backdonation from the d orbitals to the $2\pi^*$ of the CO molecules occurs [199]. This backdonation leads to a delocalization of the d electrons from the cobalt atoms and therefore reduces the Coulomb repulsion and eventually increases the coupling to the substrate conduction band electrons. Both lead to an increased exchange coupling J and therefore an increase in the observed Kondo temperature.

Another example is the creation of new magnetic nanostructures manipulating TCNE molecules and vanadium atoms deposited on Ag(100) [200]. For complexes having two V atoms, the Kondo

behavior can be quenched for different molecular arrangements, even as the spin-polarized orbitals remain unchanged. The authors trace back the origin of this behavior, with the help of DFT calculations, to the variable spin-spin (i.e., V-V) ferromagnetic coupling through a single TCNE molecule. The different configurations adopted by the V atoms and the TCNE molecule changes the distance between the V atoms and the magnetic coupling between them.

The registry of the deposited molecules with the metallic substrate has a strong influence in the Kondo screening, in particular the relative orientation of the molecules respect to the atomic lattice. This influence has been studied on iron phthalocyanines (FePc) adsorbed on Au(111) [201,202]. On the STM images measured on the FePc deposited on Au(111) at low temperature, the molecules, appear as a cross (see Fig. 48(a)), the central bright spot corresponds to the position of the Fe atom and the four lobes are the aromatic rings. As can be seen on the images the molecules are adsorbed in two configurations with a different rotation respect the atomic lattice of the Au(111) surface and are called on-top and bridge configurations [202]. On the on-top configuration the Fe atom is placed on top of one Au atom from the surface, while on the bridge configuration the Fe atom is placed on bridge position between two Au atoms from the substrate (see model in Fig. 3 in Ref. [201]). Both configurations can be distinguished in the STM images because the molecules are rotated by 15° , the rotation is induced by the improvement on the registry between the aromatic rings and the Au(111) atomic lattice.

In a first set of experiments Gao and co-workers [201] studied the system by means of scanning tunneling spectroscopy. In the dI/dV spectra measured on the molecules around the Fermi level the authors found that all the observed molecules, irrespectively of the adsorption configuration, present features at the Fermi level. For the bridge configuration a sharp peak is present on the spectra, while a dip at the Fermi level appears on the spectra measured on the molecules in the on-top configuration. Both features were associated by Gao et al. to the existence of Kondo screening in the system. Both features can be fitted with a Fano line shape and from the fitting parameters the authors extracted the corresponding Kondo temperatures, being $T_K=357$ K for the bridge configuration and $T_K=598$ K for the on-top configuration. These values are much higher than any other reported in the literature. The reason for these unrealistic high values of the Kondo temperature for both adsorption configurations could be due to the experimental procedure followed by Gao et al. It has been shown that in order to fully characterize the Kondo phenomena the evolution with temperature and magnetic field is needed [217]. In this particular case Gao et al. measured the spectra at one temperature, extracting the Kondo temperature from the fitting to the Fano function. With this procedure any systematic experimental error, like RF-noise in the system or an error in the sample temperature measurements could produce this unexpected high values for the Kondo temperature. In order to explain the Kondo resonance in the spectra the authors carried out DFT calculations and the spin-polarized partial density of states of the Fe atom presents an asymmetry in the population of the spin-up and spin-down states. The calculated magnetic moment is $\sim 1.9\mu_B$ for the Fe atoms in both adsorption configurations. The explanation given for the high values for the Kondo temperatures are based on the combination of the d -orbital character of electrons near the Fermi level within the Fe(II) d^6 system and the enhanced spin-electron coupling as consequence of the molecular bonding (see Fig. 4 on Ref. [201]).

In 2012 Minamitani et al. [202] revisited the system. As in the previous study the FePc molecules deposited on Au(111) appear as a cross in the STM images and the molecule takes two types of adsorption configurations with the molecular plane parallel to the surface and different registry for the Fe atom. Both adsorption

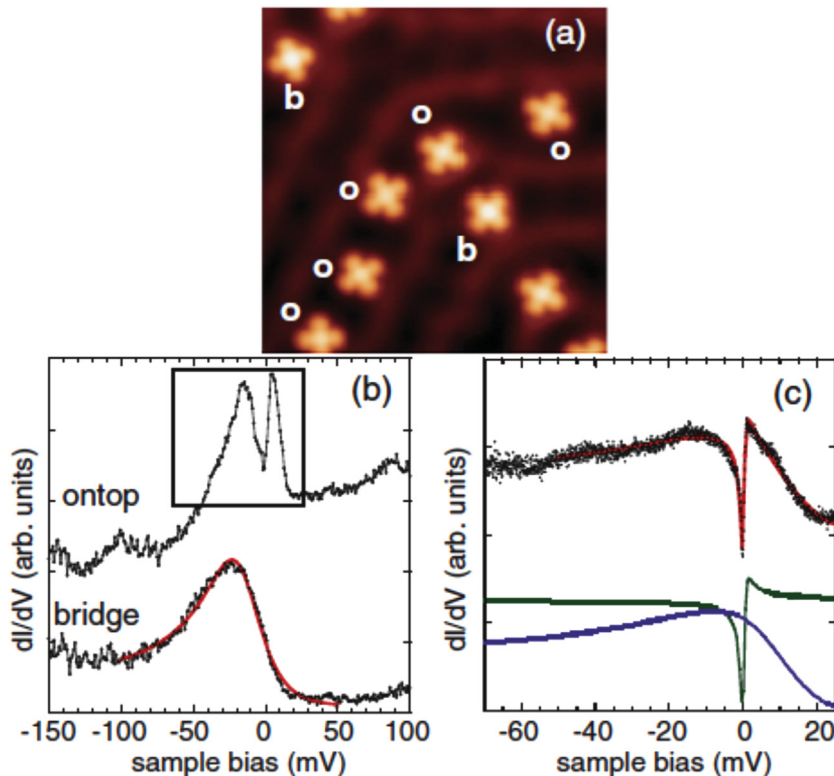


Fig. 48. (a) The topographic STM image of FePc on Au(111) taken at 0.4 K with the tunneling current $I_t=100$ pA and the sample bias $V_s=-0.1$ V. The image size is $15\text{ nm} \times 15\text{ nm}$. The on top and bridge species are specified by o and b, respectively. (b) The STS spectra were taken for both species at 0.4 K by keeping the feedback off, respectively. The red curve for the bridge species is a fit to a Fano function and gives a $T_K=200$ K. (c) High-resolution spectrum for the on top species taken in the region marked by a rectangle in (b) [The dip in (b) is broadened by using larger V_{rms}]. The green and purple curves are calculated by Fano functions and gives Kondo temperatures of $T_K=2.6$ K and $T_K=110\text{--}150$ K. The overall spectral shape is well reproduced by the linear combination (red curve) of the green and purple curves. Adapted from [202] with permission. (For interpretation of the references to color in this figure legend, the reader is referred to the web version of this article.)

configurations show characteristic spectral features near E_F (Fig. 48 (b) and (c)). For the on-top configuration species, a broad peak appears accompanied by a sharp dip structure inside the peak (top spectra in Fig. 48(b)). In contrast, only a broad peak is observed for the bridge species (low spectra in Fig. 48(b)). The spectral feature of the on-top species is well reproduced by two Fano functions, suggesting the existence of two channels for the screening of the molecular spin. The dip structure reflects the low-T Kondo channel with a temperature of $2.6\text{ K} \pm 1.4\text{ K}$ while the broad peak corresponds to the high-T Kondo channel with a temperature in the range of 110–150 K as estimated from the width by Minamitani and co-workers [202]. The broad peak observed for the bridge species is also reproduced by the Fano function and the plausible origin is a Kondo resonance with a $T_K \sim 200$ K.

To gain insight on the origin of the spectra features the authors perform measurements of the dependence of the Kondo resonance with the magnetic field applied perpendicular and parallel to the sample surface. They compare the results with ab-initio theoretical calculations. The overall LDOS features for both configurations are very similar to each other, the main difference occurs for the d_x orbitals. The peaks of the d_{zx} and d_{yz} orbitals of the top species overlap each other whereas they are separated by 100 meV for the bridge species. The origin of this difference is the local symmetry of the adsorption site. For the top configuration the fourfold symmetry is kept locally around the Fe atom and this allows the survival of the orbital degrees of freedom as reported by X-ray magnetic circular dichroism [203]. On the contrary for the bridge species the local symmetry for the ligand around the Fe atom is reduced to twofold (Fig. 2 in Ref. [202]). These results emphasize the influence of the registry between the adsorbed molecules and the substrate in the Kondo screening process.

The Kondo effect arises from the exchange interaction between the localized spins of magnetic impurities and the conduction electrons in the host metal and for this reason the characteristics of the LDOS of the surface are relevant in the screening process of the magnetic impurity. There are several ways to tailor the LDOS of the metallic host around the Fermi level, like quantum size effects, superconductivity or nanostructuring of the metallic surface.

It has been shown that quantum size effects (QSE) in ultra-thin films grown on metals [204–206] or semiconductors [207,208] strongly modifies the DOS at the Fermi level. Growing Pb films at low temperature makes possible to choose the thickness of the Pb films to place the quantum well states close or far away of the Fermi level and therefore changing the DOS of the metallic substrate. Fu et al. [209] deposited manganese phthalocyanine (MnPc) on Pb films grown at low temperature on Si(111). Using the STM tip the authors are able to move the MnPc molecules to areas of the sample with different local Pb thickness. The surface LDOS of the different areas of the sample are characterized locally by means of spatially resolved scanning tunneling spectroscopy and in the same experiment the dI/dV spectra are measured on the MnPc molecules deposited on those areas. The dI/dV spectra show features close to the Fermi level that can be fitted using a Fano line shape and the extracted Kondo temperatures oscillate with a well-defined period of 2 ML. The lowest value for the Kondo temperature occurs for the molecules located over 15 ML of Pb and the highest corresponds to 17 ML of Pb. This result highlights the importance of the LDOS of the surface in the Kondo process.

Recently, Franke et al. [210] have studied the competition of Kondo screening and superconductivity in MnPc layers grown on Pb(111) using Pb terminated tips, finding a site dependent interaction with a modulation length in the nanometer scale. Magnetic

and superconducting interaction couple electrons together and at the atomic scale both interactions can coexist and compete. By means of spatially resolved scanning tunneling spectroscopy performed at low temperature, Franke and co-workers show that MnPc deposited on Pb(111) can lie in two magnetic states as a consequence of the competition between the Kondo screening and the superconducting pair-breaking interactions. Both ground states alternate with a nanometer periodicity to form a moiré superstructure. When a magnetic adatom or molecule is adsorbed on the surface of a superconductor, its magnetic moment can interact with itinerant electrons, with spin 1/2 and with Cooper pairs that have a total spin $S=0$. Normal state electrons screen the magnetic moment of the impurity producing a Kondo resonance at the Fermi level in the dI/dV spectra. Simultaneously the magnetic impurity weakens the local coherence of the superconducting state by the creation of spin-polarized bound states in its proximity. These states appear as narrow resonances inside the superconducting energy gap, and their energy position of these resonances reflects the pair-breaking exchange interaction strength of the magnetic impurity with the Cooper pairs. Franke and co-workers have been able to measure simultaneously the energy position of the resonance inside the superconducting gap or the Pb(111) substrate and the Kondo resonance of the MnPc molecules. From the data it is clear that the MnPc molecules lie in one of the two ground states forming a quasi-periodic moiré pattern, revealing that their different quantum state is tuned by small variations of their interaction with the superconducting substrate. The resulting structure is a molecular arrangement where superconductivity and magnetism alternate at nanometer length scales.

Another way to engineer the surface LDOS is to nanostructure the surface by growing an overlayer of other material with a different lattice parameter. The overlap produces a moiré pattern that modifies periodically the properties of the surface. An example of this is obtained by the epitaxial growth of graphene on Ru(0001). The surface presents a new hexagonal super periodicity with distances of 3 nm due to the presence of a moiré pattern. The change in registry and stacking sequence associated to the moiré pattern produces a spatial modulation in the interaction between the C and the Ru atoms, going from a weak van der Waals to strong covalent interaction [211,212]. Three areas can be distinguished in the moiré pattern, the so called HCP-Top and FCC-Top for the strong interacting areas and the weak van der Waals interaction area respectively. The graphene overlayer is p-doped due to interaction with the Ru(0001) surface, as a consequence, when electron acceptor molecules, i.e. 7,7,8,8-tetracyano-*p*-quinodimethane (TCNQ), are deposited on the surface, one electron is transferred from the substrate to the molecule [213] and the resulting singly charged molecules develop a sizeable magnetic moment. Due to the low reactivity of the surface, TCNQ molecules adsorb with the molecular plane parallel to the surface and the molecular orbitals are undisturbed. For low coverages all the molecules are adsorbed on the low areas of the moiré, most of them on the HCP-Top regions and few of them on the bridge between the HCP-Top and the FCC-Top areas. The dI/dV spectra measured on molecules adsorbed on the FCC-Top and bridge positions present a feature at the Fermi level that can be fitted with a Fano line shape [46], while the molecules adsorbed on the HCP-Top areas do not present any feature. The temperature dependence of the intensity and width of this feature indicates that it is the manifestation of a Kondo screening process. The difference between both adsorption configurations is the local density of states around the Fermi level produced by the difference in the stacking sequence between graphene and the Ru(0001) atomic layers. DFT calculations show the existence of an interface state in the HCP-Top areas which becomes a surface resonance in the FCC-Top areas. The main difference is the amplitude of the state at the different atomic layers on both areas. The large amplitude of the surface resonance in the HCP-

Top areas favors a large hybridization with the TCNQ LUMO that becomes a broad resonance for both spin components, show negligible splitting and, as consequence, the magnetic moment of the charged TCNQ is quenched. On the contrary, the surface resonance presents smaller amplitude at the surface layer in the FCC-Top areas, thus reducing the overlap with the TCNQ molecules and preserving their magnetic moment. This provides an explanation for appearance of the Kondo feature in the dI/dV curves measured on the TCNQ molecules adsorbed on the different areas. Identical behavior is observed for another electron acceptor molecules, F_4 -TCNQ, deposited on the same surface [45].

The effect of organic ligands and interfacial charge transfer on the Kondo state is a rather complex problem. It has been addressed by Perera *et al.* depositing TBrPP-Co on Cu(111) [214]. TBrPP-Co molecules have their spin mainly localized at the Co atoms. Upon adsorption on Cu(111) the entire molecule becomes spin active because the organic ligands acquired spin polarization. dI/dV spectra measured in the middle of the molecules reveal the Kondo state as a dip with a width of 25 mV at the Fermi level. The dI/dV maps reveal that the entire porphyrin exhibits a Kondo signal, this behavior is observed on both isolated molecules and self-assembled molecules on the Cu(111) surface. The authors interpret this as an indication that the observed Kondo phenomenon is driven by the molecule-substrate interaction and the redistribution of the charge transferred from the substrate. The dI/dV spectra measured on different areas of a single molecule reveals changes in the Kondo temperature ranging from 107 K up to 212 K. Surprisingly the highest Kondo temperature is found when the STM tip is located over near a bromophenyl unit and not on the Co atom in the middle of the molecules. Based in DFT calculations the authors identify the mechanism for the appearance of the Kondo effect on the whole molecule. For TBrPP-Co on Cu(111) the copper atoms from the surface stabilize the double occupation of a $3d_z^2$ orbital from the cobalt atom that is located close to the surface Fermi level and has a maximal overlap with the surface. Charge transfer to the molecule changes the ligand field and this induces a transition from $3d^7$ Co(II) to $3d^8$ Co(I). It also produces the reorganization of the spin density that originally was located on the doublet Co(II) center, inducing the delocalization of the spin density and its redistribution on the porphyrin rings.

Another molecules that present a spin redistribution on the organic ligands upon adsorption are CuPc and NiPc deposited on Ag(100) [215]. Both molecules adsorb on Ag(100) with the macrocycle plane parallel to the surface and rotated by 30° respect to the [110] direction. Due to the lack of mismatch between the $d_{x^2-y^2}$ orbital and the substrate there is no charge transfer between the Cu or Ni atom and the surface, preserving both the spin of the free molecule ($S=1/2$ for the Cu and $S=0$ for the Ni). As can be seen in Fig. 49(a) and (b) the dI/dV spectra measured on the outer benzene rings present a strong zero-bias resonance, which reduces drastically towards the molecular center (Fig. 49(c)). From this results the authors conclude that the screened spin is not localized at the metal ion but delocalized in the molecular ligand states, independently of the spin of the free molecules.

The dI/dV spectra measured in a broad energy range allow the authors to identify the energy position of the HOMO and LUMO of the molecules. Charge transfer from the Ag substrate to the molecules results in the partial occupation of the gas-phase LUMO, which appears as a double-peak structure separated by 0.65 eV around the Fermi level (see Fig. 1 in Ref. [215]). This is characteristic of a partially filled orbital with Coulomb repulsion U separating the states with single and double occupancy.

Mugarza and co-workers also explore the influence of intermolecular interactions. Several studies have shown that Kondo temperature of metal-organic complexes can be manipulated by locally modifying the ligand field acting on the transition-metal ions

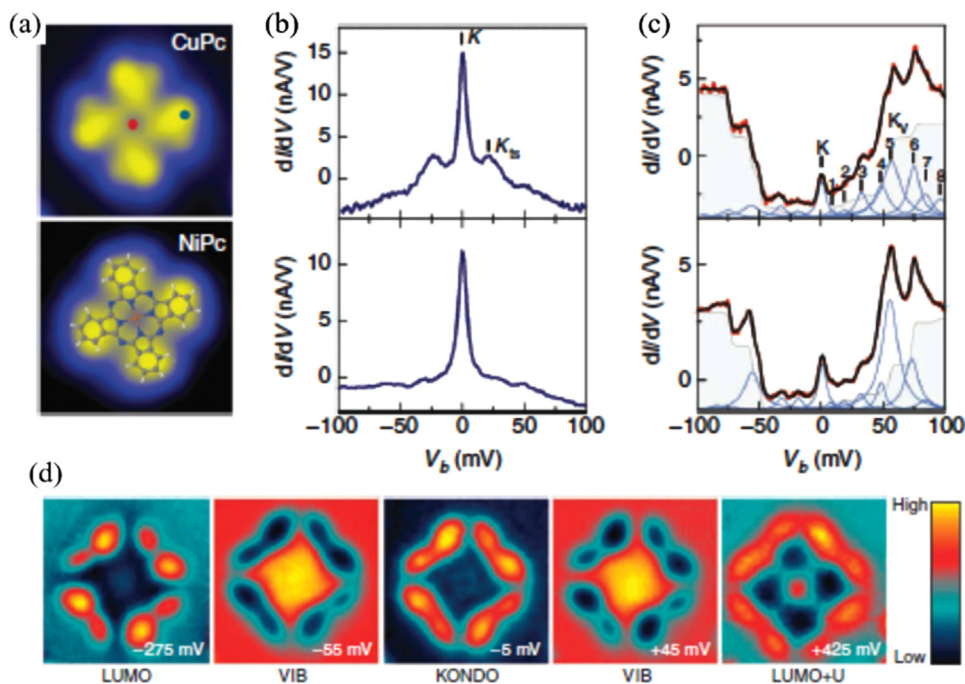


Fig. 49. (a) STM image of single CuPc (top, $I_t=72$ pA, $V_b=-5$ mV) and NiPc (bottom, $I_t=100$ pA, $V_b=-3$ mV), image size $2.5 \text{ nm} \times 2.5 \text{ nm}$. The diagram superposed to NiPc indicates the position of the metal (orange), C (grey), N (blue), and H (white) atoms. (b) dI/dV spectra of CuPc (top) and NiPc (bottom) around EF measured on benzene (blue dot) and (c) on Cu and Ni ions (red dot) ($I_t=2$ nA/1.1 nA, $V_b=-100$ mV for CuPc/NiPc). Labels denote Kondo resonances of different nature: zero-bias (K), triplet-singlet (K_t), and vibrational (K_v). Black solid lines in c are fits to the data using the sum of Lorentzian (blue) and step functions (shaded). (d) dI/dV maps of the molecular orbitals, Kondo and inelastic vibrational signals. The intensity in each map is scaled independently for maximum contrast. (For interpretation of the references to color in this figure legend, the reader is referred to the web version of this article.)

[199] or by screening the surface electron density around molecular adsorbates by other molecules [216]. For CuPc and NiPc on Ag(100) the authors show that the presence of a sizeable spin density on the organic ligand depends on the number of neighbors of the molecules. This number can be artificially manipulated by assembling molecular islands of different size and shape. The increase in the number of nearest neighbor molecules decouples gradually the molecules from the substrate, and the Kondo effect is quenched for molecules with 3 or more nearest molecular neighbors.

Chemical doping has been used to tailor the properties of organic molecular compounds. Using scanning tunneling microscopy and spectroscopy and using Li atoms as dopants Krull and co-workers [217] have been able to probe the charge transfer between the Li dopants and the CuPc and NiPc deposited on Ag(111). Both molecules, NiPc and CuPc present a Kondo resonance at the Fermi level in the dI/dV spectra measured on the molecules. When one Li atom is attached in specific positions to the molecules a charge transfer process takes place and the Kondo resonance disappears, the authors are able to determine the location of the transferred electron imaging the spatial distribution of the frontier molecular orbitals of the resulting molecular species.

Kondo lattice systems can exhibit unusual behavior that results from the interplay between onsite Kondo screening and indirect coupling between the impurity spins mediated by the conduction electrons of the host metal. The Kondo effect in single impurities suppress the magnetic moments, whereas the coupling between spins mediated by the conduction electrons stabilizes the magnetic ordering between spins. Two-dimensional Kondo lattices can be formed on metal surfaces by self-organization of molecules. Iron (II) phthalocyanine (FePc) deposited on Au(111) form a superlattice and the spectral evolution of Kondo resonance for FePc on Au(111) has been studied from isolated molecules to the superlattice by means of scanning tunneling spectroscopy [218]. As mentioned above, FePc adsorbed on Au(111) adopts two adsorption configurations called on-top and bridge [201,202]. The dI/dV

spectra measured on isolated molecules on the on-top configuration as a dip at the Fermi level. From the fitting of the dip a Kondo temperature of 2.6 K is obtained [202]. The STS spectra changes as the molecules form 2D islands. The spectra measured on each molecule presents a dip at the Fermi level whose shape depends on the number of nearest neighbors. Those molecules with two nearest neighbors presents a spectra almost identical to the one measured on isolated molecules, while the dip broadens gradually for three and four nearest neighbors. For larger clusters, the molecules at the edges present single dip that depends on the number of neighbors while the molecules at the center presents a double dip. The authors interpret this behavior as an evidence of the role of the Ruderman-Kittel-Kasuya-Yosida (RKKY) coupling after discarding the magnetic dipole interaction and the direct exchange coupling due to the overlap of 3d orbitals due to the large distance between neighbor molecules (1.47 nm). The behavior of the dip and the appearance of a double dip is explained by the authors using theoretical studies of a two-body Kondo system interacting through the RKKY coupling. It has been calculated that the antiferromagnetic (AFM) RKKY coupling broadens the Kondo resonance and reduces the intensity and in the strong coupling regime splits the peak, while a ferromagnetic (FM) coupling narrows the peak (see Ref. [218] and reference therein). The coupling driven by the surface electrons is AFM, FM and weak AFM for first, second and third nearest neighbors. The authors calculate the strength in the interactions and found that the nearest neighbor interaction is almost 5 times larger the one corresponding to the second nearest neighbor and therefore they conclude that the spectral evolution of the Kondo resonance with the number of neighbors can be rationalized using an antiferromagnetic RKKY coupling between the spin of the molecules.

Another example of Kondo lattice is a self-assembled monolayer of O_2 molecules adsorbed on the Au(110) surface at 10 K [219]. In this case the weak interaction between the gold surface and the O_2 molecules preserves the magnetic ground state of the O_2 molecules

in gas phase and leads to a Kondo resonance at the Fermi level. In gas phase the O_2 molecules present a magnetic moment of $2 \mu_B$ and the calculated magnetic moment for the molecules adsorbed on Au (110) is basically the same. The monolayer forms a ferromagnetic ground state with a rather weak exchange interaction due to the large distance between O_2 molecules. The molecules self-assemble on the surface forming two types of chains (see Ref. [219] for details). By means of spatially resolved scanning tunneling spectroscopy the authors visualized the interplay between the onsite Kondo screening and the intersite coupling, using the Kondo resonance as a local probe. The observation of Kondo screening delocalized over the entire surface and the dependence on the intermolecular distance of the coherence temperature, which is related with the intersite coupling strength [220], provides information concerning the intersite coupling in the O_2 lattice. The authors also found an enhancement on the Kondo signal between O_2 molecules, resembling the hybridization between atomic orbitals.

Recently it has been shown that metal free stable hydrocarbon π radicals deposited on Au(111) at low temperature present a Kondo resonance on the spectra measured with STS [221]. The deposition of α,γ -bis(diphenylene- β -phenylallyl) (BDPA) on Au(111) at low temperature does not affect the spin 1/2 of the free radical. The BDPA radical self-assemble in 1D chains on the surface. A typical dI/dV spectra measured on BDPA shows a narrow dip at the Fermi level. With the temperature evolution in the intensity and width of the dip the authors identify the spectra feature as the fingerprint of a Kondo resonance with a temperature of 54 K for BDPA dimers. The authors conclude that the two BDPA of a dimer are individual spin-1/2 Kondo systems correlated through the substrate.

Another example of Kondo physics for a $S=1/2$ impurity in the weak coupling regime is $C_{28}H_{25}O_2N/Au(111)$ [222]. In this case, the unpaired electron is spatially delocalized over the nitronyl-nitroxide side group of the radical instead of being localized in a

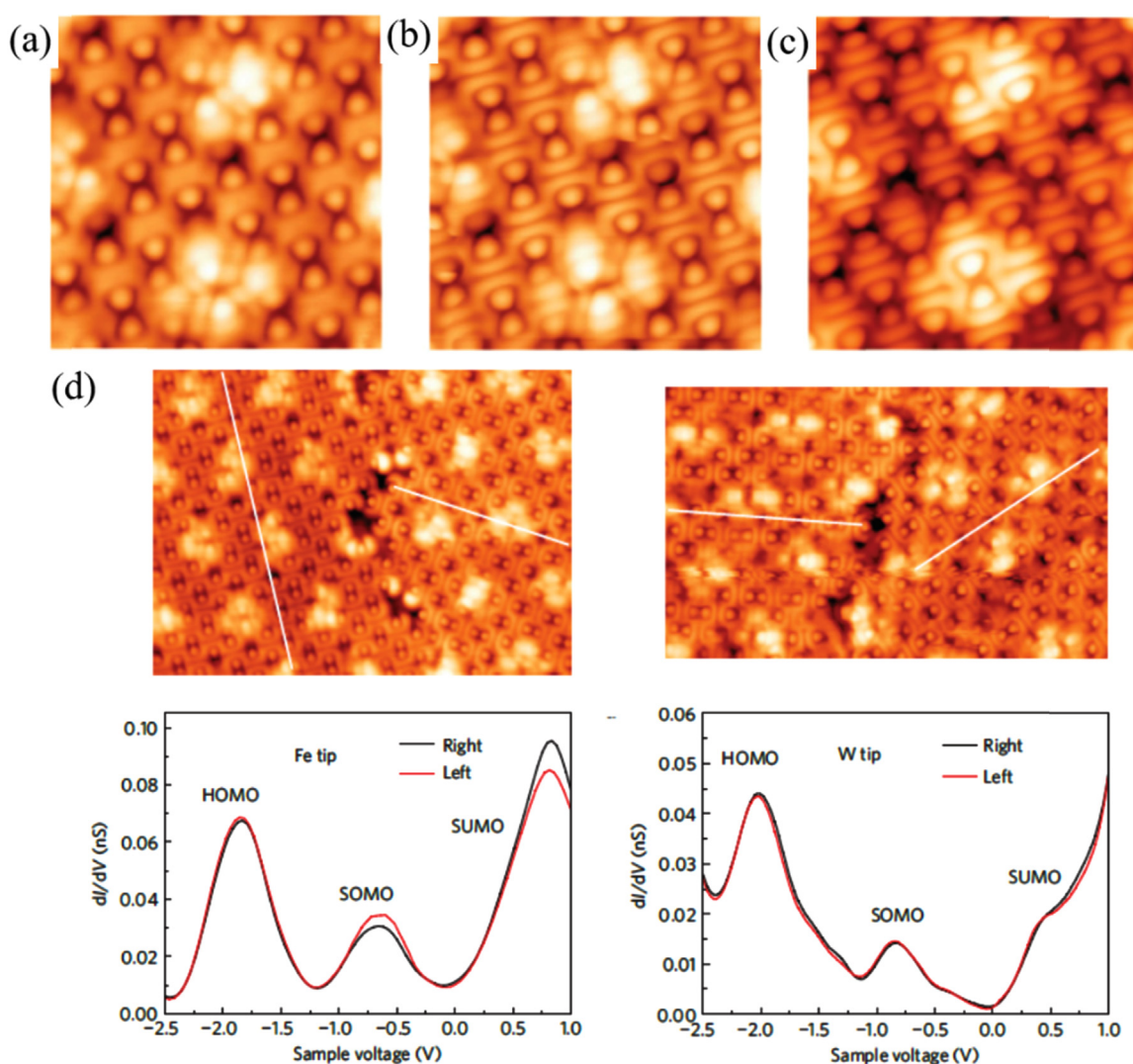


Fig. 50. Spatially extended intermolecular bands in a TCNQ monolayer adsorbed on graphene/Ru(0001). (a–c), Topographic STM images of a TCNQ monolayer on graphene/Ru(0001) recorded at $V_b = -2V$ (a), $V_b = -0.8V$ (b) and $V_b = +1.0V$ (c). (d) Upper panels STM topographic images (left: $16.7\text{ nm} \times 12.1\text{ nm}$ and right: $14\text{ nm} \times 8.5\text{ nm}$) of a TCNQ monolayer on graphene/Ru(0001) recorded the left panel with a spin-polarized tip and at $V_b = +1.5V$ and $I_t = 100\text{ pA}$, and the right panel with clean W tip and at $V_b = +1.5V$ and $I_t = 50\text{ pA}$, showing two molecular domains aligned in different directions with respect to the scanning axis. Lower panels show on the left Spin-polarized dI/dV curves averaged over three unit cells of the moiré superstructure for the left and right domains of the upper panel (red and black curves respectively). The individual curves have been taken at 4.6 K using an Fe-coated W tip with the tunneling gap stabilized at $V_b = +1.5V$ and $I_t = 100\text{ pA}$. The three peaks correspond to the HOMO (at $-1.8V$), SOMO (at $-0.7V$) and SUMO (at $+0.7V$) bands. Right panel, Spin-integrated dI/dV curves averaged over three unit cells of the moiré superstructure for the left and right domains of the upper panel (red and black curves respectively). The individual curves have been taken at 4.6 K using a W tip with the tunneling gap stabilized at $V_b = +1.5V$ and $I_t = 50\text{ pA}$. The peaks correspond to the HOMO, SOMO and SUMO bands. The white lines in the topographic panels indicate the long axis of the TCNQ molecules in the molecular domains. (For interpretation of the references to color in this figure legend, the reader is referred to the web version of this article.)

particular atom, stabilizing it against chemical reaction and charge transfer, which would quench the spin of the system. The lack of orbital degeneracy makes this system an ideal example of pure spin-1/2. The dI/dV spectra measured on the radicals at different temperatures from 1.5 K by means of spatially resolved STS show a sharp and pronounced peak at the Fermi energy, corresponding to a Kondo temperature of about 16 K. Assuming the strong limit coupling for the spin-1/2, the Kondo resonance should split in presence of a magnetic field larger than 6 T. On the contrary, the authors found a splitting for magnetic field larger than 2 T. The authors interpret this behavior as an indication of the strength in the coupling between the magnetic impurity and the conduction electrons of the substrate. From this results the authors conclude that in order to fully characterize a Kondo system the dependence of the resonance with temperature and magnetic field should be taken into account.

The Kondo resonance has been observed in a single molecular layer of a purely organic charge-transfer salt grown on Au(111) [31]. The codeposition of tetrahydrofulvalene (TTF) and TCNQ with the substrate held at room temperature, produce TTF-TCNQ layers with 1:1 stoichiometry. The differential conductance spectra measured on top of the TCNQ molecules show a prominent peak at the Fermi level that is completely absent on the TTF molecules. Changing the sample temperature and studying the evolution of the peak present at the Fermi level on the spectra measured on the TCNQ molecules the authors identify the peak as a Kondo resonance. The origin of the Kondo resonance is ascribed to charge reorganization in the molecular layer that leads to a single electron in the LUMO of the TCNQ molecules. The localization of the electron in the molecular orbital is possible because the TCNQ⁻ anions are decoupled from the metal due to the lateral interaction with the electron donor TTF molecules. The Kondo resonance has a strong dependence on the location within the TCNQ molecules, the highest intensity is found on the C(CN)₂ terminations, at the center of the molecule the amplitude is smaller and appears with two characteristic side peaks at ± 41 meV. This side peaks are interpreted as Kondo assisted inelastic tunneling.

As discussed in the previous Section (See Fig. 42), in this system a combination of spatially resolved scanning tunneling microscopy and theoretical calculations show the formation of an interface state from the complex mixing of metal and molecular states. The *k* dependence of the interface state, measured by studying the spatial distribution around defects at different energies, reveals that an anisotropic band dispersion, related to the structure of the molecular layer (see Fig. 42). The origin of the bands can be traced back to the mixture of the bulk and surface states from the metal and the TTF states. The authors suggest that tuning the strength of donor-metal (TTF-metal) interaction or the spacing between the TTF rows may allow to engineer the organic-inorganic interface and hence the functionality of the molecular thin film.

It has been shown that individual TCNQ molecules deposited on graphene grown on Ru(0001) acquire charge that is located in LUMO of the neutral molecule which splits into a single occupied molecular orbital (SOMO) and a single unoccupied molecular orbital (SUMO), as a consequence the TCNQ molecules develop a sizeable magnetic moment of 0.4 μ_B [45,46,213,223]. The magnetic moment is not quenched by the formation of dimers or larger supramolecular structures up to the full monolayer, with a value of 0.18 μ_B . The TCNQ molecules self-assembly via the formation of hydrogen bonds and develop spatially extended electronic bands which origin can be traced back to the corresponding molecular orbitals, as can be seen in Fig. 50(a–c) [223]. According to the DFT calculations presented by the authors, for the TCNQ monolayer adsorbed on graphene on Ru(0001) the magnetically ordered structure is energetically favored, with an average magnetic moment per molecule of 0.18 μ_B . An analysis of the spin density

indicates that the origin of the magnetic moment is due to unpaired spin up electrons in the almost completed filled SOMO-derived band, whereas the spin-down counterpart (SUMO-derived) is rather empty. It was predicted some time ago that the ground state for a system with a half-filled (nearly) flat bands is ferromagnetic [224–226]. By means of spin-polarized scanning tunneling microscopy and spectroscopy the authors test this predictions on samples having different molecular domains. The upper panels in Fig. 50(d) shows the constant current topographic image of the frontier between those domains, the left images is measured using a spin-polarized STM tip while the right images is measured using a clean W tip. Lower left panel on Fig. 50 (d) compares the spin-resolved dI/dV curves averaged over more than 30 molecules measured on the two domains simultaneously with the topographic images shown in the upper panel. The spin-polarized spectrum shows three characteristic peaks identified as the HOMO, SOMO and SUMO derived bands. While the intensity of the doubly occupied HOMO band does not change from one domain to the other, the intensity of the singly occupied SOMO and SUMO bands change from one domain to the other and the contrast is inverted between them as expected from the spin population of both bands. On the lower left panel in Fig. 50(d) the dI/dV curves measured with a clean W tip, as expected no difference in the intensity of the HOMO, SOMO and SUMO peaks is detected. Garnica and co-workers conclude that these results indicates the existence of long range magnetic order in the purely organic 2D layer of TCNQ molecules.

7. General conclusions

The analysis of the cases presented in this review show that the physical and chemical properties of electroactive molecules are modified in important ways when they are adsorbed on solid surfaces due to the exchange of electrons with the substrate. Since most of the technologically relevant organic molecules are strong electron donors or electron acceptors, this demonstrates that the interfaces between the electronic leads and the active material are going to be severely affected by such electron-transfer processes. Thus, understanding all such processes seems the way for a rational design of optoelectronic devices.

In this respect, the research carried out over the last decade has made impressive progress towards the understanding of adsorption, self-assembly and electronic processes involved in the formation of organic/metal interfaces. A very rich phenomenology has been found, including new substrate-mediated interactions, unprecedented chemical pathways for adsorbed organic molecules and exotic electronic behavior. Much is however still open for debate: the effect of charge-transfer in the catalytic role of solid surfaces to promote covalent binding of organic adsorbates, a more clear quantification of intermolecular versus molecule-substrate charge transfer processes or the interplay between molecular vibrations and Kondo responses are just a few examples of interesting questions that will need to be answered in forthcoming years. We hope that the ideas exposed in this review will contribute to the clarification of some key issues and the identification of some important problems that researches must face in the next future.

References

- [1] S. Reineke, F. Lindner, G. Schwartz, N. Seidler, K. Walzer, B. Lussem, K. Leo, *Nature* 459 (2009) 234.
- [2] M.J. Malachowski, J. Zmija, *Opto-Electron. Rev.* 18 (2010) 121.
- [3] P.W.M. Blom, V.D. Mihailetschi, L.J.A. Koster, D.E. Markov, *Adv. Mater.* 19

- (2007) 1551.
- [4] M. Gratzel, *Nature* 421 (2003) 586.
- [5] P. Lin, F. Yan, *Adv. Mater.* 24 (2012) 34.
- [6] M.C. Scharber, N.S. Sariciftci, *Prog. Polym. Sci.* 38 (2013) 1929.
- [7] C.A. Wolfgang Brütting, *Physics of Organic Semiconductors*, Wiley-VCH Verlag GmbH & Co., Weinheim, 2013.
- [8] E. Goiri, P. Borghetti, A. El-Sayed, J.E. Ortega, D.G. de Oteyza, *Adv. Mater.* 28 (2016) 1340.
- [9] H. Ishii, K. Sugiyama, E. Ito, K. Seki, *Adv. Mater.* 11 (1999) 605.
- [10] S. Braun, W.R. Salaneck, M. Fahlman, *Adv. Mater.* 21 (2009) 1450.
- [11] C.D. Dimitrakopoulos, P.R.L. Malenfant, *Adv. Mater.* 14 (2002) 99.
- [12] J.V. Barth, *Annu. Rev. Phys. Chem.* 58 (2007) 375.
- [13] L. Bartels, *Nat. Chem.* 2 (2010) 87.
- [14] J.V. Barth, G. Costantini, K. Kern, *Nature* 437 (2005) 671.
- [15] S. DeFeyter, F.C. DeSchryver, *J. Phys. Chem. B* 109 (2005) 4290.
- [16] R. Otero, J.M. Gallego, A.L.V. de Parga, N. Martín, R. Miranda, *Adv. Mater.* 23 (2011) 5148.
- [17] J. Lehn, *Supramolecular Chemistry: Concepts and Perspectives*, VCH-Wiley, Weinheim, 1995.
- [18] J.V. Barth, J. Weckesser, C. Cai, P. Günter, L. Bürgi, O. Jeandupeux, K. Kern, *Angew. Chem. Int. Ed.* 39 (2000) 1230.
- [19] R. Otero, M. Schöck, L.M. Molina, E. Laegsgaard, I. Stensgaard, B. Hammer, F. Besenbacher, *Angew. Chem. Int. Ed.* 44 (2005) 2270.
- [20] D. Eciya, R. Otero, L. Sanchez, J. Gallego, Y. Wang, M. Alcamí, F. Martín, N. Martín, R. Miranda, *Angew. Chem. Int. Ed.* 46 (2007) 7874.
- [21] J.A. Theobald, N.S. Oxtoby, M.A. Phillips, N.R. Champness, P.H. Beton, *Nature* 424 (2003) 1029.
- [22] J.V. Barth, *Surf. Sci.* 603 (2009) 1533.
- [23] S. Clair, S. Pons, H. Brune, K. Kern, J.V. Barth, *Angew. Chem. Int. Ed.* 44 (2005) 7294.
- [24] S. Stepanow, M. Lingenfelder, A. Dmitriev, H. Spillmann, E. Delvigne, N. Lin, X. Deng, C. Cai, J.V. Barth, K. Kern, *Nat. Mater.* 3 (2004) 229.
- [25] M. Schock, R. Otero, S. Stojkovic, F. Hummelink, A. Gourdon, E. Laegsgaard, I. Stensgaard, C. Joachim, F. Besenbacher, *J. Phys. Chem. B* 110 (2006) 12835.
- [26] S. De Feyter, F.C. De Schryver, *Chem. Soc. Rev.* 32 (2003) 139.
- [27] D. Jerome, *Chem. Rev.* 104 (2004) 5565.
- [28] H. Seo, C. Hotta, H. Fukuyama, *Chem. Rev.* 104 (2004) 5005.
- [29] G. Heimel, S. Duhm, I. Salzmann, A. Gerlach, A. Strozecka, J. Niederhausen, C. Bürker, T. Hosokai, I. Fernandez-Torrente, G. Schulze, et al., *Nat. Chem.* 5 (2013) 187.
- [30] N. Gonzalez-Lakunza, I. Fernández-Torrente, K.J. Franke, N. Lorente, A. Arnau, J.I. Pascual, *Phys. Rev. Lett.* 100 (2008) 156805.
- [31] I. Fernández-Torrente, K.J. Franke, J.I. Pascual, *Phys. Rev. Lett.* 101 (2008) 217203.
- [32] J.L. Cabellos, D.J. Mowbray, E. Goiri, A. El-Sayed, L. Floreano, D.G. de Oteyza, C. Rogero, J.E. Ortega, A. Rubio, *J. Phys. Chem. C* 116 (2012) 17991.
- [33] A. El-Sayed, P. Borghetti, E. Goiri, C. Rogero, L. Floreano, G. Lovat, D. J. Mowbray, J.L. Cabellos, Y. Wakayama, A. Rubio, et al., *ACS Nano* 7 (2013) 6914.
- [34] B. Stadtmüller, C. Henneke, S. Soubatch, F.S. Tautz, C. Kumpf, *New J. Phys.* 17 (2015) 023046.
- [35] B. Stadtmüller, D. Lüftner, M. Willenbockel, E.M. Reinisch, T. Sueyoshi, G. Koller, S. Soubatch, M.G. Ramsey, P. Puschnig, F.S. Tautz, et al., *Nat. Commun.* 5 (2014) 3685.
- [36] N. Koch, A. Gerlach, S. Duhm, H. Glowatzki, G. Heimel, A. Vollmer, Y. Sakamoto, T. Suzuki, J. Zegenhagen, J. Rabe, et al., *J. Am. Chem. Soc.* 130 (2008) 7300.
- [37] A.D. Pia, M. Riello, A. Floris, D. Stassen, T.S. Jones, D. Bonifazi, A.D. Vita, G. Costantini, *ACS Nano* 8 (2014) 12356.
- [38] C. Urban, Y. Wang, J. Rodríguez-Fernández, R. García, M. Angeles Herranz, M. Alcamí, N. Martín, F. Martín, J.M. Gallego, R. Miranda, et al., *Chem. Commun.* 50 (2014) 833.
- [39] T. Tseng, C. Urban, Y. Wang, R. Otero, S.L. Tait, M. Alcamí, D. Eciya, M. Trelka, J. M. Gallego, N. Lin, et al., *Nat. Chem.* 2 (2010) 374.
- [40] G.M. Ränger, O.T. Hofmann, L. Romaner, G. Heimel, B. Broker, R. Blum, R. L. Johnson, N. Koch, E. Zojer, *Phys. Rev. B* 79 (2009) 165306.
- [41] L. Romaner, G. Heimel, J. Bredas, A. Gerlach, F. Schreiber, R.L. Johnson, J. Zegenhagen, S. Duhm, N. Koch, E. Zojer, *Phys. Rev. Lett.* 99 (2007) 256801.
- [42] S. Bedwani, D. Wegner, M.F. Crommie, A. Rochefort, *Phys. Rev. Lett.* 101 (2008) 216105.
- [43] C. Urban, Y. Wang, J. Rodríguez-Fernández, M.Á. Herranz, M. Alcamí, N. Martín, F. Martín, J.M. Gallego, R. Otero, R. Miranda, *J. Phys. Chem. C* 118 (2014) 27388.
- [44] I. Fernández-Torrente, S. Monturet, K.J. Franke, J. Fraxedas, N. Lorente, J. I. Pascual, *Phys. Rev. Lett.* 99 (2007) 176103.
- [45] M. Garnica, F. Calleja, A.L. Vázquez, de Parga, R. Miranda, *Surf. Sci.* 630 (2014) 356.
- [46] M. Garnica, D. Stradi, F. Calleja, S. Barja, C. Díaz, M. Alcamí, A. Arnau, A. L. Vázquez de Parga, F. Martín, R. Miranda, *Nano Lett.* 14 (2014) 4560.
- [47] T. Choi, S. Bedwani, A. Rochefort, C. Chen, A.J. Epstein, J.A. Gupta, *Nano Lett.* 10 (2010) 4175.
- [48] R. Forker, T. Fritz, *Phys. Chem. Chem. Phys.* 11 (2009) 2142.
- [49] J.O. Ossó, F. Schreiber, M.I. Alonso, M. Garriga, E. Barrena, H. Dosch, *Org. Electron.* 5 (2004) 135.
- [50] J. Carrasco, A. Michaelides, M. Forster, S. Haq, R. Raval, A. Hodgson, *Nat. Mater.* 8 (2009) 427.
- [51] G. Greczynski, M. Fahlman, W.R. Salaneck, *Chem. Phys. Lett.* 321 (2000) 379.
- [52] I.G. Hill, A. Rajagopal, A. Kahn, Y. Hu, *Appl. Phys. Lett.* 73 (1998) 662.
- [53] A. Kahn, N. Koch, W. Gao, *J. Polym. Sci. Part B Polym. Phys.* 41 (2003) 2529.
- [54] S. Narioka, H. Ishii, D. Yoshimura, M. Sei, Y. Ouchi, K. Seki, S. Hasegawa, T. Miyazaki, Y. Harima, K. Yamashita, *Appl. Phys. Lett.* 67 (1995) 1899.
- [55] R. Smoluchowski, *Phys. Rev.* 60 (1941) 661.
- [56] N.D. Lang, W. Kohn, *Phys. Rev. B* 3 (1971) 1215.
- [57] X. Crispin, V. Geskin, A. Crispin, J. Cornil, R. Lazzaroni, W.R. Salaneck, J. Bredas, *J. Am. Chem. Soc.* 124 (2002) 8131.
- [58] G. Witte, S. Lukas, P.S. Bagus, C. Wöll, *Appl. Phys. Lett.* 87 (2005) 263502.
- [59] P.S. Bagus, K. Hermann, C. Wöll, *J. Chem. Phys.* 123 (2005) 184109.
- [60] N. Koch, A. Kahn, J. Ghijsen, J.-J. Pireaux, J. Schwartz, R.L. Johnson, A. Elschner, *Appl. Phys. Lett.* 82 (2003) 70.
- [61] P.S. Bagus, V. Staemmler, C. Wöll, *Phys. Rev. Lett.* 89 (2002) 096104.
- [62] C. Urban, D. Eciya, Y. Wang, M. Trelka, I. Preda, A. Vollmer, N. Lorente, A. Arnau, M. Alcamí, L. Soriano, et al., *J. Phys. Chem. C* 114 (2010) 6503.
- [63] V. De Renzi, R. Rousseau, D. Marchetto, R. Biagi, S. Scandolo, U. del Pennino, *Phys. Rev. Lett.* 95 (2005) 046804.
- [64] F. Flores, J. Ortega, H. Vazquez, *Phys. Chem. Chem. Phys.* 11 (2009) 8658.
- [65] Y. Morikawa, K. Toyoda, I. Hamada, S. Yanagisawa, K. Lee, *Curr. Appl. Phys.* 12 (Supplement 3) (2012) S2.
- [66] H. Vázquez, F. Flores, R. Oszwaldowski, J. Ortega, R. Pérez, A. Kahn, *Appl. Surf. Sci.* 234 (2004) 107.
- [67] H. Vázquez, Y.J. Dappe, J. Ortega, F. Flores, *Appl. Surf. Sci.* 254 (2007) 378.
- [68] J.I. Martínez, E. Abad, F. Flores, J. Ortega, *Phys. Status Solidi (B)* 248 (2011) 2044.
- [69] J.I. Martínez, E. Abad, C. González, J. Ortega, F. Flores, *Org. Electron.* 13 (2012) 399.
- [70] H. Vázquez, F. Flores, A. Kahn, *Org. Electron.* 8 (2007) 241.
- [71] I.F. Torrente, K.J. Franke, J.I. Pascual, *Int. J. Mass Spectrom.* 277 (2008) 269.
- [72] M. Oehzelt, N. Koch, G. Heimel, *Nat. Commun.* 5 (2014) 4174.
- [73] P. Amsalem, G. Heimel, M. Oehzelt, N. Koch (Part A), *J. Electron Spectrosc. Relat. Phenom.* 204 (2015) 177.
- [74] R.G. Parr, R.G. Pearson, *J. Am. Chem. Soc.* 105 (1983) 7512.
- [75] N. Nicotra, E. Román, J.M. Gómez-Rodríguez, J.A. Martín-Gago, J. Méndez, *Org. Electron.* 7 (2006) 287.
- [76] A. Kraft, R. Temirov, S.K.M. Henze, S. Soubatch, M. Rohlfiing, F.S. Tautz, *Phys. Rev. B* 74 (2006) 041402.
- [77] F.S. Tautz, *Prog. Surf. Sci.* 82 (2007) 479.
- [78] K. Glöckler, C. Seidel, A. Soukopp, M. Sokolowski, E. Umbach, M. Böhlinger, R. Berndt, W.-D. Schneider, *Surf. Sci.* 405 (1998) 1.
- [79] T. Wagner, A. Bannani, C. Bobisch, H. Karacuban, R. Möller, *J. Phys. Condens. Matter* 19 (2007) 056009.
- [80] S. Mannsfeld, M. Toerker, T. Schmitz-Hübsch, F. Sellam, T. Fritz, K. Leo, *Org. Electron.* 2 (2001) 121.
- [81] S. Duhm, A. Gerlach, I. Salzmann, B. Bröker, R.L. Johnson, F. Schreiber, N. Koch, *Org. Electron.* 9 (2008) 111.
- [82] N. Koch, *J. Phys. Condens. Matter* 20 (2008) 184008.
- [83] Y. Zou, L. Kilian, A. Schöll, T. Schmidt, R. Fink, E. Umbach, *Surf. Sci.* 600 (2006) 1240.
- [84] L. Romaner, D. Nabok, P. Puschnig, E. Zojer, C. Ambrosch-Draxl, *New J. Phys.* 11 (2009) 053010.
- [85] H. Vázquez, R. Oszwaldowski, P. Pou, J. Ortega, R. Pérez, F. Flores, A. Kahn, *Europhys. Lett.* 65 (2004) 802.
- [86] M. Willenbockel, D. Luftner, B. Stadtmüller, G. Koller, C. Kumpf, S. Soubatch, P. Puschnig, M.G. Ramsey, F.S. Tautz, *Phys. Chem. Chem. Phys.* 17 (2015) 1530.
- [87] S.K.M. Henze, O. Bauer, T. — Lee, M. Sokolowski, F.S. Tautz, *Surf. Sci.* 601 (2007) 1566.
- [88] A. Hauschild, K. Karki, B.C.C. Cowie, M. Rohlfiing, F.S. Tautz, M. Sokolowski, *Phys. Rev. Lett.* 94 (2005) 036106.
- [89] A. Gerlach, S. Sellner, F. Schreiber, N. Koch, J. Zegenhagen, *Phys. Rev. B* 75 (2007) 045401.
- [90] P.C. Rusu, G. Giovannetti, C. Weijtens, R. Coehoorn, G. Brocks, *Phys. Rev. B* 81 (2010) 125403.
- [91] S. Titmuss, A. Wander, D.A. King, *Chem. Rev.* 96 (1996) 1291.
- [92] G.A. Somorjai, M.A. Van Hove, *Prog. Surf. Sci.* 30 (1989) 201.
- [93] A.E. Morgan, G.A. Somorjai, *Surf. Sci.* 12 (1968) 405.
- [94] R. Raval, S. Haq, M.A. Harrison, G. Blyholder, D.A. King, *Chem. Phys. Lett.* 167 (1990) 391.
- [95] Q. Chen, N.V. Richardson, *Prog. Surf. Sci.* 73 (2003) 59.
- [96] W. Erley, H. Ibach, *Surf. Sci.* 178 (1986) 565.
- [97] S. Barja, D. Stradi, B. Borca, M. Garnica, C. Díaz, J.M. Rodríguez-García, M. Alcamí, A.L. Vázquez de Parga, F. Martín, R. Miranda, *J. Phys. Condens. Matter* 25 (2013) 484007.
- [98] J. Giergiel, S. Wells, T.A. Land, J.C. Hemminger, *Surf. Sci.* 255 (1991) 31.
- [99] C. Wackerlin, C. Iacovita, D. Chylarecka, P. Fesser, T.A. Jung, N. Ballav, *Chem. Commun.* 47 (2011) 9146.
- [100] V. Feyer, M. Graus, P. Nigge, G. Zamborlini, R.G. Acres, A. Schöll, F. Reinert, C. M. Schneider, *J. Electron Spectrosc. Relat. Phenom.* 125 (2015) (204, Part A).
- [101] Y.C. Chou, N.T. Liang, *Chem. Phys. Lett.* 106 (1984) 472.
- [102] B.H. Loo, *J. Mol. Struct.* 661–662 (2003) 451.
- [103] W. Erley, H. Ibach, *J. Phys. Chem.* 91 (1987) 2947.
- [104] D. Wegner, R. Yamachika, Y. Wang, V.W. Brar, B.M. Bartlett, J.R. Long, M. F. Crommie, *Nano Lett.* 8 (2008) 131.
- [105] T. Deilmann, P. Kruger, M. Rohlfiing, D. Wegner, *Phys. Rev. B* 89 (2014) 045405.

- [106] T. Yokoyama, S. Yokoyama, T. Kamikado, S. Mashiko, *J. Chem. Phys.* 115 (2001) 3814.
- [107] B. Milián, R. Pou-Amérgo, R. Viruela, E. Ortí, *J. Mol. Struct.* 709 (2004) 97.
- [108] J.M. Lindquist, J.C. Hemminger, *Chem. Mater.* 1 (1989) 72.
- [109] J.M. Lindquist, J.C. Hemminger, *J. Phys. Chem.* 92 (1988) 1394.
- [110] T. Katayama, K. Mukai, S. Yoshimoto, J. Yoshinobu, *Phys. Rev. B* 83 (2011) 153403.
- [111] N. Koch, S. Duhm, J.P. Rabe, A. Vollmer, R.L. Johnson, *Phys. Rev. Lett.* 95 (2005) 237601.
- [112] T. Katayama, K. Mukai, S. Yoshimoto, J. Yoshinobu, *J. Phys. Chem. Lett.* 1 (2010) 2917.
- [113] J. Rodríguez-Fernández, K. Lauwaet, M.A. Herranz, N. Martín, J.M. Gallego, R. Miranda, R. Otero, *J. Chem. Phys.* 142 (2015).
- [114] M. Poensgen, J.F. Wolf, J. Frohn, M. Giesen, H. Ibach, *Surf. Sci.* 274 (1992) 430.
- [115] L. Sánchez, R. Otero, J.M. Gallego, R. Miranda, N. Martín, *Chem. Rev.* 109 (2009) 2081.
- [116] X. Torrelles, V. Langlais, M.D. Santis, H.C.N. Tolentino, Y. Gauthier, *J. Phys. Chem. C* 114 (2010) 15645.
- [117] M. Hinterstein, X. Torrelles, R. Felici, J. Rius, M. Huang, S. Fabris, H. Fuess, M. Pedio, *Phys. Rev. B* 77 (2008) 153412.
- [118] X. Zhang, W. He, A. Zhao, H. Li, L. Chen, W.W. Pai, J. Hou, M.M.T. Loy, J. Yang, X. Xiao, *Phys. Rev. B* 75 (2007) 235444.
- [119] P.W. Murray, M.O. Pedersen, E. Laegsgaard, I. Stensgaard, F. Besenbacher, *Phys. Rev. B* 55 (1997) 9360.
- [120] S.J. Chase, W.S. Bacsa, M.G. Mitch, L.J. Pilione, J.S. Lannin, *Phys. Rev. B* 46 (1992) 7873.
- [121] M.R.C. Hunt, S. Modesti, P. Rudolf, R.E. Palmer, *Phys. Rev. B* 51 (1995) 10039.
- [122] T.R. Ohno, Y. Chen, S.E. Harvey, G.H. Kroll, J.H. Weaver, R.E. Haufler, R. E. Smalley, *Phys. Rev. B* 44 (1991) 13747.
- [123] C. Liu, Z. Qin, J. Chen, Q. Guo, Y. Yu, G. Cao, *J. Chem. Phys.* 134 (2011) 044707.
- [124] R. Felici, M. Pedio, F. Borgatti, S. Iannotta, M. Capozzi, G. Ciullo, A. Stierle, *Nat. Mater.* 4 (2005) 688.
- [125] L. Tang, X. Zhang, Q. Guo, Y. Wu, L. Wang, H. Cheng, *Phys. Rev. B* 82 (2010) 125414.
- [126] H.L. Li, K. Pussi, K.J. Hanna, L.-L. Wang, D.D. Johnson, H.-P. Cheng, H. Shin, S. Curtarolo, W. Moritz, J.A. Smerdon, et al., *Phys. Rev. Lett.* 103 (2009) 056101.
- [127] W.W. Pai, H.T. Jeng, C.-M. Cheng, C.-H. Lin, X. Xiao, A. Zhao, X. Zhang, G. Xu, X. Q. Shi, M.A. Van Hove, et al., *Phys. Rev. Lett.* 104 (2010) 036103.
- [128] X. Shi, M.A. Van Hove, R. Zhang, *Phys. Rev. B* 85 (2012) 075421.
- [129] B. Amin, S. Nazir, U. Schwingenschlögl, *Sci. Rep.* 3 (2013) 1705.
- [130] S. Gottardi, K. Müller, J.C. Moreno-López, H. Yildirim, U. Meinhardt, M. Kivala, A. Kara, M. Stöhr, *Adv. Mater. Interfaces* 1 (2014) 1300025.
- [131] T. Sirtl, J. Jelic, J. Meyer, K. Das, W.M. Heckl, W. Moritz, J. Rundgren, M. Schmittel, K. Reuter, M. Lackinger, *Phys. Chem. Chem. Phys.* 15 (2013) 11054.
- [132] M.N. Faraggi, N. Jiang, N. Gonzalez-Lakunza, A. Langner, S. Stepanow, K. Kern, A. Arnau, *J. Phys. Chem. C* 116 (2012) 24558.
- [133] Y. Wang, X. Ge, C. Manzano, J. Kröger, R. Berndt, W.A. Hofer, H. Tang, J. Cerda, *J. Am. Chem. Soc.* 131 (2009) 10400.
- [134] B. Hammer, J.K. Nørskov, *Surf. Sci.* 343 (1995) 211.
- [135] R. Hoffmann, *Rev. Mod. Phys.* 60 (1988) 601.
- [136] S.S. Sung, R. Hoffmann, *J. Am. Chem. Soc.* 107 (1985) 578.
- [137] G. Blyholder, *J. Phys. Chem.* 68 (1964) 2772.
- [138] L. Dong, P.N. Liu, N. Lin, *Acc. Chem. Res.* 48 (2015) 2765.
- [139] L. Grill, M. Dyer, L. Lafferentz, M. Persson, M.V. Peters, S. Hecht, *Nat. Nano* 2 (2007) 687.
- [140] L. Lafferentz, V. Eberhardt, C. Dri, C. Africh, G. Comelli, F. Esch, S. Hecht, L. Grill, *Nat. Chem.* 4 (2012) 215.
- [141] R. Lindner, A. Kühnle, *ChemPhysChem* 16 (2015) 1582.
- [142] J.F. Dienstmaier, D.D. Medina, M. Dogru, P. Knochel, T. Bein, W.M. Heckl, M. Lackinger, *ACS Nano* 6 (2012) 7234.
- [143] M. Treier, N.V. Richardson, R. Fasel, *J. Am. Chem. Soc.* 130 (2008) 14054.
- [144] M. Abel, S. Clair, O. Ourdjini, M. Mossoyan, L. Porte, *J. Am. Chem. Soc.* 133 (2011) 1203.
- [145] R. Coratger, B. Calmettes, M. Abel, L. Porte, *Surf. Sci.* 605 (2011) 831.
- [146] S. Weigelt, C. Busse, C. Bombis, M.M. Knudsen, K.V. Gothelf, T. Strunskus, C. Wöll, M. Dahlbom, B. Hammer, E. Lægsgaard, et al., *Angew. Chem. Int. Ed.* 46 (2007) 9227.
- [147] H. Gao, H. Wagner, D. Zhong, J. Franke, A. Studer, H. Fuchs, *Angew. Chem. Int. Ed.* 52 (2013) 4024.
- [148] D. Zhong, J. Franke, S.K. Podiyanchari, T. Blömkner, H. Zhang, G. Kehr, G. Erker, H. Fuchs, L. Chi, *Science* 334 (2011) 213.
- [149] M. Int'l Veld, P. Iavicoli, S. Haq, D.B. Amabilino, R. Raval, *Chem. Commun.* 1536 (2008).
- [150] J. Björk, *J. Phys. Condens. Matter* 28 (2016) 083002.
- [151] K. Morgenstern, *Acc. Chem. Res.* 42 (2009) 213.
- [152] M.J. Comstock, N. Levy, A. Kirakosian, J. Cho, F. Lauterwasser, J.H. Harvey, D. A. Strubbe, J.M.J. Frechet, D. Trauner, S.G. Louie, et al., *Phys. Rev. Lett.* 99 (2007) 038301.
- [153] A.S. Kumar, T. Ye, T. Takami, B. Yu, A.K. Flatt, J.M. Tour, P.S. Weiss, *Nano Lett.* 8 (2008) 1644.
- [154] W.R. Browne, B.L. Feringa, *Annu. Rev. Phys. Chem.* 60 (2009) 407.
- [155] J. Henzl, M. Mehlhorn, H. Gawronski, K. Rieder, K. Morgenstern, *Angew. Chem. Int. Ed.* 45 (2006) 603.
- [156] B. Choi, S. Kahng, S. Kim, H. Kim, H.W. Kim, Y.J. Song, J. Ihm, Y. Kuk, *Phys. Rev. Lett.* 96 (2006) 156106.
- [157] M. Alemani, M.V. Peters, S. Hecht, K. Rieder, F. Moresco, L. Grill, *J. Am. Chem. Soc.* 128 (2006) 14446.
- [158] J. Mielke, F. Leyssner, M. Koch, S. Meyer, Y. Luo, S. Selvanathan, R. Haag, P. Tegeder, L. Grill, *ACS Nano* 5 (2011) 2090.
- [159] S. Hagen, F. Leyssner, D. Nandi, M. Wolf, P. Tegeder, *Chem. Phys. Lett.* 444 (2007) 85.
- [160] V. Simic-Milosevic, M. Mehlhorn, K.-H. Rieder, J. Meyer, K. Morgenstern, *Phys. Rev. Lett.* 98 (2007) 116102.
- [161] R.J. Maurer, K. Reuter, *Angew. Chem. Int. Ed.* 51 (2012) 12009.
- [162] N. Martin, J.L. Segura, C. Seoane, J. Mater. Chem. 7 (1997) 1661.
- [163] F. Cossio, P. de la Cruz, A. de la Hoz, F. Langa, N. Martín, P. Prieto, L. Sanchez, *Eur. J. Org. Chem.* 2000 (2000) 2407.
- [164] A. Aumuler, S. Hunig, *Liebigs Ann. Chem.* 1986 (1986) 142.
- [165] J.A. Lipton-Duffin, J.A. Miwa, M. Kondratenko, F. Cicoira, B.G. Sumpter, V. Meunier, D.F. Perepichka, F. Rosei, *Proc. Natl. Acad. Sci. USA* 107 (2010) 11200.
- [166] J.A. Lipton-Duffin, O. Ivasenko, D.F. Perepichka, F. Rosei, *Small* 5 (2009) 592.
- [167] A.C. Marele, R. Mas-Balleste, L. Terracciano, J. Rodriguez-Fernandez, I. Berlanga, S.S. Alexandre, R. Otero, J.M. Gallego, F. Zamora, J.M. Gomez-Rodriguez, *Chem. Commun.* 48 (2012) 6779.
- [168] F. Bebenese, C. Bombis, S. Vadapoo, J.R. Cramer, F. Besenbacher, K.V. Gothelf, T.R. Linderroth, *J. Am. Chem. Soc.* 135 (2013) 2136.
- [169] S. Weigelt, C. Busse, C. Bombis, M.M. Knudsen, K.V. Gothelf, E. Lægsgaard, F. Besenbacher, T.R. Linderroth, *Angew. Chem. Int. Ed.* 47 (2008) 4406.
- [170] M. Di Giovannantonio, T. Kosmala, B. Bonanni, G. Serrano, N. Zema, S. Turchini, D. Catone, K. Wandelt, D. Pasini, G. Contini, et al., *J. Phys. Chem. C* 119 (2015) 19228.
- [171] R. Viruela, P.M. Viruela, E. Ortí, N. Martín, *Synth. Met.* 70 (1995) 1031.
- [172] N. Martin, R. Behnisch, M. Hanack, *J. Org. Chem.* 54 (1989) 2563.
- [173] N. Martin, M. Hanack, *J. Chem. Soc. Chem. Commun.* 1522 (1988).
- [174] G. Chen, H. Sasabe, Z. Wang, X. Wang, Z. Hong, Y. Yang, J. Kido, *Adv. Mater.* 24 (2012) 2768.
- [175] J. Zhong, X. Qin, J. Zhang, S. Kera, N. Ueno, A.T.S. Wee, J. Yang, W. Chen, *ACS Nano* 8 (2014) 1699.
- [176] A. El-Sayed, D.J. Mowbray, J.M. García-Lastra, C. Rogero, E. Goiri, P. Borghetti, A. Turak, B.P. Doyle, M. Dell'Angela, L. Floreano, et al., *J. Phys. Chem. C* 116 (2012) 4780.
- [177] B. Stadtmüller, S. Schröder, F.C. Bocquet, C. Henneke, C. Kleimann, S. Soubatch, M. Willenbockel, B. Detlefs, J. Zegenhagen, T. Lee, et al., *Phys. Rev. B* 89 (2014) 161407.
- [178] E. Barrena, D.G. de Oteyza, H. Dosch, Y. Wakayama, *ChemPhysChem* 8 (2007) 1915.
- [179] D.G. de Oteyza, J.M. García-Lastra, M. Corso, B.P. Doyle, L. Floreano, A. Morgante, Y. Wakayama, A. Rubio, J.E. Ortega, *Adv. Func. Mater.* 19 (2009) 3567.
- [180] E. Goiri, M. Matena, A. El-Sayed, J. Lobo-Checa, P. Borghetti, C. Rogero, B. Detlefs, J. Duvernay, J.E. Ortega, D.G. de Oteyza, *Phys. Rev. Lett.* 112 (2014) 117602.
- [181] T.R. Umbach, I. Fernandez-Torrente, J.N. Ladenthin, J.I. Pascual, K.J. Franke, *J. Phys. Condens. Matter* 24 (2012) 354003.
- [182] R. Otero, D. Écija, G. Fernández, J.M. Gallego, L. Sánchez, N. Martín, R. Miranda, *Nano Lett.* 7 (2007) 2602.
- [183] S. Weisz, D. Luftner, T. Ules, E.M. Reinisch, H. Kaser, A. Gottwald, M. Richter, S. Soubatch, G. Koller, M.G. Ramsey, et al., *Nat. Commun.* 6 (2015) 8287.
- [184] F.J. Himpfel, J.E. Ortega, G.J. Mankey, R.F. Willis, *Adv. Phys.* 47 (1998) 511.
- [185] A.R. Rocha, V. Garcia-suarez, S.W. Bailey, C.J. Lambert, J. Ferrer, S. Sanvito, *Nat. Mater.* 4 (2005) 335.
- [186] W.J. de Haas, J. de Boer, G.J. van den Berg, *Physica* 1 (1934) 1115.
- [187] J. Kondo, *Prog. Theor. Phys.* 32 (1964) 37.
- [188] J. Li, W. Schneider, R. Berndt, B. Delley, *Phys. Rev. Lett.* 80 (1998) 2893.
- [189] V. Madhavan, W. Chen, T. Jamneala, M.F. Crommie, N.S. Wingreen, *Science* 280 (1998) 567.
- [190] A.J. Heinrich, J.A. Gupta, C.P. Lutz, D.M. Eigler, *Science* 306 (2004) 466.
- [191] P.W. Anderson, *Phys. Rev.* 124 (1961) 41.
- [192] L.G.L. Kouwenhoven, *Phys. World* 14 (2001) 33.
- [193] U. Fano, *Phys. Rev.* 124 (1961) 1866.
- [194] K. Nagaoka, T. Jamneala, M. Grobis, M.F. Crommie, *Phys. Rev. Lett.* 88 (2002) 077205.
- [195] M. Ternes, A.J. Heinrich, W. Schneider, *J. Phys. Condens. Matter* 21 (2009) 053001.
- [196] A. Zhao, Q. Li, L. Chen, H. Xiang, W. Wang, S. Pan, B. Wang, X. Xiao, J. Yang, J. G. Hou, et al., *Science* 309 (2005) 1542.
- [197] V. Iancu, A. Deshpande, S.-W. Hla, *Nano Lett.* 6 (2006) 820.
- [198] T. Komeda, H. Isshiki, J. Liu, Y. Zhang, N. Lorente, K. Katoh, B.K. Breedlove, M. Yamashita, *Nat. Commun.* 2 (2011) 217.
- [199] P. Wahl, L. Diekhoner, G. Wittich, L. Vitali, M.A. Schneider, K. Kern, *Phys. Rev. Lett.* 95 (2005) 166601.
- [200] D. Wegner, R. Yamachika, X. Zhang, Y. Wang, T. Baruah, M.R. Pederson, B. M. Bartlett, J.R. Long, M.F. Crommie, *Phys. Rev. Lett.* 103 (2009) 087205.
- [201] L. Gao, W. Ji, Y.B. Hu, Z.H. Cheng, Z.T. Deng, Q. Liu, N. Jiang, X. Lin, W. Guo, S. X. Du, et al., *Phys. Rev. Lett.* 99 (2007) 106402.
- [202] E. Minamitani, N. Tsukahara, D. Matsunaka, Y. Kim, N. Takagi, M. Kawai, *Phys. Rev. Lett.* 109 (2012) 086602.
- [203] S. Stepanow, P.S. Miedema, A. Mugarza, G. Ceballos, P. Moras, J.C. Cezar, C. Carbone, F.M.F. de Groot, P. Gambardella, *Phys. Rev. B* 83 (2011) 220401.

- [204] R. Otero, V.ázquez de Parga, L. Amadeo, R. Miranda, *Phys. Rev. B* 66 (2002) 115401.
- [205] A.L. Vázquez de Parga, J.J. Hinarejos, F. Calleja, J. Camarero, R. Otero, R. Miranda, *Surf. Sci.* 603 (2009) 1389.
- [206] F. Calleja, A.L. Vázquez de Parga, E. Anglada, J.J. Hinarejos, R. Miranda, F. Yndurain, *New J. Phys.* 11 (2009) 123003.
- [207] T. – Chiang, *Surf. Sci. Rep.* 39 (2000) 181.
- [208] C.M. Wei, M.Y. Chou, *Phys. Rev. B* 66 (2002) 233408.
- [209] Y. Fu, S. Ji, X. Chen, X. Ma, R. Wu, C. Wang, W. Duan, X. Qiu, B. Sun, P. Zhang, et al., *Phys. Rev. Lett.* 99 (2007) 256601.
- [210] K.J. Franke, G. Schulze, J.I. Pascual, *Science* 332 (2011) 940.
- [211] A.L. Vázquez de Parga, F. Calleja, B. Borca, M.C.G. Passeggi, J.J. Hinarejos, F. Guinea, R. Miranda, *Phys. Rev. Lett.* 100 (2008) 056807.
- [212] B. Borca, S. Barja, M. Garnica, M. Minniti, A. Politano, J.M. Rodriguez-García, J. J. Hinarejos, D. Fariás, A.L. Vázquez de Parga, R. Miranda, *New J. Phys.* 12 (2010) 093018.
- [213] D. Maccariello, M. Garnica, M.A. Niño, C. Navío, P. Perna, S. Barja, A.L. Vázquez de Parga, R. Miranda, *Chem. Mater.* 26 (2014) 2883.
- [214] U.G.E. Perera, H.J. Kulik, V. Iancu, L.G.G.V. Dias da Silva, S.E. Ulloa, N. Marzari, S.-W. Hla, *Phys. Rev. Lett.* 105 (2010) 106601.
- [215] A. Mugarza, C. Krull, R. Robles, S. Stepanow, G. Ceballos, P. Gambardella, *Nat. Commun.* 2 (2011) 490.
- [216] V. Iancu, A. Deshpande, S. Hla, *Phys. Rev. Lett.* 97 (2006) 266603.
- [217] C. Krull, R. Robles, A. Mugarza, P. Gambardella, *Nat. Mater.* 12 (2013) 337.
- [218] N. Tsukahara, S. Shiraki, S. Itou, N. Ohta, N. Takagi, M. Kawai, *Phys. Rev. Lett.* 106 (2011) 187201.
- [219] Y. Jiang, Y.N. Zhang, J.X. Cao, R.Q. Wu, W. Ho, *Science* 333 (2011) 324.
- [220] S. Nakatsuji, D. Pines, Z. Fisk, *Phys. Rev. Lett.* 92 (2004) 016401.
- [221] S. Müllegger, M. Rashidi, M. Fattinger, R. Koch, *J. Phys. Chem. C* 117 (2013) 5718.
- [222] Y. Zhang, S. Kahle, T. Herden, C. Stroh, M. Mayor, U. Schlickum, M. Ternes, P. Wahl, K. Kern, *Nat. Commun.* 4 (2013) 2110.
- [223] M. Garnica, D. Stradi, S. Barja, F. Calleja, C. Diaz, M. Alcamí, N. Martin, A. L. Vazquez de Parga, F. Martin, R. Miranda, *Nat. Phys.* 9 (2013) 368.
- [224] Y. Nagaoka, *Phys. Rev.* 147 (1966) 392.
- [225] H. Tasaki, *Phys. Rev. Lett.* 69 (1992) 1608.
- [226] A. Mielke, *Phys. Rev. Lett.* 82 (1999) 4312.